Perinuclear chromatin anchoring in *Caenorhabditis elegans* embryos: CEC-4 characterization and function

Inauguraldissertation
zur
Erlangung der Würde eines Doktors der Philosophie
vorgelegt der
Philosophisch-Naturwissenschaftlichen Fakultät
der Universität Basel

von

Adriana Verenisse Gonzalez Sandoval

aus Mexico

Basel, 2017

Genehmigt von der Philosophisch-Naturwissenschaftlichen Fakultät auf Antrag von

Prof. Dr. Susan M. Gasser

Prof. Dr. Bas van Steensel

Basel, den 23 Februar 2016

Prof. Dr. Jörg Schibler

Dekan

TABLE OF CONTENTS

THESIS OVERVIEW

This PhD thesis is based on the following publications:

- Gonzalez-Sandoval A., and Gasser, S.M. Towards the functional relevance of spatial organization of chromatin in interphase nuclei. *In preparation.*
- Harr, J.C., Gonzalez-Sandoval, A. & Gasser, S.M. (2016) Histones and histone modifications in perinuclear chromatin anchoring: from yeast to man. EMBO reports, p.e201541809.
- Gonzalez-Sandoval et al. (2015). Perinuclear Anchoring of H3K9-Methylated Chromatin Stabilizes Induced Cell Fate in *C. elegans* Embryos. Cell. 163, 1333-1347.
- Gonzalez-Sandoval A., Towbin B.D., and Gasser, S.M. (2013). The formation and sequestration of heterochromatin during development. FEBS Journal. 280, 3212–3219.
- Towbin B.D., Gonzalez-Sandoval A., and Gasser, S.M. (2013). Mechanisms of heterochromatin subnuclear localization. Trends in Biochemical Sciences. Vol. 38, No. 7, 356-363.

This thesis consists of four chapters. Chapter 1 and 2 are based on published manuscript (Gonzalez-Sandoval et al., 2015). Chapter 3 includes unpublished experimental data and Chapter 4 summarizes the work and discusses future directions.

Chapter 1 is an introduction based in reviews from the Gasser lab, to which I have contributed. These are recently published (Gonzalez-Sandoval et al., 2013; Harr et al., 2016; Towbin et al., 2013) or in preparation (Gonzalez-Sandoval and Gasser S.M.). The main message of each review is kept but they are arranged or modified in a way to avoid redundancy and provide clarity. Additional relevant literature that is not discussed adequately in either of the reviews has been included. The chapter gives an updated overview of the field of spatial organization of chromatin in the interphase nucleus.

Chapter 2 presents the work published in *Cell*, 2015. It is an experimental chapter in which I present the identification, characterization and function of a novel *C. elegans* chromodomain protein called CEC-4 (*Caenorhabditis elegans* chromodomain protein 4), which mediates the anchoring of chromatin at the nuclear periphery in *C. elegans* embryos. Experiments were primarily performed by myself, but I indicate where others have carried our experimental work for this publication.

Chapter 3 presents unpublished data that further characterizes CEC-4.

Finally, Chapter 4 places the work presented in the thesis in the context of spatial chromatin organization and provides a future outlook based on this study.

CHAPTER 1: INTRODUCTION

Based on scientific reviews of the field that are published or in preparation, to which I have contributed (see Thesis Overview for list).

SUMMARY

In eukaryotic organisms, gene regulation occurs in the context of chromatin. Local modulation of DNA accessibility and contacts with other loci or distal regulatory elements (enhancers) provides a level of regulation that establishes and maintains differential transcription states. Moreover, chromatin is not randomly distributed inside the nucleus and specific types of chromatin can occupy distinct nuclear regions. In the interphase nucleus, euchromatin and heterochromatin occupy distinct space. This organization can add further constraints to fine-tune gene expression. Heterochromatin is progressively formed and becomes enriched at the nuclear periphery during differentiation in multicellular organisms. A long-standing question is whether this type of spatial segregation contributes to the control of gene expression. An understanding of the mechanisms that govern this type of nuclear organization will shed light on its functionality. Here we describe the field of nuclear organization, focusing on the segregation of chromatin near the nuclear periphery. We summarize the mechanisms that have been proposed to date to mediate such chromatin organization.

NUCLEAR ARCHITECTURE

Cell identity is determined by the specific set of genes that are expressed (and repressed) at a given time. The packaging of DNA into chromatin is critical both for the physical compaction of the genome into the nucleus and to regulate access to the genetic material for DNA-based transactions, such as transcription, replication and repair. The winding of DNA around the nucleosome, to form the basic repeat unit of chromatin, is sufficient to antagonize DNA recognition by sequence-specific binding factors (Cote et al., 1994).

On the level of the individual genes, there is a strong correlation between transcriptional activity and associated histone modifications. Histone modifications can influence the recruitment of non-histone proteins, determining the level of chromatin compaction, transcription factor binding, and RNA polymerase (Pol) elongation. Beyond the nucleosome, chromatin folds into successively higher-order structures that remain poorly described on a molecular level.

In a higher order of organization, chromosomes are not randomly positioned but rather maintain a certain "territory", with some chromosomes being more internal than others (Cremer et al., 2001; Spector, 2001). This radial distribution correlates with the density of LINE/SINE repetitive elements in mammalian cells (Meuleman et al., 2013). One example of these territories is the inactivated X-chromosome in mammals, which localizes close to the nuclear periphery and is highly compacted (reviewed in Sharma and Meister, 2015). Additionally, some chromatin segregates into foci marked by specific proteins, such as P-bodies which are enriched for Polycomb group proteins (Sexton et al., 2012). Dense-staining heterochromatin often clusters or segregates towards the nuclear periphery and around the nucleolus during differentiation. The more open, euchromatic, regions are dispersed in the nucleoplasm or underlie nuclear pores (Comings, 1980).

The functional significance of chromatin segregation is a matter of debate. It is hypothesized that compartmentalization facilitates the concentration of factors, leading to an increased efficiency of biological functions that rely on proteins present in limiting concentrations. In many cases it has been difficult to untangle whether organization is a consequence or a cause of this regulation (Meister and Taddei, 2013). How sequestration acts, remains poorly understood.

The specific aim of this thesis is to investigate the association of heterochromatin with the nuclear periphery in *C. elegans* embryos, in order to address its functionality. The following sections review our understanding of chromatin organization inside the interphase nucleus. I will first present the best characterized example of chromatin organization: the budding yeast nucleus. Even though the mechanism through which it silences chromatin is more of an exception than a paradigm for other species, some of the underlying mechanisms appear to be applicable to chromatin organization in other organisms.

Budding yeast as an example of nuclear architecture

Much of our understanding of the molecular mechanisms that drive nuclear organization stems from studies in budding yeast (*S. cerevisiae)*, even though its nucleus is small and heterochromatic domains are scarce (Taddei and Gasser, 2012). Unlike centromeres in other

species, those of budding yeast are defined by a short, non-repetitive sequence that forms a "point-like" kinetochore. Repetitive DNA and heterochromatin-like domains in yeast are found at the ends of each chromosome and at two silent mating type loci on its "sex chromosome", Chromosome III. Constitutive repression of transcription at these mating-type loci uses the same mechanism as subtelomeric domains.

Yeast chromosomes adopt a striking organization within the interphase nucleus. The centromeres anchor to the spindle-pole body (SPB) and the telomeres cluster with silent mating type loci in 3 to 8 foci distributed at perinuclear sites that are distinct from nuclear pores (reviewed in Taddei and Gasser, 2012) (Figure 1.1). This configuration reflects the so-called Rabl organization of chromosomes, which arises during mitosis when a force is placed on centromeres as they are pulled to opposite ends of the nucleus by the mitotic spindle. Telomeres are dragged behind as chromosomes segregate and this contributes to their clustering which is based on chromosome arm length, and their subnuclear positioning away from the SPB (Schober et al., 2009; Schober et al., 2008). During interphase, a large single nucleolus, which occupies nearly a third of the nuclear volume, is positioned directly opposite the SPB. The nucleolus is a scaffold not only for ribosome biogenesis, but also for tRNA (transfer RNA) genes which associate with the periphery of the nucleolus when actively transcribed (Thompson et al., 2003). However, recently it has been described that during mitotic (M) phase some tRNAs are transcribed near nuclear pores to coordinate with nuclear export. This set of tRNAs are not found close to the nucleolus at any stage (Chen and Gartenberg, 2014).

The spatial organization in yeast was originally documented using imaging techniques such as FISH (Fluorescence *in situ* hybridization), GFP-protein fusions and GFP-LacI/lacO localization. Moreover, recent studies using ligation-based Chromosome Conformation Capture (3C) technology (reviewed in de Wit and de Laat, 2012) have confirmed this polarized organization, and the importance of the nucleolus in yeast as an organizational element (Berger et al., 2008). Consistent with imaging approaches, 3C and 4C (Chromosome Conformation Capture on Chip) results detect a spatial juxtaposition of centromeres and telomeres in separate foci, but not for tRNAs, putting into question the robustness of the earlier imaging data (Duan et al., 2010; Miele et al., 2009).

The sequestration of silent domains and the SIR (Silent Information Regulator) complex in perinuclear foci (Gotta et al., 1996; Palladino et al., 1993), and the association of a subset of inducible genes at nuclear pores (Casolari et al., 2004), suggest that nuclear subcompartments may have specialized functions. This hypothesis has been tested in budding yeast in the context of transcription by several laboratories (Andrulis et al., 1998; Casolari et al., 2004; Egecioglu and Brickner, 2011; Taddei et al., 2006; Taddei et al., 2009). In particular, the clustering of silent chromatin domains encouraged scientists to test whether telomeric foci promote repression. This was achieved by tethering a gene at the nuclear envelope (NE) and placing it artificially near a telomere, through addition of a transmembrane domain. This tethering did favor silencing, but only if the reporter construct contained a "silencer", a short sequence element that targets the SIR repression complex through its interaction with sequence-specific binding factors (Andrulis et al., 1998). Besides this silencer, position-dependent repression also required that yeast telomeres were clustered in foci at the NE, leading to a local enrichment of SIR factors (Taddei et al., 2009). It was

concluded that the critical parameter for repression is proximity to sufficiently abundant pools of SIR factors, and not to the NE *per se* (Taddei et al., 2009).

While this peripheral positioning facilitates SIR-mediated silencing in wild-type cells, in some mutant conditions it is not required for repression. Notably, the loss of telomere anchoring led to the dispersion of SIR proteins from silencing foci, and allowed promiscuous repression across the genome of a handful of genes. Coincidentally, telomere-proximal promoters were derepressed (Taddei et al., 2009). This shows that presence of foci containing repressed, repetitive chromatin, affects transcription genome-wide. Additional proof for effects of spatial organization came from a gain-of-function experiment in which a gene was targeted to the nuclear pore. The promoter was roughly 2 fold more active at the pore, showing that transcription of some promoters can indeed be favored by positioning at the pore rather than in the nucleoplasm (Taddei et al., 2006). This is consistent with the finding that genes induced by heat-shock or by growth on non-glucose carbon sources shift to the nuclear periphery and associate with the nuclear pore upon activation (Akhtar and Gasser, 2007; Egecioglu and Brickner, 2011). Taken together, one can argue that the nuclear periphery can favor either repression or activation, depending on the sequence and context of the promoter as well as the NE factors to which chromatin is associated. The important principle is that position alone does not determine activity state, yet spatial juxtaposition can cooperate with cis-acting sequences and regulatory factors to favor a transcriptional state.

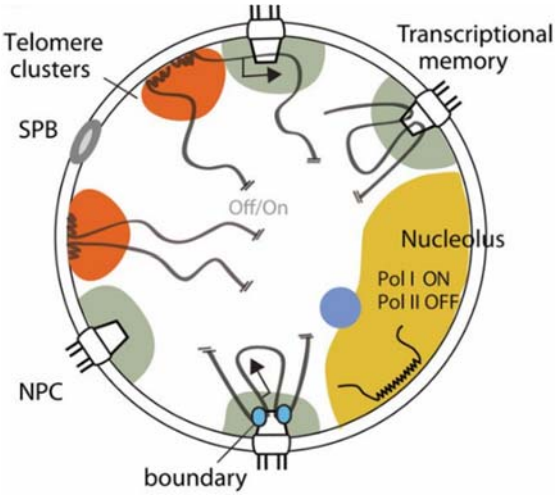

Figure 1.1. The budding yeast nucleus. The rDNA (ribosomal DNA) locus is sequestered apart from the rest of the genome in the nucleolus (in yellow) where RNA Pol I transcribes and assembles ribosome subunits and RNA Pol III transcription foci (blue circle) can be observed. Repressed telomere clusters (in orange) can be found in proximity to the nuclear periphery. Centromeres are clustered close to the Spindle Pole Body (SPB) – not depicted. Inducible genes bind the nuclear pore complex (NPC), as well as some tRNAs during M phase. Transcription of RNA Pol II genes can be found spread throughout the nucleus (Off/On). Image reprinted from (Taddei and Gasser, 2012).

The organization of chromatin such as tethering to the nuclear periphery, localization at pores or the nucleolus, can also be seen in other organisms. Yeast is a model system that has provided an advantage in understanding the molecular principles of nuclear organization.

In the following sections I will summarize our understanding of chromatin organization in other organisms, starting from the basics of chromatin types and what is known about long-range chromatin contacts and their functionality. The second half of this chapter will describe the features of chromatin that come in contact with the nuclear periphery, known factors involved in this positioning and open questions in this field of study.

CHROMATIN TYPES

Since the earliest studies on integrated gene reporters (Dobzhansky, 1936), it has been documented that the landing location or "position" of the reporter impacts expression. Unfortunately, no clear explanation of this effect was identified. Thanks to the revolution in genome wide mapping of different chromatin related factors and histone modifications, chromatin has been classified into different types (reviewed in Ciabrelli and Cavalli, 2015) giving a notion that indeed not all genomic regions share the same characteristics, and if a reporter lands close to a specific chromatin type, that neighborhood can influence its expression levels. According to these classifications, there are 'active' chromatin domains as well as 'inactive' ones (Figure 1.2). Active chromatin is marked by histone modifications such as methylation (me) of histone H3K4, K36, K79, acetylation (ac) on H3 and H4 N-terminal tail lysines and multiple factors related to active gene transcription such as RNA Pol II (Filion et al., 2010; Kharchenko et al., 2011). Inactive chromatin was found to be further subdivided depending on the combination of different factors or the lack of enrichment of some of them (reviewed in Bickmore and van Steensel, 2013; Ciabrelli and Cavalli, 2015). Relevant to our studies, we highlight two of these inactive chromatin types: (1) Polycomb-enriched which also contain the repressive histone modification H3K27me3, such as Hox clusters, X-inactivation sites and imprinted regions; (2) Lamina-associated domains (LADs) that are enriched for repressive H3K9me2 and H3K27me3 at the borders but not necessarily Heterochromatin protein 1 (HP1, a canonical reader of methylated H3K9), and tend to be gene poor (Guelen et al., 2008; Pickersgill et al., 2006). Recently, it was shown by a method called Thousands of Reporters Integrated in Parallel (TRIP) that endogenous active genes have a higher impact on expression of nearby integrated reporters (within 200 kb range), than inactive genes. It remains to be determined how propagation of the 'active' status happens. In addition, LADs were found as true attenuators of transcription, in part due to low density of functional enhancers, poor accessibility of binding factors, and degree of compaction, although all of these factors combined do not fully explain the capacity of LADs to reduce transcription. Indeed, other unknown features may contribute to the mechanisms that regulate transcription in LADs (Akhtar et al., 2013).

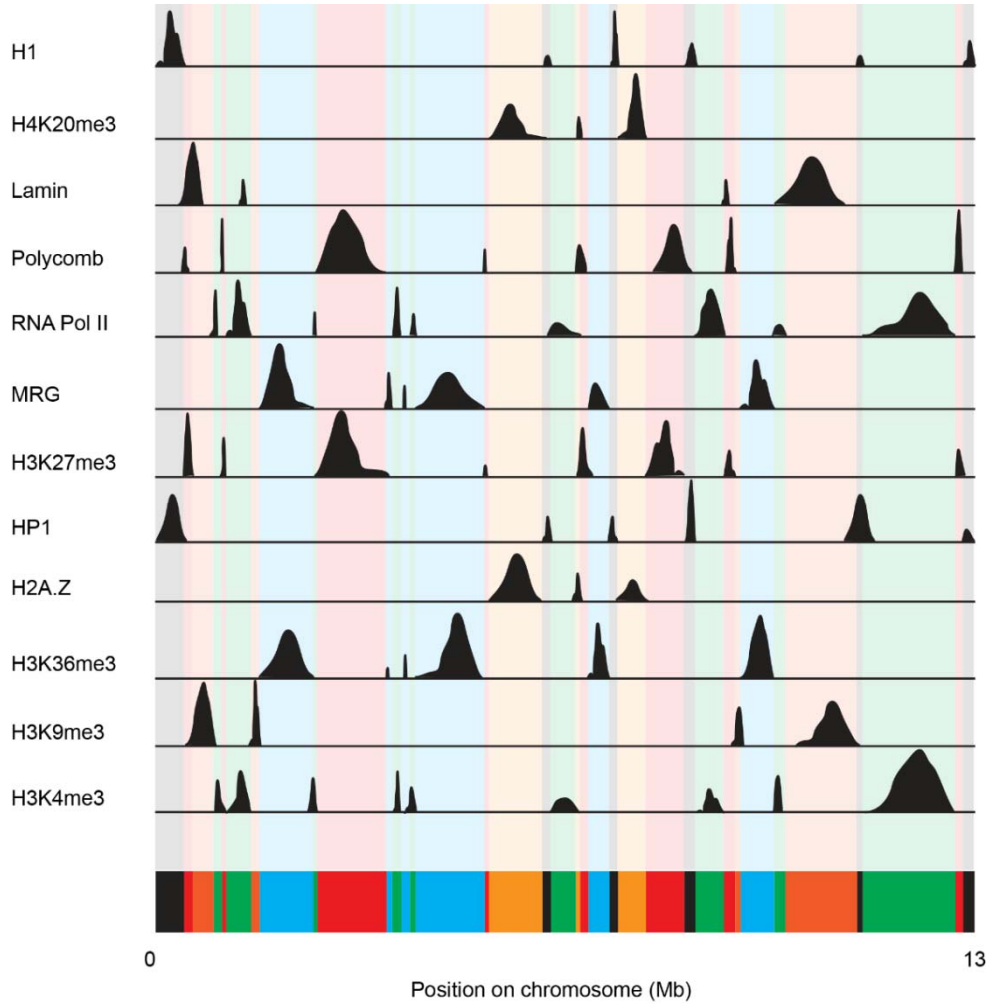

Figure 1.2. Schematic representation of chromatin types. This figure does not represent any actual data. For conceptual simplicity we just represent chromatin types with few known chromatin factors. Depending on the type of factor enriched on specific positions: proteins (Lamin, Polycomb, MRG, HP1), histones (H1, H2A.Z) or histone modifications (H3- K4me3, -K9me3, -K27me3, -K36me3 or H4K20me3), chromatin can be grouped into different categories. The overall consensus is that there are different groups of active (blue and green) and repressed (black, orange, yellow) chromatin.

Long-Range Chromatin Interactions

Transcriptional regulation is not solely through the proximal promoter region of a gene, but also distal regulatory elements, such as enhancers, have been shown to participate in such regulation. Assembly of multiple factor complexes aid in these long-range interactions, which can be intra- or inter- chromosomal contacts. Several methods have emerged to study the three-dimensional (3D) arrangement of chromatin inside the nucleus. A method that identifies the likelihood of sequence-sequence interactions, called Chromosome Conformation Capture (3C) (Dekker et al., 2002) and its derived techniques, in particular Genome-wide 3C (Hi-C), allow the definition and study of such chromatin contacts (reviewed in de Wit and de Laat, 2012). Several studies have defined units of chromatin that are in close proximity with each other in a 3D space - Topological associated domains (TADs) (Dixon et al., 2012;

Lieberman-Aiden et al., 2009; Nora et al., 2012; Sexton et al., 2012). TADs are generally conserved among different cell types and across species (Jin et al., 2013; Rao et al., 2014; Vietri Rudan et al., 2015), however Dixon et al. found discrete chromatin reorganization during lineage specification in human embryonic stem (ES) cells (Dixon et al., 2015). The insulator protein CCCTC-binding factor (CTCF) as well as Cohesin are enriched at the borders of TADs, and have been described to play a role in the formation and maintenance of long-range chromatin loops (Hadjur et al., 2009; Mishiro et al., 2009; Nativio et al., 2009). In addition, it has been shown that across species, CTCF binding orientation is conserved and sequence divergence of the binding insulation region underlies changes in local structures within TADs (Rao et al., 2014; Vietri Rudan et al., 2015).

Chromatin has been separated into two major compartments: A and B, by associations between TADs, located both in *cis* and in *trans*. The A compartment is enriched for proteins and histone modifications involved in active transcription and is correlated with early replication. The B compartment is related to inactive gene expression, enriched for inactive factors and histone marks and correlated with late replication (Dixon et al., 2012; Ryba et al., 2010). Recently, these A and B compartments have been further subdivided into two and four subcompartments respectively, thanks to higher resolution in Hi-C data (Rao et al., 2014). The relationship of chromatin contacts, global chromatin organization and gene regulation is an active area of study. Chromatin contacts among enhancers and promoters can precede gene activation and most of the contact changes have been reported within the same TAD, with relatively few associations between different TADs (Dixon et al., 2012; Jin et al., 2013; Noordermeer et al., 2011; Sexton et al., 2012). CTCF-mediated loops were strongly enriched at the border of LADs (Handoko et al., 2011), while LADs themselves were refractory to loop formation. This suggested an intimate link between the anchoring of chromatin to the nuclear lamina, and an inhibition of long-range DNA contacts mediated by CTCF (Phillips and Corces, 2009). CTCF was also found enriched around euchromatic islands within large heterochromatic domains (Wen et al., 2012), suggesting that it may also control the spread of lamin association in *cis*.

Hox gene clusters are a well-studied system of chromatin architecture. Gene expression inside a cluster is coordinated in time and space during embryonic development. These genes are colocalized in the genome in an order that corresponds to their actual expression along the body axis, which is termed collinear expression (Noordermeer and Duboule, 2013). The *HoxD* cluster is involved in vertebrate limb development, and some genes within are transcribed in two subsequent phases. Central genes are transcribed early, which will correspond to the central part of the limbs (forearm and partially the arm); later an overlapping group of genes together with genes closer to one extremity of the cluster will be expressed in the corresponding distal part of the limbs (hand). The mechanism of regulation of genes being transcribed in the early and late phases of the *HoxD* cluster involves the switch of regulatory elements between two adjacent TADs, denominated telomere-proximal and centromere-proximal domains (T-DOM and C-DOM, respectively), flanking the HoxD cluster (Andrey et al., 2013). *Hoxd11* to *Hoxd9* genes are expressed in both early and late phases of limb development. In early stages their expression is driven by T-DOM regulatory region and in late phases it is the C-DOM region which participates in control of expression (Figure 1.3A). Coincident with the switch, there is a loss of the active histone mark H3K27ac, and gain of H3K27me3 in the T-DOM region and gain of H3K27ac over the C-DOM in digits. This

study highlights the importance of chromatin contacts in the fine-tuning of gene expression during development; showing that the change of chromatin interactions of regulatory elements localized in different topological domains contributes to the timing and patterning of expression of the *HoxD* cluster. What are the factors triggering the switch of regulatory regions? Is this type of topological switch governing other type of loci through development or does it only apply to collinear gene regulation?

Recently, Lupianez et al. very elegantly addressed the impact of 3D chromatin organization on human limb development (Lupianez et al., 2015). Specifically, they studied three diseases that carry structural variations of a genomic region that encompasses the *EPHA4* gene-containing TAD and its flanking TADs. (1) Brachydactyly involves a heterozygous deletion of a 1.75-1.9 Mb region including the gene *EPHA4* and the TAD boundary to the right of the locus. Importantly, *EPHA4* inactivation alone does not cause limb skeleton changes (Helmbacher et al., 2000). (2) F-syndrome involves a heterozygous inversion of a 1.1 Mb genomic region, disrupting the orientation of a gene cluster adjacent to the *WNT6* gene, with an additional change in orientation of the left side *EPHA4*-containing TAD boundary. (3) Polydactyly holds a heterozygous 900 kb duplicated region which brings the *IHH* gene, from the left flanking TAD, in proximity to the *EPHA4*-containing TAD; in mice polysyndactyly was shown to be caused by a 600 kb deletion affecting the same region.

In this study, the authors engineered alleles in mice that mimic the rearrangements of the first two described human diseases and used an existing mouse model of polydactyly. Hi-C and 4C techniques were used to study the long-range interaction changes among these allele variants, as well as to check patterns of expression in limbs of key genes associated to these diseases: *Pax-3* for brachydactyly, *Wnt6* for F-syndrome and *Ihh* for polydactyly. For each allele variant, there was a boundary loss of the *EPHA4*-containing TAD and each of the probed genes gained contact with a regulatory region within the *EPHA4*-containing TAD (Figure 1.3B). Concomitant with this ectopic interaction, was a change in expression pattern of *Pax-3*, *Wnt6* and *Ihh* in their respective disease alleles. Interestingly, this ectopic expression was highly similar to the pattern of expression of *Epha4* for all of them, suggesting that regulatory sequences governing the expression pattern of *Epha4* were aberrantly affecting the expression of the probed genes due to their gained interaction frequency with *Epha4* TAD. Remarkably, applying the same long-range interaction experiments to fibroblasts cells of limb malformation patients revealed the same ectopic interactions. Furthermore, the authors identified a small common region (around 150 kb) between all the ectopic interactions in both mouse and human and found a cluster of enhancers that interact with *EPHA4* promoter in wild-type conditions. Confirming the importance of the TAD boundary, similar deletion alleles of brachydactyly and mouse polydactyly were produced, in which the region containing a predicted TAD boundary element was left intact (100-200 kb). Leaving the TAD boundary intact was sufficient to prevent the formation of limb abnormalities. The genes retained their endogenous expression pattern and there were no ectopic interactions with the *EPHA4*-containing TAD. Clearly, this shows that chromatin architecture, defined by TAD boundaries, is implicated in the phenotypes of the disease. In other words, once TAD borders are disrupted, ectopic interactions arise and gene mis-expression occurs, triggering morphological limb defects. It remains an open question whether other developmental genes are regulated in a similar manner.

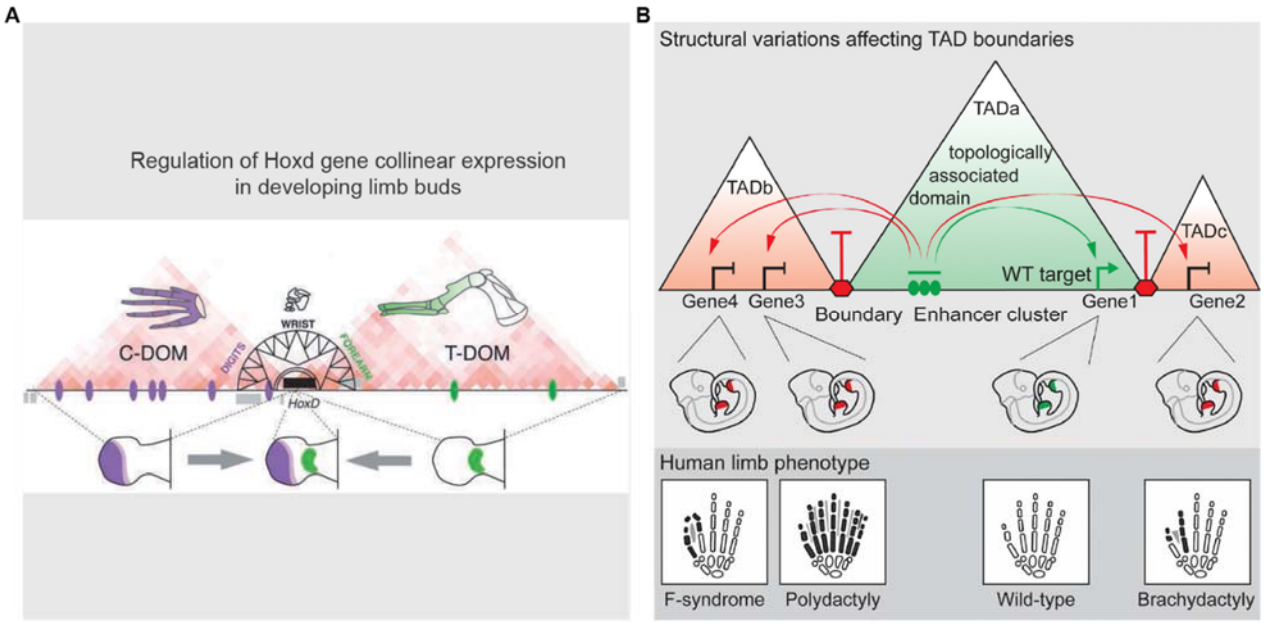

Figure 1.3. Involvement of TADs in the regulation of limb development. (A) Expression of the HoxD cluster during development of limbs involves the switch between two adjacent TADs. The telomere-proximal domain (T-DOM) regulates early transcription in the arm and forearm. The centromere-proximal domain (C-DOM) subsequently patterns the hands. During limb development, a switch occurs between landscapes as specific HoxD genes swing from one regulatory domain to the other through a conformational change. This modular organization creates a domain in-between, which will form the wrist. Image reprinted from (Andrey et al., 2013). (B) Disease-associated structural variants affecting TAD boundaries of the *EPHA4*-containing TAD (TADa), cause pathogenicity by acquiring ectopic interactions of gene promoters in TADb and TADc with the Enhancer cluster in TADa leading to altered gene expression. Gene1 = *EPHA4*, Gene2 = *PAX3*, Gene3 = *IHH*, Gene4 = *WNT6*. The different Enhancer-Gene*X* interactions lead to different malformation syndromes. Image reprinted from (Lupianez et al., 2015).

Spatial Segregation of Chromatin

A recurrent theme in nuclear organization is the spatial segregation of chromatin subtypes. Chromatin domains with high transcriptional activity are located in the nuclear center and in some cases associated with nuclear pores, while transcriptionally silent domains are associated with the nuclear periphery and the nucleolus. Although some differentiated cells such as those found in the rod photoreceptor cells of nocturnal rodents (Solovei et al., 2013) have an inverted nuclear organization, most cells from yeast to man have the conventional distribution of active and inactive domains. In the earliest stages of mammalian embryogenesis, cells are characterized by extensive chromatin remodeling, including dynamic changes in DNA methylation, histone variants and histone modifications (Fadloun et al., 2013). A rapid exchange of the core histones, H2A, H3.1, and H3.2, is seen in murine pre-implantation embryos, yet this is lost as cells transition from undifferentiated to more determined states (Boskovic et al., 2014). Unlike most somatic cells, pericentromeric major satellite sequences are initially localized around pre-nucleolar bodies and only later become clustered forming structures called chromocenters (Martin et al., 2006).

In mammals, the Barr body is one prominent structure inside the nucleus of female cells. It is localized mostly at the nuclear periphery or around the nucleolus, and contains the inactive copy of the X chromosome coated with the Xist long non-coding RNA and typical repressive histone marks of heterochromatin (DNA methylation on CG-rich promoters, Polycomb group and H3K27 and H3K9 methylation) (Brinkman et al., 2006). Inactivation of the X chromosome is needed for gene dosage compensation, as males have one X chromosome (XY) and females have two (XX). Many studies have addressed the mechanism that inactivate one X chromosome in female cells (Heard and Disteche, 2006) but the contribution of its spatial relocation remains unclear. Recently, it was described that depletion of the NE protein LBR (Lamin B Receptor) leads to an upregulation of genes on the inactive X, but no change in the position of the chromosome (McHugh et al., 2015). In contrast, the long non-coding RNA Firre was found to play a role in anchoring the inactive X to the nucleolus and maintaining the repressive H3K27me3 mark, but interestingly no gene reactivation was seen (Yang et al., 2015). Perhaps due to unchanged levels of H3K9 methylation the repressed status of the genes is unaltered, which was not tested in the mentioned study. It will be interesting to look for a factor that is required for the repositioning of the silent X towards the nuclear periphery at the very early points of inactivation, in order to understand its functional participation in the process.

Importantly, in the case of *C. elegans* the dosage compensation strategy is different, yet it is again linked to spatial nuclear organization. Hermaphrodites downregulate the expression of both copies of the X chromosome, to match the expression of the single X chromosome of males (Strome et al., 2014). Chromosome X in hermaphrodite worms is enriched for H3K27me1 in contrast to mammalian X chromosome which is enriched for H3K27me3; enrichment of H3K9 methylation happens only on the left arm of the chromosome. Even though the X chromosome modifications and dosage compensation strategy in nematodes differs from those in mammals, a molecular mechanism of perinuclear positioning and gene regulation of this chromosome has been proposed. It was shown that the X chromosome in males localizes to the nuclear periphery by interaction with nucleoporins, allowing an increase in X-linked gene expression (Sharma et al., 2014).

Another example of spatial segregation of chromatin is seen in *C. elegans* where tRNA clusters are expressed in proximity to nuclear pore proteins (Ikegami and Lieb, 2013). Stress-induced genes in particular, tend to co-localize with nuclear pores both prior to and after their induction, in organisms as diverse as yeast, flies and worms (Brickner and Walter, 2004; Dieppois et al., 2006; Kurshakova et al., 2007; Rohner et al., 2013). Therefore, one has to keep in mind that segregation of chromatin to the nuclear periphery can facilitate both activation and repression, and the outcome depends on the interactor partners at the nuclear periphery.

In addition, there have been reports of age-related changes in chromatin organization in human fibroblasts. Specifically, chromatin normally located at the nuclear periphery reorganized into foci and shifted to the nuclear center during senescence. Oncogene-induced senescence (OIS) is generated by activation of RAF1 kinase in the model system WI-38h (Jeanblanc et al., 2012) and is used as a model for aging related studies. The foci formed on OIS cells are called SAHF (senescence-associated heterochromatic foci) and are enriched for H3K9 methylation and HP1. Chandra et al. characterized the changes in chromatin organization by carrying out Hi-C on growing and senescence induced cells and observed a global change in chromatin interactions between the two cell types. Contrary to their

expectations, senescent cells had a reduction of local contacts in GC-poor LADs correlating with a loss of LMNB1 association, and a gain of new loci relocating to the nuclear periphery. As expected, the same LADs that lost local contacts, gained distal interactions being freer to interact in *trans*. Analyzing pre-senescent cells they observed that LADs that lose local contacts are first marked by a shift towards earlier replication timing. This suggests that replication, can trigger changes in chromatin organization (reviewed in Rhind and Gilbert, 2013). Finally, Progeria fibroblast (as another model for studying aging) and IOS cells shared only loss of local contacts in GC-poor LADs as a common feature, explaining that SAHF formation comes from the additional gain of distal contacts in OIS cells (Chandra et al., 2015).

The question remains, how do we reconcile the microscopy based observations of chromatin in the nucleus and the chromatin contacts measured by deep-sequencing molecular approaches? This major task will be the next required step to broaden our understanding in the functionality of nuclear organization. One has to keep in mind that microscopy based assays address single cell measurements and molecular methods are mostly based on cell populations, therefore the direct link between these approaches is not straightforward. The spatial organization of the genome involves a hierarchy of structures, from chromatin loops that connect genes with distal regulatory elements intra- or inter-chromosomally, to chromosome territories and then nuclear subcompartments (Figure 1.4). An interesting perspective of nuclear organization is reviewed in (Gibcus and Dekker, 2013). In any given cell, longer chromatin domains tend to be more stable within one cell cycle, but the pattern will not be reproduced in the subsequent cycle. In contrast, chromatin contacts between loops within TADs are variable within each cell cycle, but highly reproducible in the next cycle. Concluding that TADs are the chromatin units that confer chromatin organization in both directions, stability and reproducibility (Gibcus and Dekker, 2013). One would have to keep this in mind when trying to make the connection between the microscopy observations and the molecular approaches.

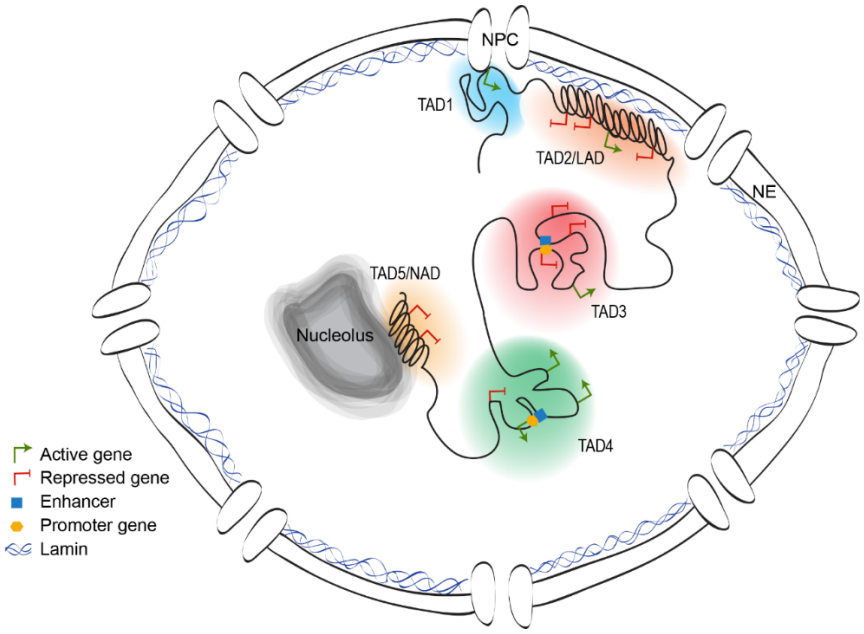

Figure 1.4. Schematic representation of the spatial segregation of chromatin inside the nucleus. TADs are units of chromatin in which long-range chromatin contacts occur – distal regulatory elements (Enhancers) interact with promoters to activate (green arrow) or repress (red arrow) genes. On

different scale, the nuclear lamina (represented by Lamin only) and the nucleolus serve as repressive nuclear compartments (TAD2/LAD and TAD5/NAD, respectively), repressed chromatin can also be found as foci in the nucleoplasm (TAD3). Active chromatin is generally found in the nucleoplasm (TAD4), but certain loci are also found actively expressed (TAD1) at nuclear pore complexes (NPC). NE – Nuclear envelope.

Spatial organization is seen across species and one distinctive feature is the enrichment of heterochromatin at the nuclear periphery. In the next section, I will discuss the emerging role of the nuclear periphery as a sub-compartment within the nucleus.

Tethering towards the nuclear lamina

Studies in organisms including yeast, worms, flies and mammals have been performed to understand the mechanism and function of the sequestration of chromatin to the nuclear periphery, although it is not fully understood yet. Below is a summary of experimental evidence of factors involved in chromatin tethering (across species) to create a broad picture and to asses our current level of understanding of the molecular mechanisms implicated in tethering.

The visualization of genetic loci in living cells by time-lapse microscopy has shown that chromatin undergoes constant Brownian-like motion in the nucleus within restricted domains (Heun et al., 2001; Marshall et al., 1997). Interestingly, silent genes that are associated with the nuclear periphery are more constrained in their movement than active genes in the nuclear center (Chubb et al., 2002; Hediger et al., 2002; Heun et al., 2001). This suggests that genes at the nuclear periphery could be molecularly tethered, albeit in a reversible manner, to a relatively immobile nuclear landmark structure. The radial distribution of chromatin subtypes change significantly during cell differentiation. This altered positioning can be observed during physiological events, such as mammalian hematopoiesis (Brown et al., 2001; Hubner et al., 2015; Kosak et al., 2007; Ugarte et al., 2015) or *C. elegans* development (Fakhouri et al.; Meister et al., 2010) and with induction of neuronal cell types from pluripotent ES cells (Dixon et al., 2015; Peric-Hupkes et al., 2010; Williams et al., 2006). While all cells of an organism contain the same DNA sequence, it is the expression of cell-type specific genes at the appropriate time that determines cell fate and function. Given that gene activity depends on transcription factor availability, histone modification and local chromatin structure (Chen and Dent, 2014; Gomez-Diaz and Corces, 2014), the inner nuclear membrane (INM) sequestration of promoters might impact these factors, or impose an added layer of regulation.

Heterochromatin is enriched in repressive histone modifications including, H3K9me2 and me3. Distribution of H3K9me2 and me3 changes with the establishment of differentiated cell states. Furthermore, the differentiation of stem cells was shown to be dependent on G9a, the H3K9 methyltransferase responsible for mono- and di-methylation (Ugarte et al., 2015). Another study reported an increase in levels of H3K9me2 during ESC differentiation, and the concurrent formation of “large domains of chromatin bearing H3K9-modifications” or LOCKs (Wen et al., 2009). In contrast, Lienert et al. found that the total level of H3K9me2 was stable during the transition from ESC to differentiated neurons, although they scored

changes at specific promoters (Lienert et al., 2011). While these varied conclusions may stem from different modes of quantitation (Filion and van Steensel, 2010; Hu et al., 2012), it is clear that methylation of H3K9 correlates with enhanced efficiency in reprogramming cell fate (Bao et al., 2015; Baxter et al., 2004; Chen et al., 2013; Sridharan et al., 2013). Indeed, independent of its level, the subnuclear distribution of H3K9me3 changes as cells differentiate, as was particularly well documented during rodent development (Solovei et al., 2009; Solovei et al., 2013). Additionally, down-regulation of both PRDM3 and PRDM16 (two H3K9-specific mono-methyltransferases) led to loss of H3K9me1, which precluded higher levels of H3K9 methylation. This alteration lead to dispersal of centromeric foci, accumulation of major satellite transcripts, and perturbed the ultrastructure of the nuclear lamina (Pinheiro et al., 2012), further implicating H3K9 methylation as an important signal on chromatin for nuclear organization. It is important to note that centromeric foci are not necessarily lamin-associated, yet there may be secondary effects from the loss of one heterochromatic structure what would impact on other chromatin domains, leading to disruption of overall chromatin organization. Alternatively, the loss of one heterochromatin compartment may feedback to influence the integrity of the lamin/LAD compartment, generating the described phenotypes indirectly.

The major ligand of H3K9 methylation is HP1, which has at least three isoforms in mammalian cells (HP1α, HP1ß and HP1γ) and two in *C. elegans* (HPL-1 and HPL-2) and *S. pombe* (Chp2 and Swi6) . All HP1 proteins contain an N-terminal chromodomain and a C-terminal chromo-shadow domain. The chromodomain specifically recognizes both H3K9me2 and me3 (Lachner et al., 2001; Nielsen et al., 2002), while the chromo-shadow domain mediates interaction with other proteins. The spacer region between the two domains binds RNA in fission yeast (Keller et al., 2012). Intriguingly, different HP1 variants have very distinct roles in the ESC-to-differentiated cell transition, and not all HP1 binding correlates with heterochromatic gene repression (Mattout et al., 2015). Furthermore, the residence time of HP1 on chromatin is very short (Cheutin et al., 2003) and in *S. pombe* its RNA binding functions are associated with the restricted spread of silent domains (Keller et al., 2013; Stunnenberg et al., 2015). Although, HP1 seems to be a good candidate for the association of heterochromatin to the nuclear periphery, its direct involvement is still not clear.

From the nuclear envelope perspective, the nuclear lamina is presented as a platform for chromatin tethering. The nuclear lamina is composed of integral INM proteins including LAP2, Emerin and MAN1 (the so-called LEM proteins) and nuclear lamins; and is present in all eukaryotes that undergo open mitosis. The mechanisms by which chromatin is tethered to it are still poorly defined (reviewed in Kind and van Steensel, 2010; Meuleman et al., 2013; Wilson and Berk, 2010). Below we describe some nuclear lamina components and their implication on chromatin tethering.

Lamins interact directly with histones and DNA *in vitro* (Goldberg et al., 1999; Luderus et al., 1992). Although it is unclear if these low affinity interactions are relevant *in vivo*, the role of lamins as a scaffold for perinuclear chromatin is supported by genetic data. Loci that were preferentially NE-associated relocated to the nuclear center upon the depletion of lamins (Mattout et al., 2011; Shevelyov et al., 2009; Towbin et al., 2010). Additionally, reduction of Lamin B1 in cultured cells was shown to alter positional chromatin organization (Malhas et al., 2007; Shimi et al., 2008). Lamin A/C has also been implicated in large scale chromatin organization (McCord et al., 2013; Solovei et al., 2013), yet mutations that

interfere with the recognition of a specific chromatin motif have not been reported. Indeed, it is likely that lamins affect chromatin positioning by altering the stability or spatial organization of lamin-associated proteins, like LEM domain proteins, LBR, and many other inner nuclear membrane proteins (Wilson and Foisner, 2010).

Two important studies have helped in our understanding of the involved of lamin together with other factors, in chromatin tethering to the nuclear periphery. Solovei et al. focused on a generalized mechanism of heterochromatin anchoring in different tissues throughout development and found anchoring to be dependent on Lamin A/C and LBR (Lamin B Receptor) (Solovei et al., 2013). Harr et al. focused on specific loci contained at the border of LADs and implicated H3K9me2/me3, H3K27me3 and the transcription factor YY1 to be involved (Harr et al., 2015) (Figure 1.5).

In the extensive study by Solovei et al., changes in heterochromatin position and gene expression were observed and correlated with alterations in NE composition in mammalian cells. In rod cells of the nocturnal rodent retina, which lack both LBR and Lamin A/C proteins, heterochromatin is positioned at the center of the nuclei. Surprisingly, the ectopic expression of LBR was sufficient to change heterochromatin localization to the nuclear periphery. Throughout a range of differentiated tissues, it was shown that LBR and Lamin A/C are differentially and often sequentially expressed, changing the patterns of genes that are tethered at the NE. Indeed, in myogenic cells the mutation of either LBR or of Lamin A/C had opposite effects on the expression of muscle-related genes during differentiation into myoblasts: loss of LBR caused gene up-regulation while loss of Lamin A/C led to down-regulation of the same subset of genes. This effect was not seen in differentiated muscle cells. These observations reinforce the potential of chromatin organization at the nuclear periphery as a means to regulate gene expression and drive differentiation. The work of Solovei et al. argues that the sequestration of heterochromatin at the NE in differentiating tissues relies on partly redundant systems requiring Lamin A/C on one hand, and LBR on the other. The authors propose a mechanism whereby LBR mediates peripheral chromatin localization during early development, while lamin A/C become more important as cells terminally differentiate (Solovei et al., 2013). However, depletion of any one of these factors, is accompanied by pleiotropic effects due to additional functions exerted by the proteins on various aspects of nuclear metabolism, rendering difficult to assess the functionality of chromatin anchoring *per se*. Another question that remained was related to the specificity of anchoring by each tethering pathway. LBR contains a Tudor domain that binds histone H4K20me2 (Hirano et al., 2012). This affinity could contribute to a developmentally controlled positioning of facultative heterochromatin, yet this histone modification is distributed broadly across the genome without significant enrichment in LADs (Barski et al., 2007). This does not exclude that in some situations, LBR-H4K20me2 interaction supports chromatin sequestration, but it is clear that this would depend on other marks or secondary interaction domains, given its broad distribution. Lamin A/C apparently requires additional proteins or factors to interact with chromatin, which in some tissues may be transcription factors or RNA Pol II regulatory complexes. LBR was also reported to bind HP1α and HP1γ (Ye and Worman, 1996). While this sounds promising, HP1α-containing chromocenters are not necessarily perinuclear and HP1γ is bound to many non-peripheral euchromatic loci (Minc et al., 1999). Moreover, ablation of HP1α or HP1β in pluripotent or differentiated embryonic stem cells did not alter pericentric heterochromatin organization (Mattout et al.,

2015). Further studies will be required to elucidate the exact mechanisms of tethering dependent on LBR and Lamin A/C.

In the study directed to elucidate the mechanisms of anchoring in mammalian cells for specific loci, Harr et al. focused on the borders of specific LADs, which are enriched for genes that are repressed in a cell-type dependent manner and are critical for cell fate determination, called variable LADs (vLADs) (Harr et al., 2015; Peric-Hupkes et al., 2010). Whereas a number of mammalian cell studies have investigated the positioning of repetitive reporters, the system used by the Reddy laboratory instead scored for unique sequences that trigger relocation to the nuclear periphery. The targeting sequences were introduced adjacent to a repetitive lacO array, which was shown to carry H3K9me2/3. In this case, however, K9 modification was not sufficient for perinuclear localization, at least in differentiated murine fibroblasts. In these fibroblasts, single integrated sequences derived from vLAD-specific DNA shifted the reporter to the INM (Harr et al., 2015; Harr and Reddy, 2015). The relocation function was reduced upon knockdown of the H3K9 methylation-depositing histone methyl transferase (HMT), SUV39H1, or by treatment with a G9a inhibitor, which also reduces H3K9 methylation. Similarly, Belmont and colleagues showed that the peripheral positioning of a randomly integrated ß-globin locus was dependent on both Suv39H-mediated H3K9me3 and G9a-mediated H3K9me2 (Bian et al., 2013). G9a inhibition had effects on endogenous sequences as well, reducing the association of LADs with the INM genome-wide (Kind et al., 2013). Finally, reduction in components of the PRC2 (Polycomb Repressive Complex 2), the H3K27 methyltransferase, and/or treatment with specific inhibitors, led to similar reductions in the perinuclear positioning vLADs (Harr et al., 2015). The question arose as to what might recruit PRC2 to vLADs, and therefore YY1, a transcription factor known to interact with PRC2 (Basu et al., 2014; Satijn et al., 2001; Srinivasan and Atchison, 2004; Wilkinson et al., 2010), was targeted to the reporter sequence. Targeted YY1 led to high levels of H3K27me3 on the tagged chromatin and enhanced its association with the INM (Harr et al., 2015). Relocation was reduced upon inhibition of the PRC2 catalytic subunit, EZH2, implicating H3K27 methylation in the process. FISH studies confirmed that the localization of vLAD-associated cell-type specific genes at the INM were sensitive to EZH2 inhibition in fibroblasts (Harr et al., 2015). It is interesting that YY1 is a transcription factor not particularly enriched at the periphery but rather dispersed throughout the nucleus, pointing out to the complexity that for specific loci, factors that are not necessarily enriched at the periphery do play a role in their positioning. Still, the extent of this mechanism to other loci remains to be studied. Are there other specific types of transcription factors, like YY1, regulating gene expression at the nuclear periphery?

In the case of LEM proteins, Emerin and MAN-1 act redundantly in the anchoring of heterochromatic arrays and endogenous chromatin in *C. elegans*. Both were associated with repression of muscle and nervous system function related genes, yet only Emerin was shown to impact the activity of neuromuscular junctions (Gonzalez-Aguilera et al., 2014; Mattout et al., 2011). In mouse fibroblasts, LAP2ß was shown to play a role in the silencing and association of the developmentally regulated IgH and Cyp3a loci to the nuclear periphery. Importantly, the association was also dependent on a sequence-specific motif found in these loci, the transcription factor cKrox, and HDAC3 (histone deacetylase 3) (Zullo et al., 2012). This shows a combinatorial effect of sequence-specific motifs and histone modifications in the positioning of genes towards the nuclear periphery, yet it is not a generalized mechanism.

Barrier to Autointegration Factor (BAF) can be found at the nuclear periphery due to its associations with DNA, certain histones, LEM proteins, Lamin A, and certain transcription factors (Margalit et al., 2007). It has been suggested that BAF is the link between chromatin and the nuclear periphery thanks to its multiple interactions at the nuclear lamina, though the specificity of this binding to heterochromatin remains unclear, since it has also been shown to associate with active histone marks (Montes de Oca et al., 2011).

Samp1 is an INM protein connected to LINC (linker of nucleoskeleton and cytoskeleton) complexes, and was shown in HeLa cells to have an impact on heterochromatin localization. However, the Samp1 dominant negative mutant compromised nuclear integrity and mislocalized nuclear lamina proteins such as Emerin, Sun-1 and LaminA/C, making it difficult to understand if the effect is direct or indirect (Gudise et al., 2011). Another example in HeLa cells is the PRR14 (PRoline-Rich protein 14) protein, which was shown to localize at the nuclear periphery, interact with lamin and bind HP1α at the onset of anaphase to promote chromatin re-tethering after mitosis. Depletion of this factor caused defects in nuclear structure, and partial loss of perinuclear attachment of H3K9 methylated chromatin (Poleshko et al., 2013). To date, PPR14 is the only example where there is a clear bridge of nuclear lamina and H3K9 methylated chromatin through binding of HP1. Further studies of PPR14 expression in different cell types are needed to understand its physiological implications; although its intrinsic impact on nuclear structure might bring difficulties in the conclusions related to anchoring function alone.

In addition to the above mentioned INM associated proteins and their potential roles in regulation of nuclear organization, the INM proteome is very complex, containing over 100 different proteins that are cell-type specific (Malik et al., 2010; Wong et al., 2014). Overexpression of 5 Nuclear Envelope Transmembrane (NET) proteins (NET5, NET29, NET39, NET45 and NET47), led to a dramatic shift of chromosome 5 towards the nuclear periphery in fibroblast cells where is normally internal. These proteins are differentially expressed in a tissue specific manner. NET45 and NET47 are preferentially expressed in liver cells coincidental with a peripheral position of chromosome 5. Depletion of any of these two NETs resulted in a shift towards an internal position for this specific chromosome (Zuleger et al., 2013). Unfortunately the impact of this reorganization in gene control or other effect remains to be studied, as well as the mechanism by which these NETs recognize specific chromosomes.

The apparent redundancy in tethering mechanisms and the high number of INM proteins suggests that the answers of mechanism and functionality of tethering to the nuclear periphery, will not be as straight forward as one would expect, particularly in mammalian systems (de Las Heras and Schirmer, 2014; Wong et al., 2014). Many studies have implicated specific histone modifications in this process and this suggests they are a common denominator in this process. Further research to understand the combinatorial factors and tissue specific roles will be required to decipher the mechanism and functional relevance of perinuclear sequestration.

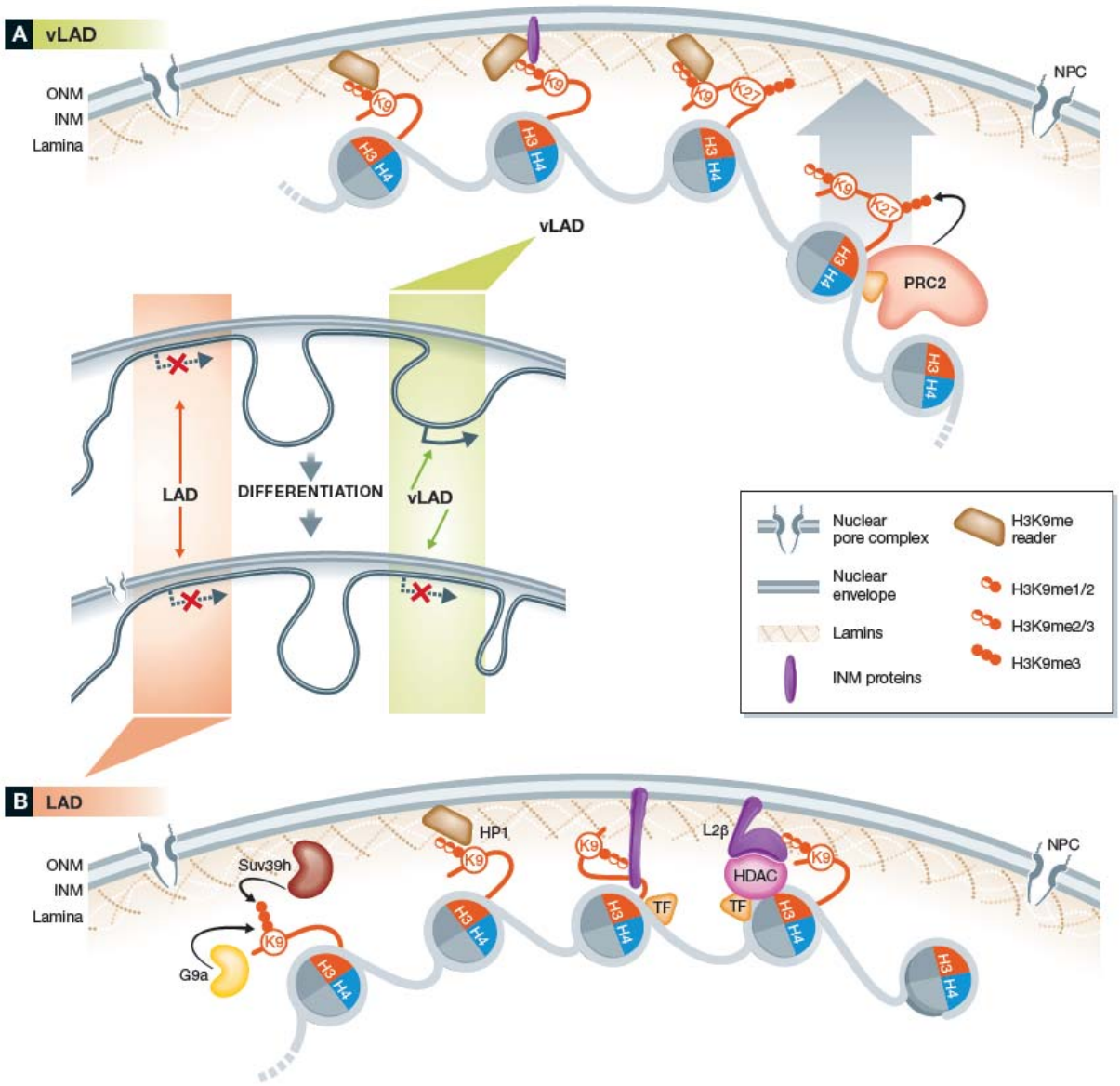

Figure 1.5. Anchoring chromatin to the nuclear periphery in mammalian cells. (A) vLAD anchoring mechanisms. Borders of vLADs are enriched for both H3K9me2 and H3K27me3 and shift to the nuclear periphery in a manner dependent on PRC2 activity as well as on Suv39H1 and G9a. (B) Mechanisms implicated in the anchoring of constitutive/common LADs. They depend on H3K9 methylation deposited by G9a and Suv39h and involve ligands which may include HP1 and other unknown methylation readers. Transcription factor interactions with INM proteins, such as the cKrox/HDAC3/Lap2ß bridge, may also be relevant for tissue-specific LADs. Image reprinted from (Harr et al., 2016).

The last section of this introduction is dedicated to discussing a mechanism of tethering identified in *C. elegans* due to its importance for the work presented in this thesis.

PERINUCLEAR CHROMATIN SEGREGATION VIA H3K9 METHYLATION IN *C. ELEGANS*

C. elegans has been used effectively to examine the impact of nuclear organization on gene expression during differentiation (reviewed in Meister et al., 2011; Meister and Taddei, 2013). Using LacI/lacO tagged integrated arrays bearing tissue-specific promoters, Meister et al. successfully demonstrated a role for promoter-bound factors in the subnuclear positioning of developmentally regulated genes (Meister et al., 2010). Several developmentally regulated promoters, including muscle specific, intestine specific and neuronal specific ones, were analyzed for cell-type specific subnuclear organization during development. In early embryos, small transgenes bearing inactive tissue-specific promoters were found to be randomly distributed throughout the nucleus. Over the course of differentiation, a spatial segregation of the transgenes was observed, which depended strictly on the transcriptional status of the promoter. Inactive promoters shifted to the nuclear periphery, while active promoters were sequestered internally, in differentiated tissues (Meister et al., 2010). This was not true in the relatively undifferentiated nuclei of early embryos, where only very large arrays carrying 300-500 copies of either housekeeping or tissue-specific promoters, were found at the NE (Towbin et al., 2010). These large arrays carry marks typical for heterochromatin, including histone H3K9 and H3K27 methylation , in a manner dependent on the number of repeats (50 were insufficient, while 250 were enough to generate a heterochromatic state) (Towbin et al., 2010). Nonetheless, the activation of a tissue-specific promoter could overcome the anchoring of the repressed arrays. Indeed, several lines of evidence argue that the internal shift of developmentally regulated genes depends on factors that bind the relevant promoters, driving gene activation.

A genome-wide RNAi screen was carried out using these large *C. elegans* gene arrays to identify the mechanisms that link heterochromatin to the INM. Whereas loss of various chromatin modifiers led to a loss of transcriptional repression, only one RNAi target released the array from the nuclear periphery. This RNAi target was a pair of closely related genes that encode S-adenosyl methionine synthetase (SAMS – *sams-3* and *sams-4*). Loss of these enzymes reduced histone methylation globally, leading to both transcriptional up-regulation and the release of the array from the NE. Many other RNAi clones led to derepression without affecting localization, underscoring the fact that peripheral anchoring is not sufficient to silence. A second targeted screen was performed to identify the relevant HMTs necessary for array attachment at the NE. The screen tested 12 single and double mutants' combinations of putative HMTs in *C. elegans*. The majority of the different mutants were defective in array silencing, but not in array anchoring. Only the combined elimination of two HMTs, MET-2 and SET-25 showed that heterochromatic arrays were released as efficiently as in a SAMS-3/-4 knockdown. MET-2 is the worm homolog of human SetDB1/ESET, while the catalytic domain of SET-25 is human G9a-like. The former experiments, together with mass spectroscopy analysis of the histone methylation status in single and double mutants, allowed one to conclude that (1) both HMTs target specifically lysine 9 of histone H3, (2) H3K9me1 and -me2 are sufficient for array anchoring, and H3K9me3 as well can mediate this contact, (3) and finally that the trimethylated state was needed for transcriptional silencing (Towbin et al., 2012). Since chromatin bearing H3K9me1 and me2 was not repressed, one can conclude that the level of H3K9 methylation distinguishes a perinuclear anchoring signal from transcriptional repression, even though they are on the same methylation pathway.

To understand the orchestration of how a heterochromatin subcompartment can be formed, strains were created that expressed either MET-2 or SET-25 fused to the red fluorescent protein mCherry. Interestingly, MET-2 was enriched in the cytoplasm, where it appears to act on cytoplasmic histones, prior to their incorporation into chromatin. Such an activity has previously been described for a human homolog of MET-2 (ESET/SetDB1) (Andersen and Horvitz, 2007; Bessler et al., 2010). In contrast to MET-2, mCherry::SET-25 was located in the nucleus and formed foci. These foci were enriched at the NE and co-localized with transgene arrays. A version of SET-25 that lacked its catalytic domain was still able to interact with peripheral heterochromatin, although its binding required that H3K9me3 had been deposited (for example, by an intact SET-25 molecule). Thus, SET-25 is recruited to the nuclear periphery by its affinity for chromatin carrying H3K9me3, which is the mark that this HMT uniquely deposits. It does not get sequestered by H3K9me1 or me2, although exactly how it recognizes the mark is unknown, as SET-25 does not contain a canonical me-lysine recognition domain. Sequestration of SET-25 at the NE is proposed to help ensure the faithful establishment and/or maintenance of the silent state (Towbin et al., 2012) (Figure 1.6). It remained unresolved what component of the nuclear lamina recognizes the H3K9me1, me2 or me3 marks, and whether it is one or several proteins that tether the modified histones. The binding of HP1 homologue (HPL-2) and/or LIN-61, an MBT (Malignant Brain Tumor) domain protein that also recognizes H3K9me2/me3, can repress transcription but neither is involved directly in anchorage of the H3K9metylated chromatin (Koester-Eiserfunke and Fischle, 2011; Towbin et al., 2012). Downregulation of HPL-1 also affects transcription of endogenous loci, but is not sufficient to derepress the transgenic array, and it also does not appear to be essential for silent chromatin anchoring at the NE (Studencka et al., 2012; Towbin et al., 2012).

Importantly, we note that although H3K9 methylation is essential for anchoring in early *C. elegans* embryos, this pathway is not the only heterochromatin-anchoring mechanism functioning in worms. At later developmental stages, such as the first larval stage, when most cells have acquired a cell-type specific pattern of gene expression and morphology, sequences that were released from the INM in H3K9-methylation deficient embryos became re-anchored, although H3K9 methylation remains absent (Towbin et al., 2012). Thus, alternative pathways for heterochromatin anchoring are induced during terminal differentiation, perhaps explaining the unexpected finding that *C. elegans* embryos lacking all histone H3K9 methylation still develop into adult worms with the full range of differentiated tissues. One pathway that has already been characterized is the anchorage of *C. elegans* telomeric repeats (Ferreira et al., 2013). These repeats are anchored at the nuclear envelope and become increasingly peripheral in terminally differentiated cells. Their anchorage is not dependent on H3K9 methylation, but requires a factor that recognizes the ss telomeric overhang (POT-1) and an inner nuclear membrane SUN domain protein, SUN-1. The interaction is also affected by sumoylation, reminiscent of telomere anchoring in budding yeast (Ferreira et al., 2011; Ferreira et al., 2013).

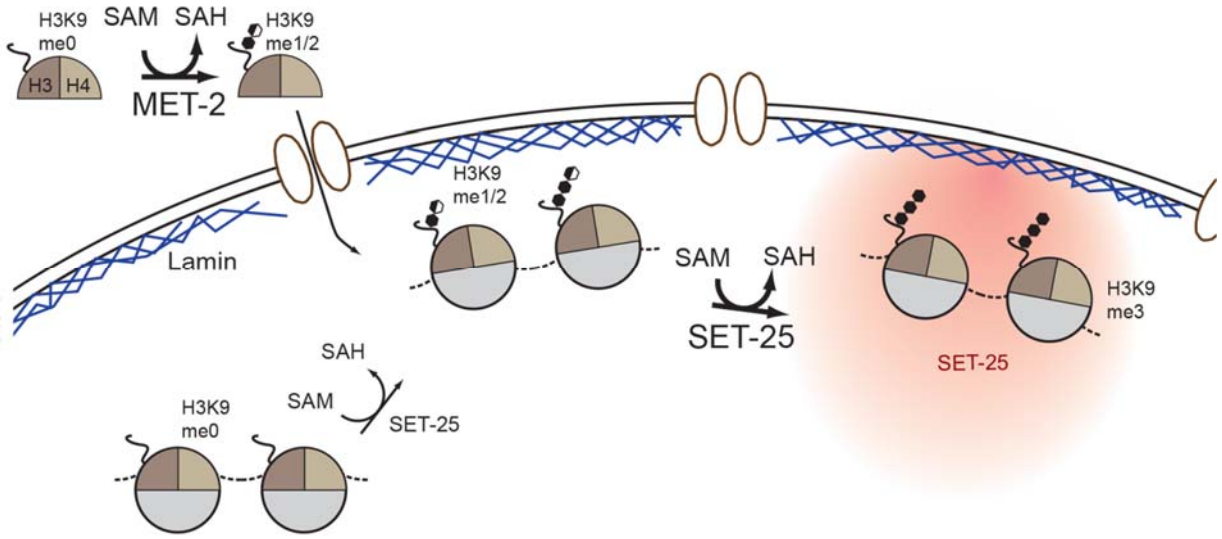

Figure 1.6. A self-reinforcing mechanism for perinuclear anchoring and silencing of heterochromatin. The step-wise establishment of H3K9me3 involves deposition of H3K9me1/2 by cytoplasmic MET-2 prior to nucleosome assembly, and trimethylation by nuclear foci-associated SET-25. H3K9me1/2 initiates perinuclear chromatin targeting, and H3K9me3 is needed for complete array silencing and enhanced attachment. SET-25 requires its own reaction product, H3K9me3, to accumulate in perinuclear foci. Image reprinted from (Towbin et al., 2012).

SCOPE OF THESIS PROJECT

Despite the progress made in identifying different components at the nuclear periphery which help anchor chromatin (in many cases redundantly), for most of these factors the specificity of their interaction with chromatin remained undemonstrated. As mentioned above for lamins, some factors may indirectly influence chromatin association by perturbing the localization or stability of other tethers. The fact that some of these related anchoring factors are known to have additional functions besides chromatin anchorage, complicates the study of chromatin sequestration function.

Knowing that H3K9 methylation is required for anchoring of *C. elegans* heterochromatin in embryos (Towbin et al., 2012), we used a genetic approach to identify H3K9 methylation readers that would function as tethers of heterochromatin to the nuclear periphery.

Chapter 2 describes the work done with the goal of identifying this type of anchor protein in *C. elegans* embryos. In particular, we utilized RNAi to down-regulate each gene containing a potential histone methylation binding domain, based on characterized binding motif. We next scanned for the loss of perinuclear position of an integrated high-copy number array that is fluorescently tagged by GFP-LacI (Meister et al., 2010). We identified an undescribed chromodomain protein, CEC-4, as a positive hit for array de-localization and went on to characterize it molecularly using cell biology and functionally by assaying its effects on transcription, development and cell-type stability under conditions of induced cell fate. Our data show that in *C. elegans* early embryos the perinuclear chromodomain protein CEC-4 directly binds endogenous H3K9me-containing chromatin and anchors it to the nuclear periphery. *In vitro*, the CEC-4 chromodomain recognizes me1-, me2- and me-3 K9 in a histone

H3 peptide, with equal affinity. Remarkably, CEC-4 is not necessary for transcriptional silencing of endogenous genes nor of our heterochromatic array, whereas methylation of H3K9 is. Lack of CEC-4 presents no visually obvious phenotype on the life cycle of worms. Nevertheless, CEC-4 is needed for the stable commitment of embryos to a forced induction of muscle specification, unveiling potential chromatin anchoring contribution to cell fate commitment.

Chapter 3 describes additional characterization of *cec-4* null mutant worms, our attempts to understand the localization of perinuclear localization of CEC-4, as well as trial experiments to understand the relationship between known factors related to H3K9 and loss of anchoring.

Chapter 4 summarizes conclusions from the thesis project and indicates future directions that will help us understand the relevance of nuclear organization.

REFERENCES

Akhtar, A., and Gasser, S.M. (2007). The nuclear envelope and transcriptional control. Nat Rev Genet *8*, 507-517.

Akhtar, W., de Jong, J., Pindyurin, A.V., Pagie, L., Meuleman, W., de Ridder, J., Berns, A., Wessels, L.F., van Lohuizen, M., and van Steensel, B. (2013). Chromatin position effects assayed by thousands of reporters integrated in parallel. Cell *154*, 914-927.

Andersen, E.C., and Horvitz, H.R. (2007). Two *C. elegans* histone methyltransferases repress *lin-3* EGF transcription to inhibit vulval development. Development *134*, 2991-2999.

Andrey, G., Montavon, T., Mascrez, B., Gonzalez, F., Noordermeer, D., Leleu, M., Trono, D., Spitz, F., and Duboule, D. (2013). A switch between topological domains underlies HoxD genes collinearity in mouse limbs. Science *340*, 1234167.

Andrulis, E.D., Neiman, A.M., Zappulla, D.C., and Sternglanz, R. (1998). Perinuclear localization of chromatin facilitates transcriptional silencing. Nature *394*, 592-595.

Bao, X., Wu, H., Zhu, X., Guo, X., Hutchins, A.P., Luo, Z., Song, H., Chen, Y., Lai, K., Yin, M., *et al.* (2015). The p53-induced lincRNA-p21 derails somatic cell reprogramming by sustaining H3K9me3 and CpG methylation at pluripotency gene promoters. Cell research *25*, 80--92.

Barski, A., Cuddapah, S., Cui, K., Roh, T.-Y., Schones, D.E., Wang, Z., Wei, G., Chepelev, I., and Zhao, K. (2007). High-resolution profiling of histone methylations in the human genome. Cell *129*, 823--837.

Basu, A., Wilkinson, F.H., Colavita, K., Fennelly, C., and Atchison, M.L. (2014). YY1 DNA binding and interaction with YAF2 is essential for Polycomb recruitment. Nucleic acids research *42*, 2208--2223.

Baxter, J., Sauer, S., Peters, A., John, R., Williams, R., Caparros, M.-L., Arney, K., Otte, A., Jenuwein, T., Merkenschlager, M., *et al.* (2004). Histone hypomethylation is an indicator of epigenetic plasticity in quiescent lymphocytes. The EMBO journal *23*, 4462--4472.

Berger, A.B., Cabal, G.G., Fabre, E., Duong, T., Buc, H., Nehrbass, U., Olivo-Marin, J.C., Gadal, O., and Zimmer, C. (2008). High-resolution statistical mapping reveals gene territories in live yeast. Nat Methods *5*, 1031-1037.

Bessler, J.B., Andersen, E.C., and Villeneuve, A.M. (2010). Differential Localization and Independent Acquisition of the H3K9me2 and H3K9me3 Chromatin Modifications in the *Caenorhabditis elegans* Adult Germ Line. PLoS Genet *6*, e1000830.

Bian, Q., Khanna, N., Alvikas, J., and Belmont, A.S. (2013). beta-Globin cis-elements determine differential nuclear targeting through epigenetic modifications. J Cell Biol *203*, 767-783.

Bickmore, W.A., and van Steensel, B. (2013). Genome architecture: domain organization of interphase chromosomes. Cell *152*, 1270-1284.
Boskovic, A., Eid, A., Pontabry, J., Ishiuchi, T., Spiegelhalter, C., Raghu Ram, E.V., Meshorer, E., and Torres-Padilla, M.E. (2014). Higher chromatin mobility supports totipotency and precedes pluripotency in vivo. Genes Dev *28*, 1042-1047.
Brickner, J.H., and Walter, P. (2004). Gene Recruitment of the Activated INO1 Locus to the Nuclear Membrane. PLoS Biology *2*, e342.
Brinkman, A.B., Roelofsen, T., Pennings, S.W., Martens, J.H., Jenuwein, T., and Stunnenberg, H.G. (2006). Histone modification patterns associated with the human X chromosome. EMBO Rep *7*, 628-634.
Brown, K.E., Amoils, S., Horn, J.M., Buckle, V.J., Higgs, D.R., Merkenschlager, M., and Fisher, A.G. (2001). Expression of [alpha]- and [beta]-globin genes occurs within different nuclear domains in haemopoietic cells. Nat Cell Biol *3*, 602.
Casolari, J.M., Brown, C.R., Komili, S., West, J., Hieronymus, H., and Silver, P.A. (2004). Genome-wide localization of the nuclear transport machinery couples transcriptional status and nuclear organization. Cell *117*, 427-439.
Chandra, T., Ewels, P.A., Schoenfelder, S., Furlan-Magaril, M., Wingett, S.W., Kirschner, K., Thuret, J.Y., Andrews, S., Fraser, P., and Reik, W. (2015). Global reorganization of the nuclear landscape in senescent cells. Cell Rep *10*, 471-483.
Chen, B., Gilbert, L.A., Cimini, B.A., Schnitzbauer, J., Zhang, W., Li, G.-W., Park, J., Blackburn, E.H., Weissman, J.S., Qi, L.S.*, et al.* (2013). Dynamic imaging of genomic loci in living human cells by an optimized CRISPR/Cas system. Cell *155*, 1479--1491.
Chen, M., and Gartenberg, M.R. (2014). Coordination of tRNA transcription with export at nuclear pore complexes in budding yeast. Genes Dev *28*, 959-970.
Chen, T., and Dent, S.Y.R. (2014). Chromatin modifiers and remodellers: regulators of cellular differentiation. Nature reviews Genetics *15*, 93--106.
Cheutin, T., McNairn, A.J., Jenuwein, T., Gilbert, D.M., Singh, P.B., and Misteli, T. (2003). Maintenance of stable heterochromatin domains by dynamic HP1 binding. Science (New York, NY) *299*, 721--725.
Chubb, J.R., Boyle, S., Perry, P., and Bickmore, W.A. (2002). Chromatin motion is constrained by association with nuclear compartments in human cells. Curr Biol *12*, 439-445.
Ciabrelli, F., and Cavalli, G. (2015). Chromatin-driven behavior of topologically associating domains. J Mol Biol *427*, 608-625.
Comings, D.E. (1980). Arrangement of chromatin in the nucleus. Human Genetics *53*.
Cote, J., Quinn, J., Workman, J.L., and Peterson, C.L. (1994). Stimulation of GAL4 derivative binding to nucleosomal DNA by the yeast SWI/SNF complex. Science *265*, 53-60.
Cremer, M., von Hase, J., Volm, T., Brero, A., Kreth, G., Walter, J., Fischer, C., Solovei, I., Cremer, C., and Cremer, T. (2001). Non-random radial higher-order chromatin arrangements in nuclei of diploid human cells. Chromosome Res *9*, 541-567.
de Las Heras, J.I., and Schirmer, E.C. (2014). The nuclear envelope and cancer: a diagnostic perspective and historical overview. Adv Exp Med Biol *773*, 5-26.
de Wit, E., and de Laat, W. (2012). A decade of 3C technologies: insights into nuclear organization. Genes Dev *26*, 11-24.
Dekker, J., Rippe, K., Dekker, M., and Kleckner, N. (2002). Capturing Chromosome Conformation. Science *295*, 1306-1311.
Dieppois, G., Iglesias, N., and Stutz, F. (2006). Cotranscriptional Recruitment to the mRNA Export Receptor Mex67p Contributes to Nuclear Pore Anchoring of Activated Genes. Mol Cell Biol *26*, 7858-7870.

Dixon, J.R., Jung, I., Selvaraj, S., Shen, Y., Antosiewicz-Bourget, J.E., Lee, A.Y., Ye, Z., Kim, A., Rajagopal, N., Xie, W.*, et al.* (2015). Chromatin architecture reorganization during stem cell differentiation. Nature *518*, 331-336.
Dixon, J.R., Selvaraj, S., Yue, F., Kim, A., Li, Y., Shen, Y., Hu, M., Liu, J.S., and Ren, B. (2012). Topological domains in mammalian genomes identified by analysis of chromatin interactions. Nature *485*, 376-380.
Dobzhansky, T. (1936). Position effects on genes. Biological Reviews Cambridge Philosophical Society *11*, 364-384.
Duan, Z., Andronescu, M., Schutz, K., McIlwain, S., Kim, Y.J., Lee, C., Shendure, J., Fields, S., Blau, C.A., and Noble, W.S. (2010). A three-dimensional model of the yeast genome. Nature *465*, 363-367.
Egecioglu, D., and Brickner, J.H. (2011). Gene positioning and expression. Curr Opin Cell Biol *23*, 338-345.
Fadloun, A., Eid, A., and Torres-Padilla, M.E. (2013). Mechanisms and dynamics of heterochromatin formation during mammalian development: closed paths and open questions. Curr Top Dev Biol *104*, 1-45.
Fakhouri, T.H.I., Stevenson, J., Chisholm, A.D., and Mango, S.E. Dynamic Chromatin Organization during Foregut Development Mediated by the Organ Selector Gene PHA-4/FoxA. PLoS Genet *6*, e1001060.
Ferreira, H.C., Luke, B., Schober, H., Kalck, V., Lingner, J., and Gasser, S.M. (2011). The PIAS homologue Siz2 regulates perinuclear telomere position and telomerase activity in budding yeast. Nat Cell Biol *13*, 867-874.
Ferreira, H.C., Towbin, B.D., Jegou, T., and Gasser, S.M. (2013). The shelterin protein POT-1 anchors Caenorhabditis elegans telomeres through SUN-1 at the nuclear periphery. J Cell Biol *203*, 727-735.
Filion, G.J., van Bemmel, J.G., Braunschweig, U., Talhout, W., Kind, J., Ward, L.D., Brugman, W., de Castro, I.J., Kerkhoven, R.M., Bussemaker, H.J.*, et al.* (2010). Systematic protein location mapping reveals five principal chromatin types in Drosophila cells. Cell *143*, 212-224.
Filion, G.J., and van Steensel, B. (2010). Reassessing the abundance of H3K9me2 chromatin domains in embryonic stem cells. Nature genetics *42*, 4; author reply 5--6.
Gibcus, J.H., and Dekker, J. (2013). The hierarchy of the 3D genome. Mol Cell *49*, 773-782.
Goldberg, M., Harel, A., Brandeis, M., Rechsteiner, T., Richmond, T.J., Weiss, A.M., and Gruenbaum, Y. (1999). The tail domain of lamin Dm0 binds histones H2A and H2B. Proc Natl Acad Sci U S A *96*, 2852-2857.
Gomez-Diaz, E., and Corces, V.G. (2014). Architectural proteins: regulators of 3D genome organization in cell fate. Trends Cell Biol *24*, 703-711.
Gonzalez-Aguilera, C., Ikegami, K., Ayuso, C., de Luis, A., Iniguez, M., Cabello, J., Lieb, J.D., and Askjaer, P. (2014). Genome-wide analysis links emerin to neuromuscular junction activity in Caenorhabditis elegans. Genome biology *15*, R21.
Gonzalez-Sandoval, A., Towbin, B.D., and Gasser, S.M. (2013). The formation and sequestration of heterochromatin during development: delivered on 7 September 2012 at the 37th FEBS Congress in Sevilla, Spain. FEBS J *280*, 3212-3219.
Gonzalez-Sandoval, A., Towbin, B.D., Kalck, V., Cabianca, D.S., Gaidatzis, D., Hauer, M.H., Geng, L., Wang, L., Yang, T., Wang, X.*, et al.* (2015). Perinuclear Anchoring of H3K9-Methylated Chromatin Stabilizes Induced Cell Fate in C. elegans Embryos. Cell *163*, 1333-1347.
Gotta, M., Laroche, T., Formenton, A., Maillet, L., Scherthan, H., and Gasser, S.M. (1996). The clustering of telomeres and colocalization with Rap1, Sir3, and Sir4 proteins in wild-type Saccharomyces cerevisiae. J Cell Biol *134*, 1349-1363.

Gudise, S., Figueroa, R.A., Lindberg, R., Larsson, V., and Hallberg, E. (2011). Samp1 is functionally associated with the LINC complex and A-type lamina networks. J Cell Sci *124*, 2077-2085.
Guelen, L., Pagie, L., Brasset, E., Meuleman, W., Faza, M.B., Talhout, W., Eussen, B.H., de Klein, A., Wessels, L., de Laat, W.*, et al.* (2008). Domain organization of human chromosomes revealed by mapping of nuclear lamina interactions. Nature *453*, 948-951.
Hadjur, S., Williams, L.M., Ryan, N.K., Cobb, B.S., Sexton, T., Fraser, P., Fisher, A.G., and Merkenschlager, M. (2009). Cohesins form chromosomal cis-interactions at the developmentally regulated IFNG locus. Nature *460*, 410-413.
Handoko, L., Xu, H., Li, G., Ngan, C.Y., Chew, E., Schnapp, M., Lee, C.W.H., Ye, C., Ping, J.L.H., Mulawadi, F.*, et al.* (2011). CTCF-mediated functional chromatin interactome in pluripotent cells. Nat Genet *43*, 630-638.
Harr, J.C., Gonzalez-Sandoval, A., and Gasser, S.M. (2016). Histones and histone modifications in perinuclear chromatin anchoring: from yeast to man. EMBO Rep.
Harr, J.C., Luperchio, T.R., Wong, X., Cohen, E., Wheelan, S.J., and Reddy, K.L. (2015). Directed targeting of chromatin to the nuclear lamina is mediated by chromatin state and A-type lamins. J Cell Biol *208*, 33-52.
Harr, J.C., and Reddy, K.L. (2015). Tagged Chromosomal Insertion Site System: A Method to Study Lamina-Associated Chromatin.
Heard, E., and Disteche, C.M. (2006). Dosage compensation in mammals: fine-tuning the expression of the X chromosome. Genes Dev *20*, 1848-1867.
Hediger, F., Dubrana, K., and Gasser, S.M. (2002). Myosin-like proteins 1 and 2 are not required for silencing or telomere anchoring, but act in the Tel1 pathway of telomere length control. J Struct Biol *140*, 79-91.
Helmbacher, F., Schneider-Maunoury, S., Topilko, P., Tiret, L., and Charnay, P. (2000). Targeting of the EphA4 tyrosine kinase receptor affects dorsal/ventral pathfinding of limb motor axons. Development *127*, 3313-3324.
Heun, P., Laroche, T., Shimada, K., Furrer, P., and Gasser, S.M. (2001). Chromosome Dynamics in the Yeast Interphase Nucleus. Science *294*, 2181-2186.
Hirano, Y., Hizume, K., Kimura, H., Takeyasu, K., Haraguchi, T., and Hiraoka, Y. (2012). Lamin B receptor recognizes specific modifications of histone H4 in heterochromatin formation. The Journal of biological chemistry *287*, 42654--42663.
Hu, S., Cheng, L., and Wen, B. (2012). Large chromatin domains in pluripotent and differentiated cells. Acta biochimica et biophysica Sinica *44*, 48--53.
Hubner, B., Lomiento, M., Mammoli, F., Illner, D., Markaki, Y., Ferrari, S., Cremer, M., and Cremer, T. (2015). Remodeling of nuclear landscapes during human myelopoietic cell differentiation maintains co-aligned active and inactive nuclear compartments. Epigenetics Chromatin *8*, 47.
Ikegami, K., and Lieb, J.D. (2013). Integral nuclear pore proteins bind to Pol III-transcribed genes and are required for Pol III transcript processing in C. elegans. Mol Cell *51*, 840-849.
Jeanblanc, M., Ragu, S., Gey, C., Contrepois, K., Courbeyrette, R., Thuret, J.Y., and Mann, C. (2012). Parallel pathways in RAF-induced senescence and conditions for its reversion. Oncogene *31*, 3072-3085.
Jin, F., Li, Y., Dixon, J.R., Selvaraj, S., Ye, Z., Lee, A.Y., Yen, C.A., Schmitt, A.D., Espinoza, C.A., and Ren, B. (2013). A high-resolution map of the three-dimensional chromatin interactome in human cells. Nature *503*, 290-294.
Keller, C., Adaixo, R., Stunnenberg, R., Woolcock, K.J., Hiller, S., and Buhler, M. (2012). HP1(Swi6) mediates the recognition and destruction of heterochromatic RNA transcripts. Mol Cell *47*, 215-227.

Keller, C., Kulasegaran-Shylini, R., Shimada, Y., Hotz, H.-R., and Bhler, M. (2013). Noncoding RNAs prevent spreading of a repressive histone mark. Nature structural \& molecular biology *20*, 994--1000.
Kharchenko, P.V., Alekseyenko, A.A., Schwartz, Y.B., Minoda, A., Riddle, N.C., Ernst, J., Sabo, P.J., Larschan, E., Gorchakov, A.A., Gu, T.*, et al.* (2011). Comprehensive analysis of the chromatin landscape in Drosophila melanogaster. Nature *471*, 480-485.
Kind, J., Pagie, L., Ortabozkoyun, H., Boyle, S., de Vries, S.S., Janssen, H., Amendola, M., Nolen, L.D., Bickmore, W.A., and van Steensel, B. (2013). Single-cell dynamics of genome-nuclear lamina interactions. Cell *153*, 178-192.
Kind, J., and van Steensel, B. (2010). Genome-nuclear lamina interactions and gene regulation. Curr Opin Cell Biol *22*, 320-325.
Koester-Eiserfunke, N., and Fischle, W. (2011). H3K9me2/3 Binding of the MBT Domain Protein LIN-61 Is Essential for Caenorhabditis elegans Vulva Development. PLoS Genetics *7*, e1002017.
Kosak, S.T., Scalzo, D., Alworth, S.V., Li, F., Palmer, S., Enver, T., Lee, J.S.J., and Groudine, M. (2007). Coordinate Gene Regulation during Hematopoiesis Is Related to Genomic Organization. PLoS Biology *5*, e309.
Kurshakova, M.M., Krasnov, A.N., Kopytova, D.V., Shidlovskii, Y.V., Nikolenko, J.V., Nabirochkina, E.N., Spehner, D., Schultz, P., Tora, L., and Georgieva, S.G. (2007). SAGA and a novel Drosophila export complex anchor efficient transcription and mRNA export to NPC. EMBO J *26*, 4956-4965.
Lachner, M., O'Carroll, D., Rea, S., Mechtler, K., and Jenuwein, T. (2001). Methylation of histone H3 lysine 9 creates a binding site for HP1 proteins. Nature *410*, 116--120.
Lieberman-Aiden, E., van Berkum, N.L., Williams, L., Imakaev, M., Ragoczy, T., Telling, A., Amit, I., Lajoie, B.R., Sabo, P.J., Dorschner, M.O.*, et al.* (2009). Comprehensive Mapping of Long-Range Interactions Reveals Folding Principles of the Human Genome. Science *326*, 289-293.
Lienert, F., Mohn, F., Tiwari, V.K., Baubec, T., Roloff, T.C., Gaidatzis, D., Stadler, M.B., and Schbeler, D. (2011). Genomic prevalence of heterochromatic H3K9me2 and transcription do not discriminate pluripotent from terminally differentiated cells. PLoS genetics *7*, e1002090.
Luderus, M.E., de Graaf, A., Mattia, E., den Blaauwen, J.L., Grande, M.A., de Jong, L., and van Driel, R. (1992). Binding of matrix attachment regions to lamin B1. Cell *70*, 949-959.
Lupianez, D.G., Kraft, K., Heinrich, V., Krawitz, P., Brancati, F., Klopocki, E., Horn, D., Kayserili, H., Opitz, J.M., Laxova, R.*, et al.* (2015). Disruptions of topological chromatin domains cause pathogenic rewiring of gene-enhancer interactions. Cell *161*, 1012-1025.
Malhas, A., Lee, C.F., Sanders, R., Saunders, N.J., and Vaux, D.J. (2007). Defects in lamin B1 expression or processing affect interphase chromosome position and gene expression. J Cell Biol *176*, 593-603.
Malik, P., Korfali, N., Srsen, V., Lazou, V., Batrakou, D.G., Zuleger, N., Kavanagh, D.M., Wilkie, G.S., Goldberg, M.W., and Schirmer, E.C. (2010). Cell-specific and lamin-dependent targeting of novel transmembrane proteins in the nuclear envelope. Cellular and molecular life sciences : CMLS *67*, 1353--1369.
Margalit, A., Brachner, A., Gotzmann, J., Foisner, R., and Gruenbaum, Y. (2007). Barrier-to-autointegration factor--a BAFfling little protein. Trends in cell biology *17*, 202--208.
Marshall, W.F., Straight, A., Marko, J.F., Swedlow, J., Dernburg, A., Belmont, A., Murray, A.W., Agard, D.A., and Sedat, J.W. (1997). Interphase chromosomes undergo constrained diffusional motion in living cells. Curr Biol *7*, 930-939.
Martin, C., Beaujean, N., Brochard, V., Audouard, C., Zink, D., and Debey, P. (2006). Genome restructuring in mouse embryos during reprogramming and early development. Dev Biol *292*, 317-332.

Mattout, A., Aaronson, Y., Sailaja, B.S., Raghu Ram, E.V., Harikumar, A., Mallm, J.P., Sim, K.H., Nissim-Rafinia, M., Supper, E., Singh, P.B., *et al.* (2015). Heterochromatin Protein 1beta (HP1beta) has distinct functions and distinct nuclear distribution in pluripotent versus differentiated cells. Genome biology *16*, 213.
Mattout, A., Pike, Brietta L., Towbin, Benjamin D., Bank, Erin M., Gonzalez-Sandoval, A., Stadler, Michael B., Meister, P., Gruenbaum, Y., and Gasser, Susan M. (2011). An EDMD Mutation in *C. elegans* Lamin Blocks Muscle-Specific Gene Relocation and Compromises Muscle Integrity. Current biology : CB *21*, 1603-1614.
McCord, R.P., Nazario-Toole, A., Zhang, H., Chines, P.S., Zhan, Y., Erdos, M.R., Collins, F.S., Dekker, J., and Cao, K. (2013). Correlated alterations in genome organization, histone methylation, and DNA-lamin A/C interactions in Hutchinson-Gilford progeria syndrome., pp. 260--269.
McHugh, C.A., Chen, C.K., Chow, A., Surka, C.F., Tran, C., McDonel, P., Pandya-Jones, A., Blanco, M., Burghard, C., Moradian, A., *et al.* (2015). The Xist lncRNA interacts directly with SHARP to silence transcription through HDAC3. Nature *521*, 232-236.
Meister, P., Mango, S.E., and Gasser, S.M. (2011). Locking the genome: nuclear organization and cell fate. Current Opinion in Genetics & Development *21*, 167-174.
Meister, P., and Taddei, A. (2013). Building silent compartments at the nuclear periphery: a recurrent theme. Curr Opin Genet Dev.
Meister, P., Towbin, B.D., Pike, B.L., Ponti, A., and Gasser, S.M. (2010). The spatial dynamics of tissue-specific promoters during C. elegans development. Genes & Development *24*, 766-782.
Meuleman, W., Peric-Hupkes, D., Kind, J., Beaudry, J.B., Pagie, L., Kellis, M., Reinders, M., Wessels, L., and van Steensel, B. (2013). Constitutive nuclear lamina-genome interactions are highly conserved and associated with A/T-rich sequence. Genome Res *23*, 270-280.
Miele, A., Bystricky, K., and Dekker, J. (2009). Yeast silent mating type loci form heterochromatic clusters through silencer protein-dependent long-range interactions. PLoS Genet *5*, e1000478.
Minc, E., Allory, Y., Worman, H.J., Courvalin, J.-C., and Buendia, B. (1999). Localization and phosphorylation of HP1 proteins during the cell cycle in mammalian cells. Chromosoma *108*, 220--234.
Mishiro, T., Ishihara, K., Hino, S., Tsutsumi, S., Aburatani, H., Shirahige, K., Kinoshita, Y., and Nakao, M. (2009). Architectural roles of multiple chromatin insulators at the human apolipoprotein gene cluster. EMBO J *28*, 1234-1245.
Montes de Oca, R., Andreassen, P.R., and Wilson, K.L. (2011). Barrier-to-Autointegration Factor influences specific histone modifications. Nucleus *2*, 580-590.
Nativio, R., Wendt, K.S., Ito, Y., Huddleston, J.E., Uribe-Lewis, S., Woodfine, K., Krueger, C., Reik, W., Peters, J.-M., and Murrell, A. (2009). Cohesin Is Required for Higher-Order Chromatin Conformation at the Imprinted <italic>IGF2-H19</italic> Locus. PLoS Genet *5*, e1000739.
Nielsen, P.R., Nietlispach, D., Mott, H.R., Callaghan, J., Bannister, A., Kouzarides, T., Murzin, A.G., Murzina, N.V., and Laue, E.D. (2002). Structure of the HP1 chromodomain bound to histone H3 methylated at lysine 9. Nature *416*, 103--107.
Noordermeer, D., de Wit, E., Klous, P., van de Werken, H., Simonis, M., Lopez-Jones, M., Eussen, B., de Klein, A., Singer, R.H., and de Laat, W. (2011). Variegated gene expression caused by cell-specific long-range DNA interactions. Nat Cell Biol *13*, 944-951.
Noordermeer, D., and Duboule, D. (2013). Chromatin architectures and Hox gene collinearity. Curr Top Dev Biol *104*, 113-148.

Nora, E.P., Lajoie, B.R., Schulz, E.G., Giorgetti, L., Okamoto, I., Servant, N., Piolot, T., van Berkum, N.L., Meisig, J., Sedat, J., *et al.* (2012). Spatial partitioning of the regulatory landscape of the X-inactivation centre. Nature *485*, 381-385.
Palladino, F., Laroche, T., Gilson, E., Axelrod, A., Pillus, L., and Gasser, S.M. (1993). SIR3 and SIR4 proteins are required for the positioning and integrity of yeast telomeres. Cell *75*, 543-555.
Peric-Hupkes, D., Meuleman, W., Pagie, L., Bruggeman, S.W., Solovei, I., Brugman, W., Graf, S., Flicek, P., Kerkhoven, R.M., van Lohuizen, M., *et al.* (2010). Molecular maps of the reorganization of genome-nuclear lamina interactions during differentiation. Mol Cell *38*, 603-613.
Phillips, J.E., and Corces, V.G. (2009). CTCF: Master Weaver of the Genome. Cell *137*, 1194-1211.
Pickersgill, H., Kalverda, B., de Wit, E., Talhout, W., Fornerod, M., and van Steensel, B. (2006). Characterization of the Drosophila melanogaster genome at the nuclear lamina. Nat Genet *38*, 1005-1014.
Pinheiro, I., Margueron, R., Shukeir, N., Eisold, M., Fritzsch, C., Richter, F.M., Mittler, G., Genoud, C., Goyama, S., Kurokawa, M., *et al.* (2012). Prdm3 and Prdm16 are H3K9me1 methyltransferases required for mammalian heterochromatin integrity. Cell *150*, 948-960.
Poleshko, A., Mansfield, K.M., Burlingame, C.C., Andrake, M.D., Shah, N.R., and Katz, R.A. (2013). The human protein PRR14 tethers heterochromatin to the nuclear lamina during interphase and mitotic exit. Cell Rep *5*, 292-301.
Rao, S.S., Huntley, M.H., Durand, N.C., Stamenova, E.K., Bochkov, I.D., Robinson, J.T., Sanborn, A.L., Machol, I., Omer, A.D., Lander, E.S., *et al.* (2014). A 3D map of the human genome at kilobase resolution reveals principles of chromatin looping. Cell *159*, 1665-1680.
Rhind, N., and Gilbert, D.M. (2013). DNA replication timing. Cold Spring Harb Perspect Biol *5*, a010132.
Rohner, S., Kalck, V., Wang, X., Ikegami, K., Lieb, J.D., Gasser, S.M., and Meister, P. (2013). Promoter- and RNA polymerase II-dependent hsp-16 gene association with nuclear pores in Caenorhabditis elegans. J Cell Biol *200*, 589-604.
Ryba, T., Hiratani, I., Lu, J., Itoh, M., Kulik, M., Zhang, J., Schulz, T.C., Robins, A.J., Dalton, S., and Gilbert, D.M. (2010). Evolutionarily conserved replication timing profiles predict long-range chromatin interactions and distinguish closely related cell types. Genome Res *20*, 761-770.
Satijn, D.P., Hamer, K.M., den Blaauwen, J., and Otte, A.P. (2001). The polycomb group protein EED interacts with YY1, and both proteins induce neural tissue in Xenopus embryos. Molecular and cellular biology *21*, 1360--1369.
Schober, H., Ferreira, H., Kalck, V., Gehlen, L.R., and Gasser, S.M. (2009). Yeast telomerase and the SUN domain protein Mps3 anchor telomeres and repress subtelomeric recombination. Genes Dev *23*, 928-938.
Schober, H., Kalck, V.r., Vega-Palas, M.A., Van Houwe, G., Sage, D., Unser, M., Gartenberg, M.R., and Gasser, S.M. (2008). Controlled exchange of chromosomal arms reveals principles driving telomere interactions in yeast. Genome Research *18*, 261-271.
Sexton, T., Yaffe, E., Kenigsberg, E., Bantignies, F., Leblanc, B., Hoichman, M., Parrinello, H., Tanay, A., and Cavalli, G. (2012). Three-dimensional folding and functional organization principles of the Drosophila genome. Cell *148*, 458-472.
Sharma, R., Jost, D., Kind, J., Gomez-Saldivar, G., van Steensel, B., Askjaer, P., Vaillant, C., and Meister, P. (2014). Differential spatial and structural organization of the X chromosome underlies dosage compensation in C. elegans. Genes Dev *28*, 2591-2596.
Sharma, R., and Meister, P. (2015). Dosage compensation and nuclear organization: cluster to control chromosome-wide gene expression. Curr Opin Genet Dev *37*, 9-16.

Shevelyov, Y.Y., Lavrov, S.A., Mikhaylova, L.M., Nurminsky, I.D., Kulathinal, R.J., Egorova, K.S., Rozovsky, Y.M., and Nurminsky, D.I. (2009). The B-type lamin is required for somatic repression of testis-specific gene clusters. Proc Natl Acad Sci U S A *106*, 3282-3287.
Shimi, T., Pfleghaar, K., Kojima, S., Pack, C.G., Solovei, I., Goldman, A.E., Adam, S.A., Shumaker, D.K., Kinjo, M., Cremer, T.*, et al.* (2008). The A- and B-type nuclear lamin networks: microdomains involved in chromatin organization and transcription. Genes Dev *22*, 3409-3421.
Solovei, I., Kreysing, M., Lanctot, C., Kosem, S., Peichl, L., Cremer, T., Guck, J., and Joffe, B. (2009). Nuclear architecture of rod photoreceptor cells adapts to vision in mammalian evolution. Cell *137*, 356-368.
Solovei, I., Wang, A.S., Thanisch, K., Schmidt, C.S., Krebs, S., Zwerger, M., Cohen, T.V., Devys, D., Foisner, R., Peichl, L.*, et al.* (2013). LBR and lamin A/C sequentially tether peripheral heterochromatin and inversely regulate differentiation. Cell *152*, 584-598.
Spector, D.L. (2001). Nuclear domains. J Cell Sci *114*, 2891-2893.
Sridharan, R., Gonzales-Cope, M., Chronis, C., Bonora, G., McKee, R., Huang, C., Patel, S., Lopez, D., Mishra, N., Pellegrini, M.*, et al.* (2013). Proteomic and genomic approaches reveal critical functions of H3K9 methylation and heterochromatin protein-1γ in reprogramming to pluripotency. Nature cell biology *15*, 872--882.
Srinivasan, L., and Atchison, M.L. (2004). YY1 DNA binding and PcG recruitment requires CtBP. Genes \& development *18*, 2596--2601.
Strome, S., Kelly, W.G., Ercan, S., and Lieb, J.D. (2014). Regulation of the X chromosomes in Caenorhabditis elegans. Cold Spring Harb Perspect Biol *6*.
Studencka, M., Konzer, A., Moneron, G., Wenzel, D., Opitz, L., Salinas-Riester, G., Bedet, C., Kruger, M., Hell, S.W., Wisniewski, J.R.*, et al.* (2012). Novel roles of Caenorhabditis elegans heterochromatin protein HP1 and linker histone in the regulation of innate immune gene expression. Mol Cell Biol *32*, 251-265.
Stunnenberg, R., Kulasegaran-Shylini, R., Keller, C., Kirschmann, M.A., Gelman, L., and Bhler, M. (2015). H3K9 methylation extends across natural boundaries of heterochromatin in the absence of an HP1 protein. The EMBO journal.
Taddei, A., and Gasser, S.M. (2012). Structure and function in the budding yeast nucleus. Genetics *192*, 107-129.
Taddei, A., Van Houwe, G., Hediger, F., Kalck, V., Cubizolles, F., Schober, H., and Gasser, S.M. (2006). Nuclear pore association confers optimal expression levels for an inducible yeast gene. Nature *441*, 774-778.
Taddei, A., Van Houwe, G., Nagai, S., Erb, I., van Nimwegen, E., and Gasser, S.M. (2009). The functional importance of telomere clustering: global changes in gene expression result from SIR factor dispersion. Genome Res *19*, 611-625.
Thompson, M., Haeusler, R.A., Good, P.D., and Engelke, D.R. (2003). Nucleolar clustering of dispersed tRNA genes. Science *302*, 1399-1401.
Towbin, Benjamin D., González-Aguilera, C., Sack, R., Gaidatzis, D., Kalck, V., Meister, P., Askjaer, P., and Gasser, Susan M. (2012). Step-Wise Methylation of Histone H3K9 Positions Heterochromatin at the Nuclear Periphery. Cell *150*, 934-947.
Towbin, B.D., Gonzalez-Sandoval, A., and Gasser, S.M. (2013). Mechanisms of heterochromatin subnuclear localization. Trends Biochem Sci *38*, 356-363.
Towbin, B.D., Meister, P., Pike, B.L., and Gasser, S.M. (2010). Repetitive transgenes in C. elegans accumulate heterochromatic marks and are sequestered at the nuclear envelope in a copy-number- and lamin-dependent manner. Cold Spring Harb Symp Quant Biol *75*, 555-565.
Ugarte, F., Sousae, R., Cinquin, B., Martin, E.W., Krietsch, J., Sanchez, G., Inman, M., Tsang, H., Warr, M., Passegue, E.*, et al.* (2015). Progressive Chromatin Condensation and

H3K9 Methylation Regulate the Differentiation of Embryonic and Hematopoietic Stem Cells. Stem Cell Reports *5*, 728-740.
Vietri Rudan, M., Barrington, C., Henderson, S., Ernst, C., Odom, D.T., Tanay, A., and Hadjur, S. (2015). Comparative Hi-C reveals that CTCF underlies evolution of chromosomal domain architecture. Cell Rep *10*, 1297-1309.
Wen, B., Wu, H., Loh, Y.H., Briem, E., Daley, G.Q., and Feinberg, A.P. (2012). Euchromatin islands in large heterochromatin domains are enriched for CTCF binding and differentially DNA-methylated regions. BMC Genomics *13*, 566.
Wen, B., Wu, H., Shinkai, Y., Irizarry, R.A., and Feinberg, A.P. (2009). Large histone H3 lysine 9 dimethylated chromatin blocks distinguish differentiated from embryonic stem cells. Nature genetics *41*, 246--250.
Wilkinson, F., Pratt, H., and Atchison, M.L. (2010). PcG recruitment by the YY1 REPO domain can be mediated by Yaf2. Journal of cellular biochemistry *109*, 478--486.
Williams, R.R.E., Azuara, V., Perry, P., Sauer, S., Dvorkina, M., Jorgensen, H., Roix, J., McQueen, P., Misteli, T., Merkenschlager, M.*, et al.* (2006). Neural induction promotes large-scale chromatin reorganisation of the Mash1 locus. J Cell Sci *119*, 132-140.
Wilson, K.L., and Berk, J.M. (2010). The nuclear envelope at a glance. J Cell Sci *123*, 1973-1978.
Wilson, K.L., and Foisner, R. (2010). Lamin-binding Proteins. Cold Spring Harb Perspect Biol *2*, a000554.
Wong, X., Luperchio, T.R., and Reddy, K.L. (2014). NET gains and losses: the role of changing nuclear envelope proteomes in genome regulation. Curr Opin Cell Biol *28*, 105-120.
Yang, F., Deng, X., Ma, W., Berletch, J.B., Rabaia, N., Wei, G., Moore, J.M., Filippova, G.N., Xu, J., Liu, Y.*, et al.* (2015). The lncRNA Firre anchors the inactive X chromosome to the nucleolus by binding CTCF and maintains H3K27me3 methylation. Genome biology *16*, 52.
Ye, Q., and Worman, H.J. (1996). Interaction between an integral protein of the nuclear envelope inner membrane and human chromodomain proteins homologous to Drosophila HP1. The Journal of biological chemistry *271*, 14653--14656.
Zuleger, N., Boyle, S., Kelly, D.A., de las Heras, J.I., Lazou, V., Korfali, N., Batrakou, D.G., Randles, K.N., Morris, G.E., Harrison, D.J.*, et al.* (2013). Specific nuclear envelope transmembrane proteins can promote the location of chromosomes to and from the nuclear periphery. Genome biology *14*, R14.
Zullo, J.M., Demarco, I.a., Pique-Regi, R., Gaffney, D.J., Epstein, C.B., Spooner, C.J., Luperchio, T.R., Bernstein, B.E., Pritchard, J.K., Reddy, K.L.*, et al.* (2012). DNA sequence-dependent compartmentalization and silencing of chromatin at the nuclear lamina. Cell *149*, 1474--1487.

CHAPTER 2: PERINUCLEAR ANCHORING OF H3K9-METHYLATED CHROMATIN STABILIZES INDUCED CELL FATE IN *C. ELEGANS* EMBRYOS

Adriana Gonzalez-Sandoval,[1,2] Benjamin D. Towbin,[1,5] Veronique Kalck,[1] Daphne S. Cabianca,[1] Dimos Gaidatzis,[1,3] Michael H. Hauer,[1,2] Liqing Geng,[4] Li Wang,[4] Teddy Yang,[4] Xinghao Wang,[4] Kehao Zhao,[4] and Susan M. Gasser[1,2]

[1]Friedrich Miescher Institute for Biomedical Research, Maulbeerstrasse 66, CH-4058 Basel, Switzerland
[2]Faculty of Natural Sciences, University of Basel, Klingelbergstrasse 50/70, CH-4056 Basel, Switzerland
[3]Swiss Institute of Bioinformatics, CH-4058 Basel, Switzerland
[4]China Novartis Institute of Biomedical Research Co, Ltd. Bldg 3, Lane 3728 Jinke Road, Pudong New Area, Shanghai 201203, China
[5]Present address: Department of Molecular Cell Biology, The Weizmann Institute of Science, Rehovot 76100, Israel

Published in *Cell*, Volume 163, Issue 6, p1333–1347, 3 December 2015

A.G.-S. contributed to experiments in Figure 1 with exception of panel C and F contributed by V.K. and M.H.H respectively. Figure 2 data was contributed by A.G.-S. panels A and C, V.K. panel B and D.C. panel D. Figure 3 results were generated by collaborators from C-NIBR (L.G., L.W., T.Y., X.W. and K.Z.). Figure 4 panels A and B results were performed by A.G.-S. and panel C by D.C. For Figure 5 all genome-wide analyses were performed by D.G. with material provided by A.G-S. and confirmations in panels E and F; panel C was generated by V.K. Finally, Figure 6 results were performed by A.G.-S.

In relation to the supplemental experiments, A.G.-S., B.D.T. and V.K. contributed to Figure S1. Figure S2 contributed by A.G.-S. and V.K. Collaborators from C-NIBR performed experiments for Figure S3 and S4. Figure S5 data was contributed by A.G.-S and genome-wide analysis by D.G. Finally, Figure S6 experiments were contributed by A.G.-S.

SUMMARY

Interphase chromatin is organized in distinct nuclear sub-compartments, reflecting its degree of compaction and transcriptional status. In *C. elegans* embryos, H3K9 methylation is necessary to silence and to anchor repeat-rich heterochromatin at the nuclear periphery. In a screen for perinuclear anchors of heterochromatin, we identified a previously uncharacterized *C. elegans* chromodomain protein, CEC-4. CEC-4 binds preferentially mono-, di-, or tri-methylated H3K9 and localizes at the nuclear envelope independently of H3K9 methylation and nuclear lamin. CEC-4 is necessary for endogenous heterochromatin anchoring, but not for transcriptional repression, in contrast to other known H3K9 methyl-binders in worms, which mediate gene repression but not perinuclear anchoring. When we ectopically induce a muscle differentiation program in embryos, *cec-4* mutants fail to commit fully to muscle cell fate. This suggests that perinuclear sequestration of chromatin during development helps restrict cell differentiation programs by stabilizing commitment to a specific cell fate.

Please cite this article in press as: Gonzalez-Sandoval et al., Perinuclear Anchoring of H3K9-Methylated Chromatin Stabilizes Induced Cell Fate in *C. elegans* Embryos, Cell (2015), http://dx.doi.org/10.1016/j.cell.2015.10.066

Article

Cell

Perinuclear Anchoring of H3K9-Methylated Chromatin Stabilizes Induced Cell Fate in *C. elegans* Embryos

Adriana Gonzalez-Sandoval,[1,2] Benjamin D. Towbin,[1,5] Veronique Kalck,[1] Daphne S. Cabianca,[1] Dimos Gaidatzis,[1,3] Michael H. Hauer,[1,2] Liqing Geng,[4] Li Wang,[4] Teddy Yang,[4] Xinghao Wang,[4] Kehao Zhao,[4] and Susan M. Gasser[1,2,*]

[1]Friedrich Miescher Institute for Biomedical Research, Maulbeerstrasse 66, CH-4058 Basel, Switzerland

[2]Faculty of Natural Sciences, University of Basel, Klingelbergstrasse 50/70, CH-4056 Basel, Switzerland

[3]Swiss Institute of Bioinformatics, CH-4058 Basel, Switzerland

[4]China Novartis Institute of Biomedical Research Co, Ltd. Bldg 3, Lane 3728 Jinke Road, Pudong New Area, Shanghai 201203, China

[5]Present address: Department of Molecular Cell Biology, The Weizmann Institute of Science, Rehovot 76100, Israel

*Correspondence: susan.gasser@fmi.ch

http://dx.doi.org/10.1016/j.cell.2015.10.066

SUMMARY

Interphase chromatin is organized in distinct nuclear sub-compartments, reflecting its degree of compaction and transcriptional status. In *Caenorhabditis elegans* embryos, H3K9 methylation is necessary to silence and to anchor repeat-rich heterochromatin at the nuclear periphery. In a screen for perinuclear anchors of heterochromatin, we identified a previously uncharacterized *C. elegans* chromodomain protein, CEC-4. CEC-4 binds preferentially mono-, di-, or tri-methylated H3K9 and localizes at the nuclear envelope independently of H3K9 methylation and nuclear lamin. CEC-4 is necessary for endogenous heterochromatin anchoring, but not for transcriptional repression, in contrast to other known H3K9 methyl-binders in worms, which mediate gene repression but not perinuclear anchoring. When we ectopically induce a muscle differentiation program in embryos, *cec-4* mutants fail to commit fully to muscle cell fate. This suggests that perinuclear sequestration of chromatin during development helps restrict cell differentiation programs by stabilizing commitment to a specific cell fate.

INTRODUCTION

Cues stemming from the spatial organization of chromatin are widely thought to influence the function of eukaryotic genomes. Indeed, chromatin assumes distinct patterns of distribution in the interphase nucleus in response to cell-type-specific gene expression (reviewed in Meister et al., 2011; Talamas and Capelson, 2015). Dense-staining heterochromatin and repressed tissue-specific genes are sequestered at the inner nuclear membrane (INM) in both plant and animal cells. In metazoans, an INM-associated network of the intermediate filament protein lamin and other associated proteins provides a scaffold that helps the interphase nucleus reform after mitosis (Nigg, 1992).

The chromatin that associates with the nuclear lamina (lamin-associated domains or LADs) is generally gene poor, transcriptionally silent, and enriched for repressive histone marks (Gerstein et al., 2010; Guelen et al., 2008; Ikegami et al., 2010; Pickersgill et al., 2006). Importantly, in *C. elegans* embryos the integrity of two histone methyltransferases (HMTs) that target histone H3K9, MET-2, and SET-25 was shown to be essential for the peripheral localization of heterochromatin (Towbin et al., 2012). Perturbed H3K9 methylation also partially compromised proper heterochromatin organization in mammalian cells (Kind et al., 2013; Pinheiro et al., 2012). However, no nuclear envelope protein has yet been identified that anchors H3K9-methylated chromatin specifically.

Studies of nuclear organization during the development of multicellular organisms or of embryonic stem cell (ESC) differentiation in vitro showed that perinuclear chromatin sequestration is a dynamic process that changes with cell-type-specific gene expression (Fussner et al., 2010; Harr et al., 2015; Meister et al., 2010; Peric-Hupkes et al., 2010). Important genetic studies of Solovei et al. (2013) showed that heterochromatin tethering in differentiated mammalian cells depends on two partially redundant pathways that reflect the sequential induction through development of lamin B receptor (LBR) and lamin A/C. In some mouse tissues both LBR and lamin A/C are expressed; in others, expression of only one is sufficient to ensure the conventional sequestration of heterochromatin at the INM. In the absence of both perinuclear components, heterochromatin accumulated at the nuclear core (Solovei et al., 2013).

Despite these genetic implications, it was unclear what bridges chromatin to LBR or lamin A/C. LBR has been shown to bind the chromodomain (CD) of Heterochromatin proteins 1α and γ (HP1α and HP1γ; (Ye and Worman, 1996), which are hallmarks of heterochromatin. But HP1α-containing chromocenters are not necessarily perinuclear, and HP1γ is bound to many euchromatic loci positioned away from INM (Minc et al., 1999). Moreover, complete ablation of HP1α or β in either pluripotent or differentiated ESCs does not change chromocenter positioning (Mattout et al., 2015). Mammalian LBR also binds histone H4K20me2 in vitro through its C-terminal Tudor domain (Hirano et al., 2012), yet H4K20me2 is

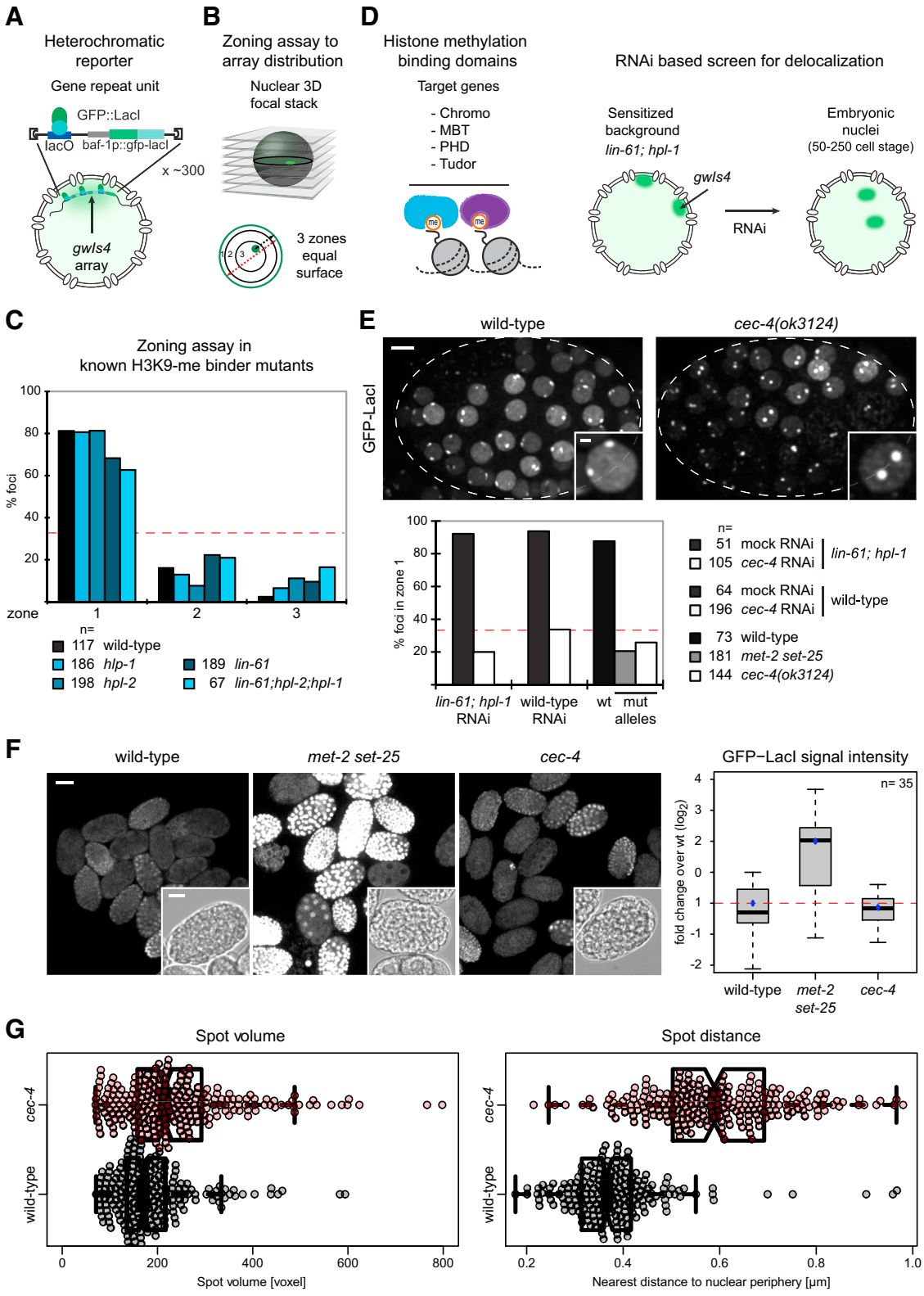

Figure 1. *cec-4* Is Required for Anchoring and Compaction of a Heterochromatic Array

(A) Heterochromatic transgene array *gwIs4 [baf-1p::GFP-lacI::let-858 3′UTR; myo-3p::RFP]* reporter.

(B) Zoning assay for array distribution. Radial position is determined relative to the INM, and values are binned into three concentric zones.

(legend continued on next page)

broadly distributed without enrichment on LADs (Barski et al., 2007).

Whereas mammalian lamins were reported to bind AT-rich DNA and histone dimers in vitro (reviewed in Wilson and Foisner, 2010), this affinity cannot account for selective heterochromatin binding. Nor is it explained by lamin A/C interaction with transcription factors or the barrier to autointegration factor (BAF), which may link specific promoters to lamins (Kubben et al., 2012; Meuleman et al., 2013). Similarly, the lamin associated Lap2β interacts with HDAC3 and the transcription factor cKrox, a ligand of GAGA motifs, leading to the repression and perinuclear anchoring of a subset of mammalian promoters (Zullo et al., 2012). Yet LADs extend far beyond promoters, coinciding instead with extensive domains of H3K9 methylation (Towbin et al., 2012).

Alternatively, nuclear lamins may act indirectly by providing a stable platform for the localization of other INM proteins (e.g., Lap2β, Emerin and Man1 [Brachner and Foisner, 2011]). Indeed, depletion of the *C. elegans* lamin, LMN-1, mislocalizes Emerin (EMR-1) and Man1 (LEM-2), and the worm Emerin in turn helps stabilize repressed muscle and neuronal genes at the INM in differentiated worm tissues (González-Aguilera et al., 2014). Yet neither Emerin nor Man1 bind heterochromatin directly. A similar indirect effect was ascribed to mammalian SAMP-1, an INM protein connected to LINC (linker of nucleo- and cytoskeleton) complex, whose loss compromises nuclear integrity and leads to Emerin, SUN-1, and Lamin A/C mislocalization (Gudise et al., 2011). Finally, loss of PRR14, a perinuclear HP1-binding protein, altered perinuclear attachment of H3K9-methylated domains in mammalian nuclei, yet led to general defects in nuclear structure, raising the question of indirect effect on DNA localization (Poleshko et al., 2013).

Here we exploit the power of RNAi screens in the nematode *C. elegans* to find a methyl-H3K9-specific perinuclear anchor for heterochromatin. We have individually downregulated genes that harbor characteristic histone methylation binding motifs and monitored changes in the perinuclear anchoring of heterochromatin in early embryos. We identified a previously uncharacterized *C. elegans* CD protein, CEC-4, as our only positive hit. CEC-4 localizes at the INM where it directly binds endogenous H3K9-methylated chromatin through its CD's aromatic cage. CEC-4 is not necessary for the transcriptional silencing of either endogenous genes or a heterochromatic reporter, although the methylation of H3K9 and its ligands HPL-2 and LIN-61 are. Despite this, a reproducible fraction of *cec-4* embryos were unable to maintain the muscle specification induced by a pulse of HLH-1 (MyoD) expression. We suggest that perinuclear sequestration of chromatin contributes to cell fate commitment under conditions of perturbed development.

RESULTS

CEC-4 Is a Chromodomain Factor that Anchors a Heterochromatic Array

To search for proteins involved in the anchoring of methylated H3K9 chromatin, we designed an RNAi screen with a fluorescent reporter for perinuclear heterochromatin positioning in *C. elegans* embryos. Our reporter is an integrated plasmid array, *gwIs4*, which expresses the GFP-LacI fusion protein under control of the ubiquitously active *baf-1* promoter. GFP-LacI binds a *lacO* site that occurs once per 3.5 kb (~300x), generating a fluorescent focus that binds the INM in embryonic nuclei (Figure 1A). The histones on the array are trimethylated on H3K9 and H3K27, but lack H3K4 methylation, and have reduced gene expression, thereby recapitulating conserved features of heterochromatin (Meister et al., 2010; Towbin et al., 2010). Array position is determined with a zoning assay in which radial distances from the spot to the nuclear periphery, scored in the focal plane in which the spot is the brightest, are binned into 3 zones of equal surface (Figure 1B). Deviation from 33% indicates nonrandom localization.

The *C. elegans* genome encodes 65 proteins that contain methyl-lysine/-arginine binding motifs, namely CD, MBT (malignant brain tumor), PHD (plant homeodomain) and Tudor domains (Table S1; reviewed in Taverna et al., 2007). This set of proteins includes HPL-1 and HPL-2, homologs of HP1, a highly conserved CD protein that binds methylated H3K9 to silence heterochromatin (Nestorov et al., 2013). HPL-1 co-localizes with the heterochromatic *gwIs4* array in worm embryos and appears to repress transcription in a promoter-specific manner working together with the H1 variant HIS-24 in larvae (Studencka et al., 2012a). HPL-2 binds H3K9me2/3 as well as H3K27me2/3 in vitro, and it is needed to repress large heterochromatic arrays in both embryos and germline cells, as well as to fine-tune other gene expression events (Couteau et al., 2002; Studencka et al., 2012b). A third H3K9me2/me3 ligand is the MBT-domain protein LIN-61, whose loss compromises vulva development, silencing of heterochromatic arrays, and a neuron-specific reporter in somatic cells (Koester-Eiserfunke and Fischle, 2011; Zheng et al., 2013). Remarkably, elimination of these known H3K9me ligands,

(C) Array distribution quantitation, as described in (B), in early embryos (50–250 cell stage) of indicated genotypes (Tables S1 and S3). Red line = random distribution of 33%.

(D) Design of candidate RNAi screen in *lin-61;hpl-1* deficient strain. L1 larvae subjected to RNAi for candidates listed in Table S3, and embryonic progeny screened for array delocalization.

(E) Z-projection of representative embryos bearing *gwIs4* in WT and *cec-4(ok3124)* strains. Insets: single nuclei. Scale bar, 5 or 2 μm, respectively. Array distribution, zone 1 data in early embryos as indicated, n = foci scored per condition. Pair-wise comparisons of mock RNAi and WT conditions with *cec-4* RNAi or mutant yielded p values < 0.001 by χ^2 test.

(F) Z-projection of GFP fluorescence in embryos of indicated genotype with *gwIs4*. Insets: bright field. Scale bar, 20 or 10 μm, respectively. Quantified signal intensity displayed as box plot in $\log_2$ scale, whiskers = 1st and 3rd quartiles. Black lines: median, blue dots: mean, red dashed line: baseline = mean of WT. n = embryos scored.

(G) 3D spot volume and distance from INM in WT and *cec-4(ok3124)* embryos. Notched box plots overlapping individual measurements as above. n = 209 and 237, respectively, from five embryos each; pair-wise comparisons with p-values < 0.001 by Student's t test.

See also Figure S1.

singly or in combination, had little impact on the perinuclear sequestration of the *gwIs4* heterochromatic array, although the mutants did lose transcriptional repression (Figure 1C; Towbin et al., 2012).

Conscious that anchor redundancy might be a concern, we downregulated other methyl-binding candidates by RNAi in *hpl-1;lin-61* double mutant embryos. Only one RNAi target, *cec-4,* which encodes an uncharacterized CD protein, affected the perinuclear anchoring of the heterochromatic reporter (Figures 1D and 1E). The percentage of heterochromatic foci in the outermost nuclear zone dropped from 92% to 20%, following *cec-4* RNAi (Figures 1E and S1B). Although *cec-3/eap-1* has been described as an H3K9me1-3 binder involved in neuron-specific gene expression (Greer et al., 2014; Zheng et al., 2013), *cec-3* RNAi had no impact on heterochromatin anchoring in our screen (data not shown).

The effect of *cec-4* RNAi on array position did not depend on the absence of LIN-61 or HPL-1, for the same RNAi in WT worms yielded identical array delocalization (Figures 1E and S1B). To rule out off-target effects of *cec-4* RNAi, we scored array position in embryos carrying the null mutant *cec-4(ok3124),* which lacks the 5′ UTR and first 2 exons (Figure S1A). The genetic ablation of *cec-4* phenocopied *cec-4* RNAi, yielding full array detachment from the INM, identical to that scored in embryos that lack H3K9 methylation; i.e., the *met-2 set-25* double mutant (Towbin et al., 2012). Thus, the CD-encoding *cec-4* gene is required, like H3K9-methylation, for the perinuclear anchoring of heterochromatic arrays in *C. elegans* early embryos.

We examined the effect of *cec-4* ablation on gene expression by quantifying the fluorescent intensity of GFP-LacI, which is expressed from a housekeeping promoter on the *gwIs4* array. Although the expression levels are strongly upregulated in *met-2 set-25* mutant, deletion of *cec-4* did not alter GFP-LacI expression in embryos (Figure 1F). Both H3K9me3 and the enzyme mediating this terminal modification, SET-25, remained enriched on the delocalized array in *cec-4* mutant embryos (Figures S1C and S1D), consistent with the observed transcriptional repression. We conclude that CEC-4-mediated anchoring is not essential for heterochromatic array repression. Nonetheless, coupled with the loss of anchoring we scored a significant decompaction of the reporter, upon release from the INM. Monitored by a quantitative 3D volume rendering protocol, we found that the mean volume expanded from about 192 to 239 voxels upon *cec-4* deletion (Figure 1G).

CEC-4 Localizes Intrinsically to the Nuclear Periphery

We next examined the subcellular localization of CEC-4. A mCherry-tagged version of *cec-4* was integrated as a site-specific, single-copy genomic insertion under control of its endogenous *cec-4* promoter and 3′UTR (Figure S2A). Confocal fluorescence microscopy of CEC-4-mCherry (CEC-4-mCh) showed that the protein forms a ring at the nuclear periphery at all embryonic stages (Figure 2A). This distribution persisted in larval and adult differentiated tissues and in the germline of adult worms (Figure 2D; data not shown). CEC-4 localization was independent of H3K9 methylation; the same perinuclear CEC-4-mCh ring was found in the *met-2 set-25* mutant, in which H3K9 is unmethylated and heterochromatin was delocalized and expressed (Figure 2C). Only in mitosis did CEC-4-mCh become dispersed (data not shown), much like lamins, which undergo phosphorylation by cyclinB/Cdk in mitosis (Nigg, 1992).

Quantification of fluorescence intensity of CEC-4-mCh in L1 larval stage showed protein level variation in a tissue-specific fashion. CEC-4 is weakly expressed in intestine, highly expressed in muscle, and is found at intermediate levels in almost every other tissue (Figure 2D). This unequal tissue-specific expression was not observed for an EMR-1 fusion construct designed and integrated in a similar manner (EMR-1-mCherry; Figures 2D and S2A).

To characterize CEC-4's nuclear rim pattern further, we imaged embryos at 100 nm resolution using super-resolution structured illumination microscopy (SR-SIM). The CEC-4-mCh ring resolved into a perinuclear, punctate pattern (Figure 2B), and counterlabeling of nuclear pores or LMN-1 (lamin) showed CEC-4 in the same concentric plane as lamin and is situated mostly between pores (Figure 2B). Lamin and CEC-4-mCh were in very close proximity, yet could be resolved as distinct foci (low yellow signal in red/green channel merge; Figure 2B), suggesting that CEC-4 might localize to the INM independently of lamin. Indeed, after treating these worms with *lmn-1* RNAi, CEC-4 perinuclear ring persisted (data not shown). The same was true after RNAi against Emerin, LEM-2, SUN-1, UNC-84, BAF-1, and all other known *C. elegans* INM components (Table S6).

We reasoned that if CEC-4 localizes independently of lamin, it might also associate with the nuclear envelope of budding yeast, which lacks lamin entirely (reviewed in Taddei and Gasser, 2012). Indeed, when expressed as a GFP fusion protein under control of the *GAL1* promoter, CEC-4-GFP formed a perinuclear ring at INM of yeast nuclei (Figure S2B). To map the domain that directs CEC-4 to the INM, we expressed complementary N- and C-terminal fragments of CEC-4, fused to GFP. Both yielded a diffuse nuclear distribution (Figure S2C), suggesting that the integrity of the holoprotein is necessary for INM enrichment (Figure S2C). Similar results were obtained with similar constructs expressed ectopically in *C. elegans* (data not shown). Finally, in yeast as in worms, ablation of known INM and pore basket proteins (Table S7) did not alter CEC-4-GFP localization. We therefore propose that either CEC-4 has an intrinsic affinity for the INM, or else it binds a conserved but uncharacterized membrane component.

CEC-4 Chromodomain Preferentially Binds Methylated H3K9

Based on sequence analysis, the CEC-4 CD (aa 82–141) shares 42% identity with mammalian HP1α CD and 33% with HPL-1/2 CDs, yet CEC-4 lacks the HP1-specific chromoshadow and RNA-binding hinge domains (Couteau et al., 2002). Protein comparison failed to reveal a strict homolog of CEC-4 in mammalian genomes, apart from the CD and a second conserved motif, here called PD (putative domain, aa 25–76), which is found in other CD-containing proteins (Figure 3A).

The CEC-4 CD has a canonical secondary structure like mammalian HP1 and Pc3 (Fischle et al., 2003b), with an aromatic cage containing two tyrosine residues that are predicted to recognize methylated lysine within the H3 ARK(S/T) motif. To characterize the specificity of CEC-4 CD binding, we expressed

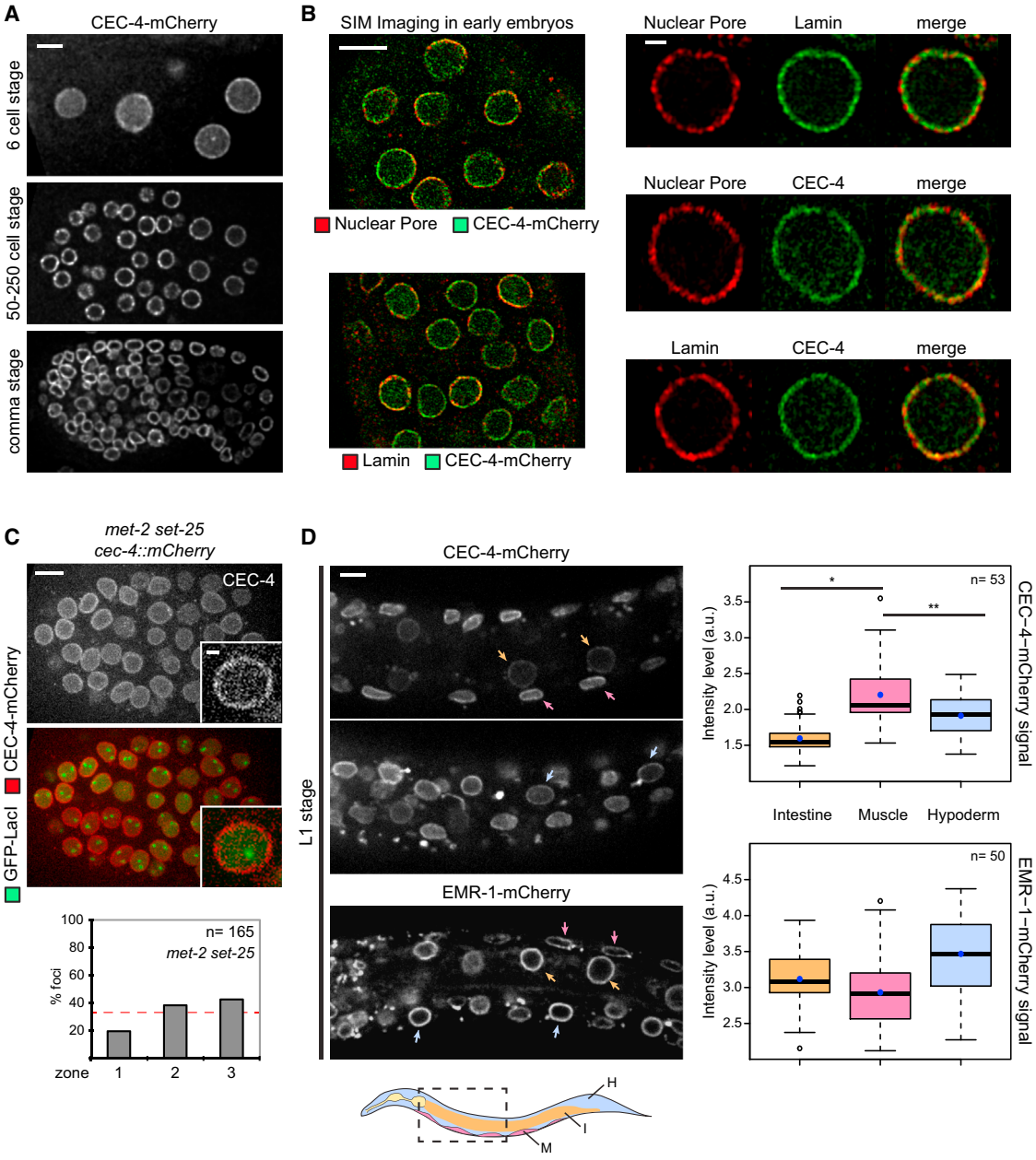

Figure 2. Perinuclear CEC-4 Localization Is Independent of H3K9 Methylation, and Varies from Tissue to Tissue

(A) Single plane images of indicated embryo stages expressing CEC-4-mCh.

(B) SR-SIM microscopy of CEC-4-mCh transgenic embryos, counterstained for nuclear pores, lamin or mCherry. Embryo sections and single nuclear planes shown.

(C) Z-projection of CEC-4-mCh in *met-2 set-25* mutant background; images of mCherry alone and merged with *gwIs4* GFP-LacI signal are shown. Insets: single plain nuclei. Quantification of array distribution, n = foci scored.

(D) Single plane confocal images of CEC-4- and EMR-1-mCh transgenic L1 larvae; scheme of L1 worm color-coded by tissue, M: muscle, I: intestine, H: hypoderm. Measured mCh signal intensity displayed as box plots in a.u. as in Figure 1. Black circles = outliers, n = number of nuclei per tissue; pair-wise comparisons for * and **p value < 0.001 in Wilcoxon test. Scale bar, 5 μm in whole/section embryos and larvae; 2μm in single nuclei/insets.

See also Figure S2.

and purified the WT CD-containing fragment of CEC-4 (CEC-4 CD; aa 25–141) and a mutated version of the same fragment (Y87A and Y111A; CEC-4 cd-2YA; Figures 3A and S3A), bearing point mutations that should disrupt the aromatic cage. Using magnetic beads coated with unmethylated (me0) or tri-methylated (me3) H3K9 peptide (aa 1–20+Cys), we found that the WT CEC-4 CD bound a H3K9me3 peptide specifically, while the CEC-4 cd-2YA mutant fragment did not (Figure 3B).

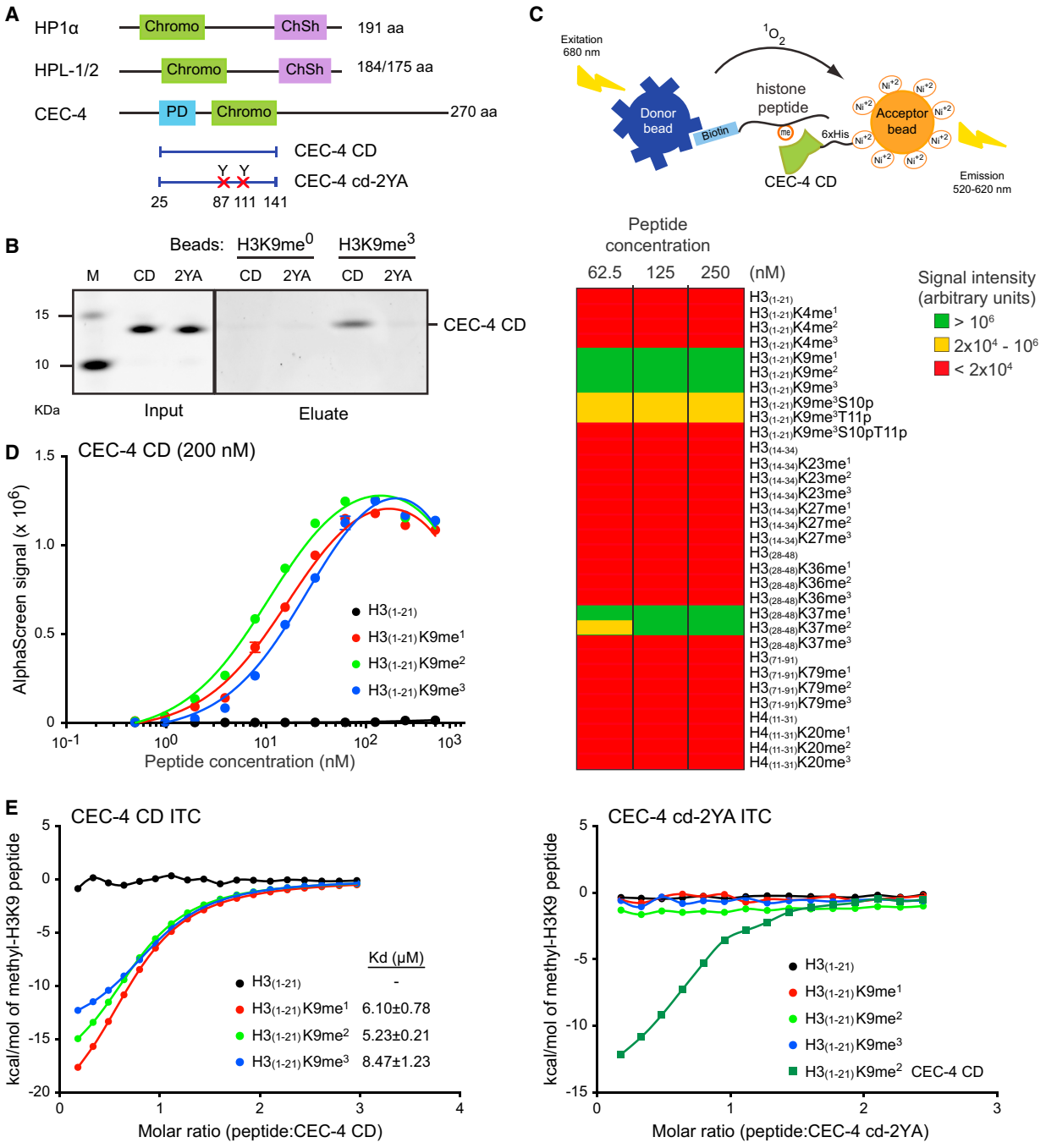

Figure 3. CEC-4 CD Binds Methylated H3K9 Peptides

(A) Schematic comparison of *H. sapiens* HP1α, *C. elegans* HPL-1/2 and CEC-4. CD (green), purple: chromoshadow (ChSh) domain, blue: conserved PD. Purified CEC-4 CD fragments in blue; red X = Y87A and Y111A mutations.

(B) Pull-down of recombinant His-tagged CEC-4 CD fragments (A) by unmodified or me3-H3K9 resin-immobilized peptides. Protein visualized by SYPRO Ruby staining.

(C) AlphaScreen scheme: donor and acceptor microbeads coated with 188 different biotinylated peptides and His-tagged CEC-4 CD, respectively. Interaction produces a fluorescent signal through singlet oxygen ($^1O_2$) transfer from donor to Ni^{+2} ions on acceptor beads. Three peptide concentrations tested with equal amounts of CEC-4 CD (200 nM). Color-coded results reflect signal intensity (see Table S4 for rest of library).

(D) Dose-response binding curves for indicated H3K9 peptides with CEC-4 CD in AlphaScreen assay.

(E) Quantitation of binding affinities of H3K9 peptides to CEC-4 CD and cd-2YA mutant determined by ITC. In (D) and (E) solid lines represent a nonlinear least-square fit using one-sided fitting equation.

See also Figures S3 and S4.

We evaluated CEC-4 CD specificity by scoring interaction with a range of modified and unmodified histone tail peptides in a quantitative chemiluminiscence assay (Alpha Screen; Taouji et al., 2009). We screened the ALTA Biosciences library, which contains 188 histone tail ligands each with a different epigenetic modification (Table S4; Figure 3C). Consistent with the pull-down assay, strong interaction signals were detected almost exclusively between CEC-4 CD and a peptide of histone H3 bearing me1-, me2-, or me3-K9. Intriguingly, CEC-4 affinity for H3K9me3-containing peptides was compromised by additionally phosphorylating S10 and/or T11 (Figure 3C and Table S4). Such modifications have been proposed to release HP1 from chromatin in mitosis (Fischle et al., 2003a).

The interaction of CEC-4 CD with methylated H3K9 was confirmed by serial dilutions of each peptide in the AlphaScreen (Figure 3D) and IC_{50} (half maximal inhibitory concentration) was determined by peptide displacement. CEC-4 CD bound to me1-, me-2, or me3-K9 H3 peptides with similar affinities (Figure S3C). We then measured binding energies using Isothermal Titration Calorimetry (ITC). Dissociation constants (Kd) for CEC-4 CD bound to the methylated H3K9 peptides ranged from 5 to 9 μM. There was a slight preference for me2 and no detectable binding to the unmodified H3 peptide (Figures 3E, S3D, and S4A). Similar Kd values have been reported for human, mouse, and *Drosophila* HP1 homologs (reviewed in Steffen et al., 2012). The interaction requires the characteristic aromatic cage of the CEC-4 CD, as CEC-4 cd-2YA gave only background level interaction (Figures 3E and S4A). We conclude that CEC-4 CD recognizes H3K9me1, me2, and me3. Its affinity for all three methyl-H3K9 forms is consistent with the fact that heterochromatic arrays remain peripherally sequestered in the *set-25* mutant, which has H3K9me1/me2, but no H3K9me3 (Towbin et al., 2012).

In addition to its strong affinity to H3K9me-peptides, we detected interaction of the CEC-4 CD with me1- or me-2 H3K37 (aa 28–48; Figures 3C and S3B; Table S4). Methylation of H3K37 has not been reported to occur in native *C. elegans* chromatin and was not detected in our own mass spectrometry of embryonic histones (data not shown; Towbin et al., 2012). To date, the only documented occurrence of H3K37me1 is in tandem with H3K36me1 at origins of replication in budding yeast, outside of S phase (Unnikrishnan et al., 2010). However, CEC-4 did not recognize H3K36me. In addition, CEC-4 CD had significantly lower affinity for H3K37me than for methylated H3K9 (Figures S3D, S3E, and S4B). Thus, the physiological relevance of this second binding site is unclear.

The CEC-4 CD Is Essential for Heterochromatin Anchoring in Embryos, but Is Redundant in Differentiated Tissues

The single-copy CEC-4-mCh fully restores array anchoring in the *cec-4* null mutant. It is enriched on the anchored heterochromatic reporter due to its affinity for H3K9me (Figures 4A and S2C). An identical integration construct bearing the aromatic cage mutations described above (CEC-4cd-2YA-mCh) did not complement for anchoring, nor did it bind to the array (Figure 4B). Thus, disruption of the CEC-4 CD aromatic cage is sufficient to disrupt the anchoring of heterochromatin at the INM in embryos and the binding of methylated H3K9 peptides in vitro. On the other hand, CD integrity is not involved in CEC-4 localization, given that CEC-4cd-2YA-mCh forms a perinuclear ring like WT CEC-4-mCh (Figure 4B).

In contrast to the situation in embryos, the ablation of *cec-4* did not provoke relocalization of the heterochromatic array in differentiated L1 larval tissues, such as intestine and hypoderm (Figure 4C). The same was observed in the *met-2 set-25* double mutant (Towbin et al., 2012). It appears, therefore, that compensatory or redundant mechanisms for anchoring heterochromatin are induced in the differentiated tissues of the L1 larva. It is unclear whether these mechanisms are fully independent of CEC-4 or if CEC-4 contributes to tissue-specific anchoring in a redundant manner (Figure 2D). Both the redundancy and tissue-specificity aspects are reminiscent of lamin A/C and LBR effects in mice (Solovei et al., 2013).

Loss of CEC-4 Alters the Spatial Distribution of Endogenous Chromosome Arms

Thus far integrated transgenic arrays were used as a surrogate for heterochromatin. To see if CEC-4 affects the distribution of endogenous chromatin, we performed LEM-2 chromatin immunoprecipitation coupled to deep sequencing (ChIP-seq) in WT and mutant embryos. *C. elegans* chromosomes are holocentric and lack pericentric satellite heterochromatin but are enriched for H3K9 methylation and repetitive elements along the distal arms of all autosomes and the left arm of chromosome X(Gerstein et al., 2010; Ikegami et al., 2010). Previous ChIP and lamin-Dam-ID studies had shown that chromosome arms are proximal to the INM in *C. elegans* embryos, larvae, and adults. Moreover, the loss of H3K9 methylation (*met-2 set-25*) was enough to compromise INM-anchoring of the repeat-rich autosomal arms (González-Aguilera et al., 2014; Ikegami et al., 2010; Towbin et al., 2012).

We used ChIP-seq to map LEM-2-binding along endogenous sequences in WT, *cec-4*, and *met-2 set-25* embryos. Euclidian distances were measured showing high similarity between replicas. Hierarchical clustering resolved WT LEM-2 ChIP as different from either mutant, while the *met-2 set-25* and *cec-4* mutants clustered together (Figure S5A). All input samples were very similar. Plotting the LEM-2 signals along the chromosomal sequences showed that distal arms lost anchoring in *cec-4* null embryos to the same degree as in the H3K9me-deficient *met-2 set-25* mutant (Figures 5A and S5B).

As expected, LEM-2 binding along wild-type autosomes was polarized: chromosome arms were enriched at the INM and centers were depleted. This polarization was reduced for each autosome similarly in both mutants. The integrated LEM-2 signal on each chromosomal extremity was plotted against the signal integrated over each center, to visualize the effects of the mutations (Figure 5B). We conclude that the INM binding of the endogenous repeat-rich domains on chromosome arms requires H3K9 methylation and its recognition by CEC-4. Nonetheless, other positioning pathways likely exist, since chromosome extremities were displaced to different degrees.

In many organisms heterochromatin is also clustered around the nucleolus, the site of rDNA transcription by RNA Pol I (Padeken and Heun, 2014). The *C. elegans* rDNA is found on the

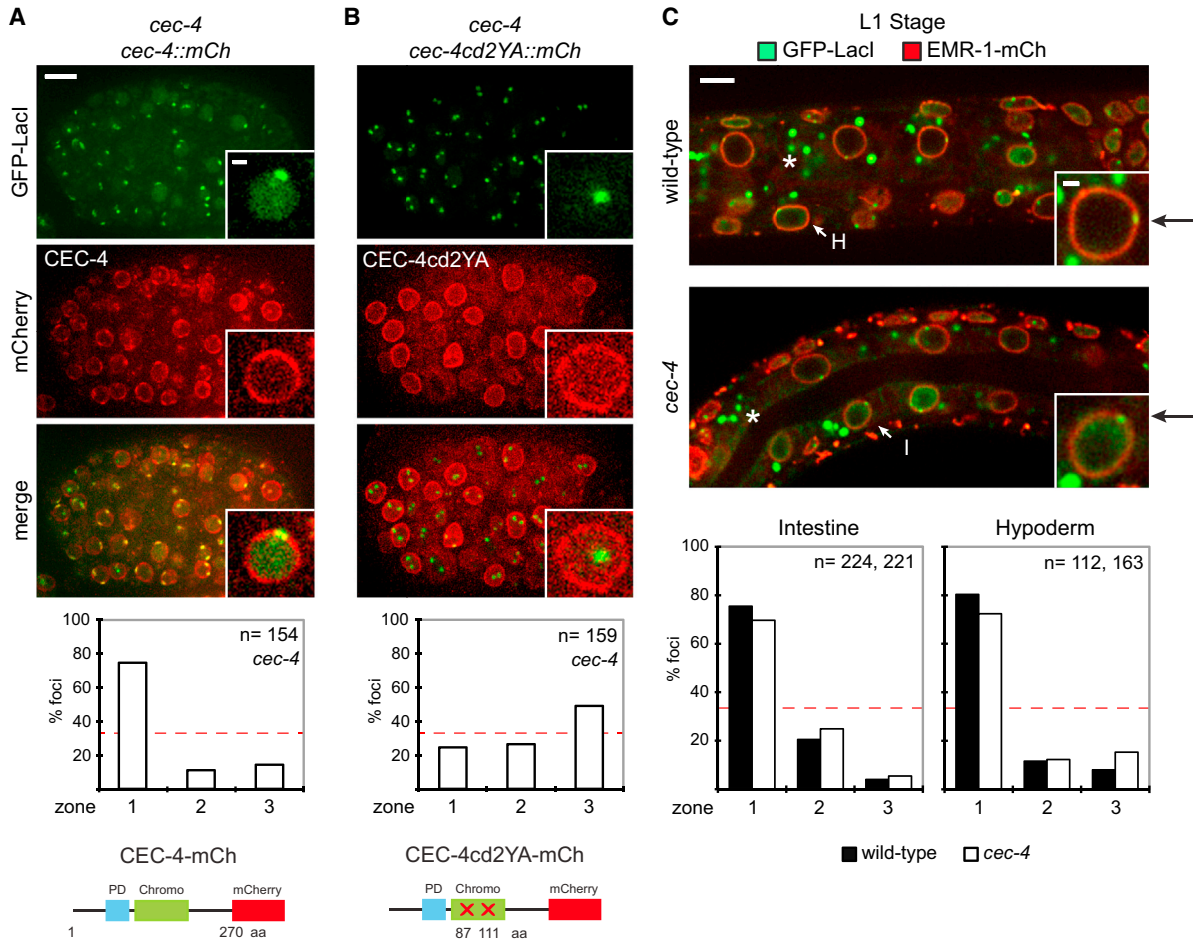

Figure 4. CEC-4 CD-H3K9me Recognition Required for Heterochromatic Array Anchoring in Embryos, while Larvae Have Compensatory Pathway(s)

(A) Z-projections showing co-localization of *gwIs4* GFP-LacI signal with CEC-4-mCh in *cec-4* null embryos. Insets: single nucleus. Zoning assay for array distribution, n = foci scored. Schematic view of transgenic protein expressed.

(B) Same as (A), except that CEC-4 transgene contains CD mutations (CEC-4cd2YA-mCh). Pair-wise comparison of (A) and (B) graphs with p value < 0.001, χ^2 test.

(C) Single plane images of L1 stage worms containing *gwIs4* and EMR-1-mCh in indicated genotypes. White arrows indicate hypoderm (H) or intestine (I) cells; * marks granule intestine foci. Insets: intestine nuclei, black arrows = array foci. Zoning assay on indicated tissues, n = foci scored per condition. Scale bars, 5 μm in embryos/L1 sections and 2 μm in single nuclei.

See also Figure S2.

distal arms of ChrI and ChrV in heterochromatic regions (Figure 5A). We therefore checked whether nucleoli change their radial position in the *cec-4* mutant by staining for a conserved marker of the nucleolus, fibrillarin (Figure 5A). In embryos lacking CEC-4, nucleoli shifted quantitatively away from the perinuclear lamin (Figure 5C), confirming that CEC-4 contributes profoundly to the positioning of endogenous chromatin in embryos.

Monitoring Gene Expression in the Absence of CEC-4

It has long been debated whether nuclear localization is sufficient to influence gene expression. To test this we generated gene expression profiles (RNA-seq) of WT, *met-2 set-25*, and *cec-4* mutant embryos. Pairwise comparison of two independent biological replicas of mutant and WT samples showed a reproducible upregulation (>4-fold) of a large number of genes in embryos lacking H3K9 methylation (*met-2 set-25)*, whereas the loss of CEC-4 led to robust upregulation of a single gene, *srw-85* (Figure 5D). The modest effect of *cec-4* mutation on gene expression is consistent with our results from the array-borne GFP-LacI (Figure 1F). In the case of endogenous genes in early embryos, the lack of derepression might simply reflect the absence of transcription factors needed for tissue-specific gene expression. However, given that the loss of H3K9 methylation does upregulate many genes in embryos, it is more likely that H3K9me-ligands other than CEC-4 mediate gene repression. Analysis of datasets in 500 bp windows across the whole genome, for potential changes in non-genic regions, yielded similar results to the gene-centric analysis; only genomic

windows spanning the *srw-85* locus were reproducibly upregulated in *cec-4(ok3124)* (Figure S5C).

The dramatic induction of *srw-85* (> 16-fold) upon displacement from the INM is a notable exception (Figures 5A and 5D–5F). Its derepression correlates strongly with subnuclear position, and not with H3K9 methylation state, as it was not derepressed in *met-2* or *set-25* single mutant embryos, which retain anchoring (Towbin et al., 2012). SRW-85 is a member of the *C. elegans* chemoreceptor family of seven transmembrane G protein-coupled receptors (7TM-GPCR). The gene sits on ChrV-right, along with 90% of the 145 *srw* family members, and is normally expressed in non-ASE type (gustatory) neurons (Etchberger et al., 2007). Given that surrounding genes are not equally upregulated (Figure S5D), we conclude that *srw-85* is an exception rather than the rule. CEC-4, unlike other H3K9 methylation readers, serves primarily to position chromatin, although the H3K9me2/me3 modification it recognizes also mediates transcriptional silencing.

Perinuclear Anchoring Helps Stabilize an Ectopically Induced Cell Differentiation Program

We examined *cec-4* mutant worms for developmental defects. Surprisingly, we found no drop in brood size nor embryonic lethality (either at 20°C or 26°C). We scored no reproducible differences in the developmental timing of embryonic stages, and except for a slight increase in the proportion of male progeny, proliferation appeared normal under standard laboratory conditions (data not shown). Given that alternative anchoring pathways are induced in L1 larvae, we sought to test the role of CEC-4-mediated chromatin tethering specifically in embryos.

To this end, we used an assay that induces muscle cell specification in embryos in response to a cell-type independent burst of HLH-1 (MyoD) expression, a master regulator for muscle differentiation (Fukushige and Krause, 2005). Induction of HLH-1 is driven by the *hsp-16.2* heat-shock (HS) promoter on a transgene array (*HS::hlh-1*) and is achieved by placing embryos at 34°C for 10 min; about 24 hr after, efficiency of induction can be monitored by morphology and muscle-specific gene expression (Figure 6A). To test whether *cec-4* mutant alters the efficiency of muscle induction, we introduced the *HS::hlh-1* transgene and the *gwIs4* array into WT and *cec-4* mutant, using the latter as a fluorescent reporter for muscle-specific gene expression (*myo-3p::RFP*). At 40 min after HS, *hlh-1* mRNA was expressed at comparable levels in both genotypes, as was the downstream muscle specific myosin, *myo*-3, at 24 hr after HS (Figure 6B).

We induced HLH-1 expression at different time points during synchronized embryonic growth and monitored the outcome by microscopy. A striking difference between WT and mutant embryos was noted when we exposed the bean stage (~560 cells; 300 min growth at 22.5°C) to the HLH-1 pulse (Figure 6C–6F). Whereas 100% of the wild-type embryos turned into lumps of muscle-like cells with muscle-twitching behavior, among the heat-shocked *cec-4* null embryos a reproducible 25% continued to develop, reaching the point of hatching from the eggshell despite their documented HLH-1 expression (Figure 6C and 6D). These hatched larva-like organisms were clearly abnormal, as they were disrupted by the slightest manipulation and failed to survive. Nonetheless, they had progressed well beyond embryonic stages and did not manifest the muscle morphology of their WT counterparts (Figure 6C and 6E). To rule out a general temperature sensitivity of *cec-4* deletion, we exposed the mutant embryos lacking the *HS::hlh-1* to HS, yet observed no effect on development: all embryos yielded normal larvae (Figure 6C).

After HLH-1 induction, the fluorescent reporter *myo-3p::RFP* was detected in patches of cells in both genotypes, with an overall higher intensity in WT cells (Figures 6E and S6A). The subset of *cec-4* mutant embryos that became muscle, like the WT embryos, showed twitching behavior. In contrast, the *cec-4* null hatched larva-like worms had a dispersed *myo-3p::RFP* expression pattern throughout the organism, which was distinct from the usual *myo-3* expression pattern in L1 larvae body wall muscle (Figure 6E). We could complement the *cec-4* deletion by introducing the tagged CEC-4-mCh; indeed, this restored the normal WT response to HLH-1 induction, and 100% of the embryos became muscle cells. In contrast, complementing with CEC-4cd2YA-mCh yielded results reminiscent of the *cec-4* null, albeit less penetrant (Figure S6B).

The inefficiency of the *cec-4* mutant for muscle tissue conversion in response to MyoD, appears to reflect an inability to lock in the muscle specification program and repress other differentiation programs. In other words, despite high level expression of HLH-1, the *cec-4* mutant appeared to remain more permissive to other differentiation signals and therefore continued to develop other tissues while expressing muscle-specific genes. We confirmed this by tracking an intestine cell marker that is not expressed in either genotype at the bean stage when we perform HS. The reporter (kind gift of G.-J. Hendriks and H. Grosshans, personal communication) expresses a GFP-tagged nuclear pore protein from an L1-stage gut-specific promoter (*nhx-2*). At 18 hr after HS, we find that the fluorescent gut marker (*nhx-2p::npp-9::GFP*) was detected in 94.5% of *cec-4* mutant embryos, but significantly less in WT (39.6%; Figure 6F).

Given the fragility of the hatched larvae-like structures, neither immunostaining nor manual isolation for RNA-seq was possible. However, their morphology alone allows one to conclude that a significant fraction of the *cec-4* mutant embryos failed to restrict gene expression to the muscle program. Thus, the perinuclear sequestration of silent genes by CEC-4 in embryonic stages appears to help stabilize the HLH-1-induced muscle cell fate.

DISCUSSION

Perinuclear Chromatin Sequestration through Histone H3K9 Methylation

Heterochromatin, or transcriptionally silenced chromatin, is often juxtaposed to the INM in eukaryotic organisms. Previous work has identified H3K9 methylation as essential for heterochromatin anchoring in worms (Towbin et al., 2012) and important in mammalian cells (Kind et al., 2013; Pinheiro et al., 2012). However, no INM anchor that selectively binds this epigenetic mark was known. Here we describe CEC-4 as a perinuclear *C. elegans* protein which is necessary for the tethering of endogenous chromatin bearing me1-, me2-, or me3-H3K9 histones. Its CD's aromatic cage is necessary for H3K9me binding in vitro and

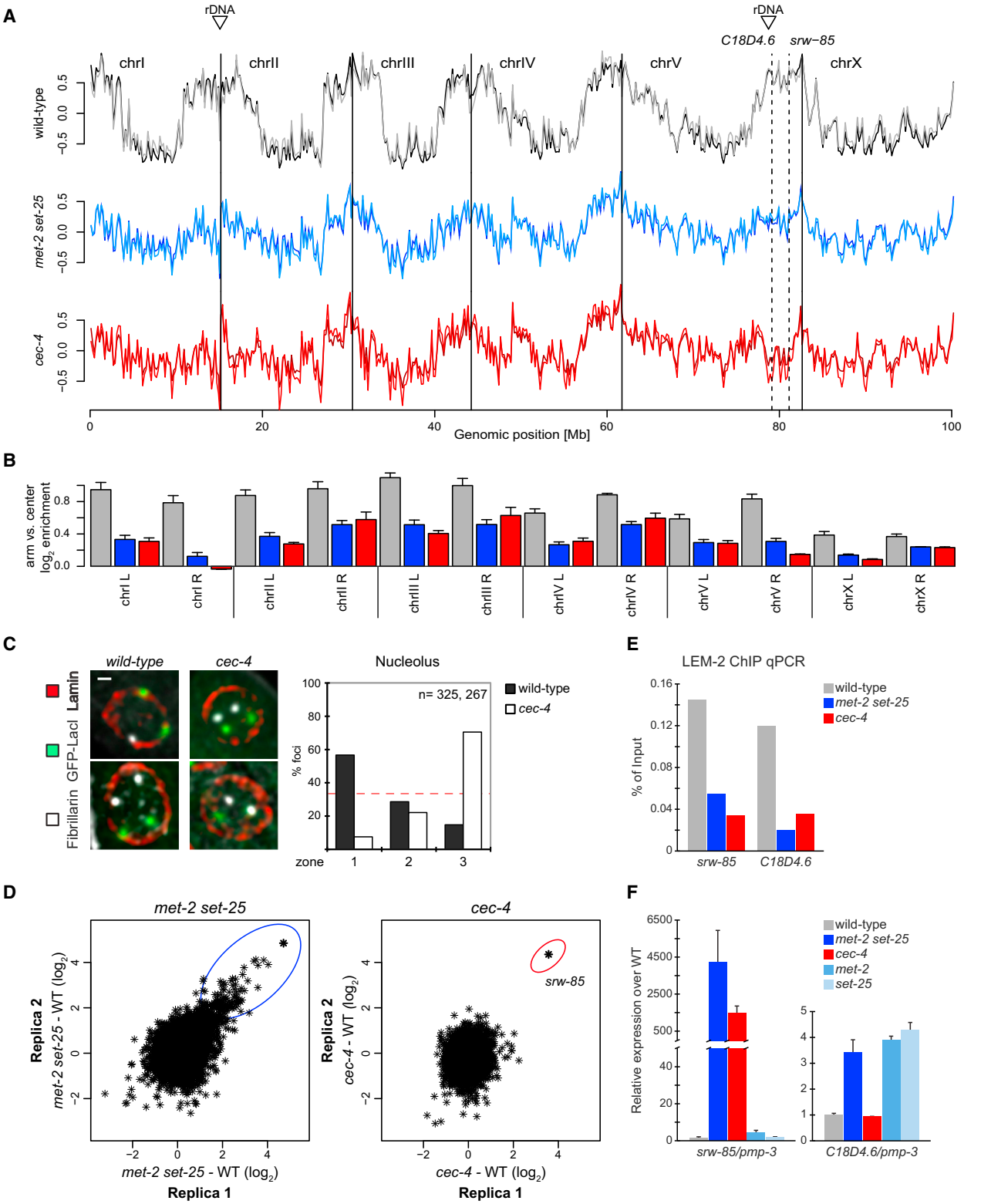

Figure 5. CEC-4 Influences Anchoring of Endogenous Chromatin and Nucleoli, but Not Silencing

(A) LEM-2 ChIP-seq profiles over chromosomes are shown for two independent replicas of early embryos of WT (gray/dark gray), *met-2 set-25* (blue/light blue), and *cec-4* (red/light red) mutants. Dashed line shows *srw-85* and *C18D4.6* genes, and triangles show rDNA clusters.

(legend continued on next page)

in vivo. Ablation of CEC-4 delocalizes heterochromatin, but does not necessarily lead to its derepression, whereas loss of histone H3K9 methylation compromises both. Other H3K9me-ligands (HP1 homologs HPL-1 and HPL-2, or LIN-61) contribute to transcriptional repression by binding H3K9me2 or me3, but do not mediate perinuclear anchoring. This bifurcation in function of a single methylated lysine in a histone tail, through divergent sets of methyl-lysine readers, provides a paradigm for how epigenetic states can coordinate distinct activities. In this case, chromatin can be anchored without silencing and silenced without anchoring, even though the two functions are correlated through H3K9 methylation. H3K9me1/me2 is sufficient for tethering through CEC-4, while H3K9me3 is needed for gene repression mediated by other H3K9me-readers (Figure 7). It remains to be seen if CEC-4 and other H3K9me readers interact.

CEC-4 Contributes to the Robustness of Ectopically Induced Differentiation

This finding gave us the opportunity to examine what happens during development when heterochromatin anchorage is compromised, without loss of H3K9 methylation or the transcriptional repression it mediates. Although *cec-4* mutant embryos yielded normal adult worms when development proceeded unperturbed, we were able to demonstrate a function for heterochromatin anchoring in early development by inducing muscle differentiation with ectopic expression of MyoD (HLH-1). Unlike the WT strain, a significant fraction of *cec-4* deficient embryos (about 25%) did not maintain the muscle fate provoked by HLH-1 induction (Figure 6) and continued to develop. In contrast, the induction of muscle cell fate and repression of alternative programs of differentiation occurred in 100% of the WT bean-staged embryos. The failure of the mutant to sustain an HLH-1-induced muscle program could either mean that CEC-4 actively supports muscle-specific gene expression, or else that it helps repress other tissue-specific programs. Given that muscle markers were expressed in heat-shocked *cec*-4 mutant embryos and that muscles develop normally in the mutant without HS, we favor the latter hypothesis: upon loss of CEC-4-mediated heterochromatin sequestration, non-muscle programs may not be properly repressed during ectopic muscle induction. This is consistent with earlier studies that showed a clear spatial segregation of active and inactive tissue-specific genes in differentiated cells of *C. elegans* larvae (Meister et al., 2010).

Because *cec-4* ablation per se seems to have a very limited effect on normal transcription patterns, we propose that CEC-4-mediated tethering does not control gene repression directly, but instead influences events that prepare genes for tissue-restricted patterns. These events might be the remodeling of epigenetic states (e.g., through histone deacetylases that bind the nuclear envelope [Zullo et al., 2012]), the sequestration of promoters away from their regulators, or the timing of replication of tissue-specific genes (Hiratani et al., 2008). These changes may not directly repress transcription, but rather change the compaction state of chromatin as a prerequisite for stage-specific repression. Indeed, the INM-released arrays in *cec-4* mutants are less compact (Figure 1), although we did not detect less histone H3K9 methylation by genome-wide ChIP (data not shown).

ESC differentiation studies have shown that the timing of replication of genes, and their reassembly into chromatin following replication, are compromised by spatial misorganization (reviewed in Hiratani et al., 2009). Moreover, it has been suggested that altered replication timing precedes commitment to differentiation-related expression patterns (Hiratani et al., 2008). Thus, we propose that CEC-4-mediated chromatin positioning and compaction may contribute to a replication timing program, which in turn reinforces appropriate gene repression. We expect that the compromised commitment of *cec-4* mutant is not restricted to muscle differentiation, but rather is a general mechanism that becomes important when normal development is perturbed. Whereas the ectopic HLH-1 induction is definitely a strong perturbation, less dramatic perturbations during development may rely on spatial sequestration to ensure proper patterns of tissue-specific gene expression.

Extending Nuclear Anchoring Mechanisms to Other Organisms

Although CEC-4 is the first CD protein reported to form a ring at the nuclear perimeter autonomously, CEC-4's anchoring function becomes either redundant or replaced by other mechanisms in L1 larvae, the stage at which most cells reached terminal differentiation. We note that heterochromatin can be anchored in differentiated tissues without H3K9 methylation, and without HPL-1, HPL-2, or LIN-61 (Studencka et al., 2012b; Towbin et al., 2012). Another CD protein, CEC-3, had no impact on embryonic array distribution in our screen, although it appears to restrain the expression of a neuronal specific transcription factor in larvae (Greer et al., 2014; Zheng et al., 2013). Thus, four H3K9me binders—HPL-1, HPL-2, LIN-61 and CEC-3—contribute to transcriptional silencing during development, while CEC-4 specifically sequesters H3K9me-containing chromatin in embryos. CEC-4 may also contribute to heterochromatin anchoring in some differentiated worm tissues, albeit in a redundant manner (data not shown).

(B) LEM-2 ChIP enrichment of arms (left or right) compared with corresponding center plotted for each genotype. Error bars = SEM.
(C) Representative merged color, single plane nuclei are shown for WT and *cec-4* mutant stained for anti-fibrillarin, lamin, and *gwIs4* array (anti-GFP), Scale bar, 2 μm. Zoning assay of nucleolar foci in 50–250 cell stage embryos, n = foci scored; pair-wise comparison p value < 0.001, χ^2 test.
(D) Relative gene expression profiles as scatter plots of *met-2 set*-25 and cec-*4* mutants versus WT early embryo extracts. Genes significantly changed are circled, bold star = *srw-85*.
(E) LEM-2 ChIP qPCR for *srw-85* and *C18D4.6* genes. ChIP values as a percentage of respective input DNA.
(F) Gene expression levels of indicated genotypes by qRT-PCR, normalized to *pmp-3* gene and shown relative to WT expression. Error bars = SEM of 3 biological replicas.
See also Figure S5.

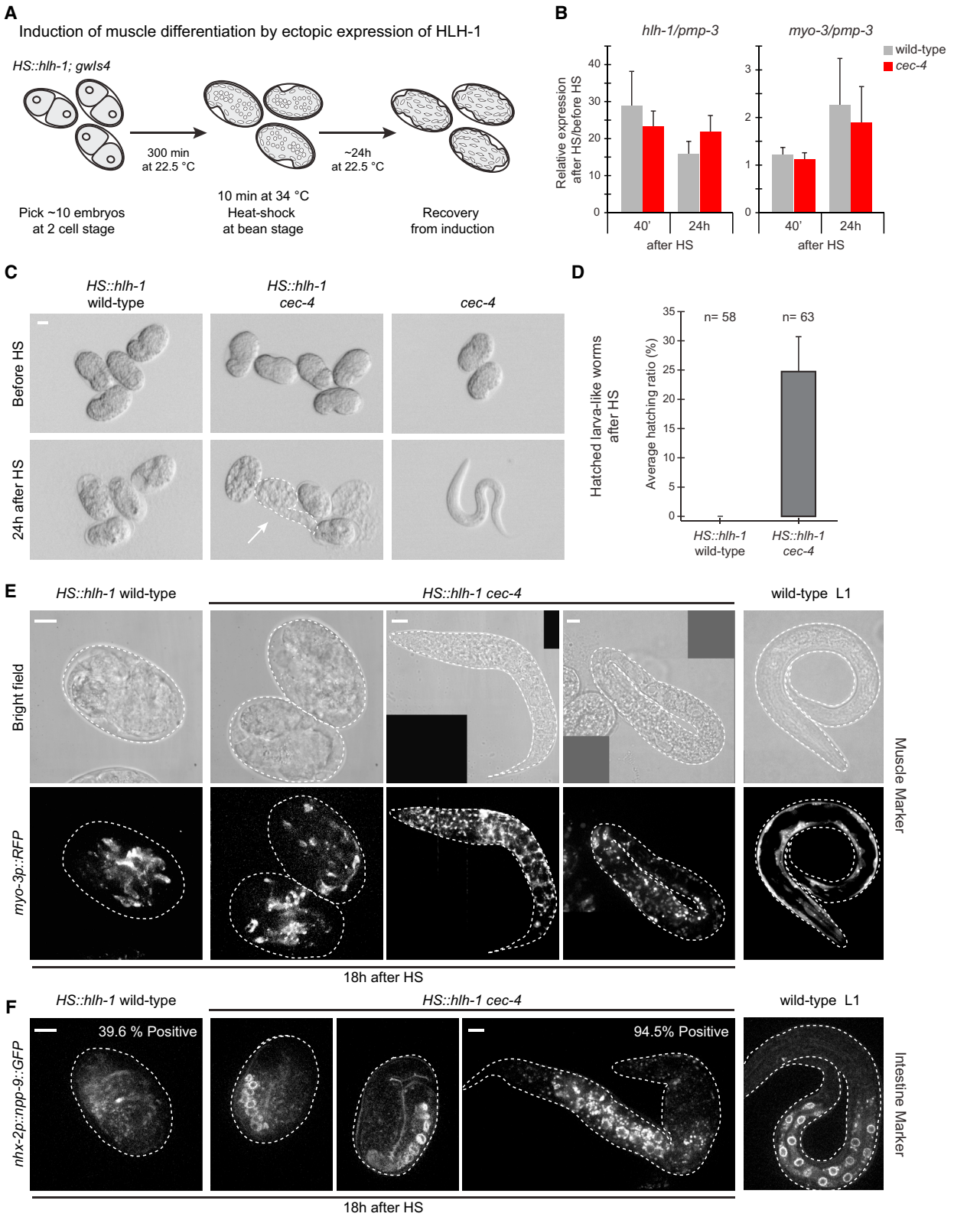

Figure 6. Lack of CEC-4 Impairs the Commitment of Embryos to a Forced Muscle Differentiation

(A) Experimental flow for forced muscle differentiation by HS induction of the master regulator HLH-1. See main text and Supplemental Experimental Procedures.

(legend continued on next page)

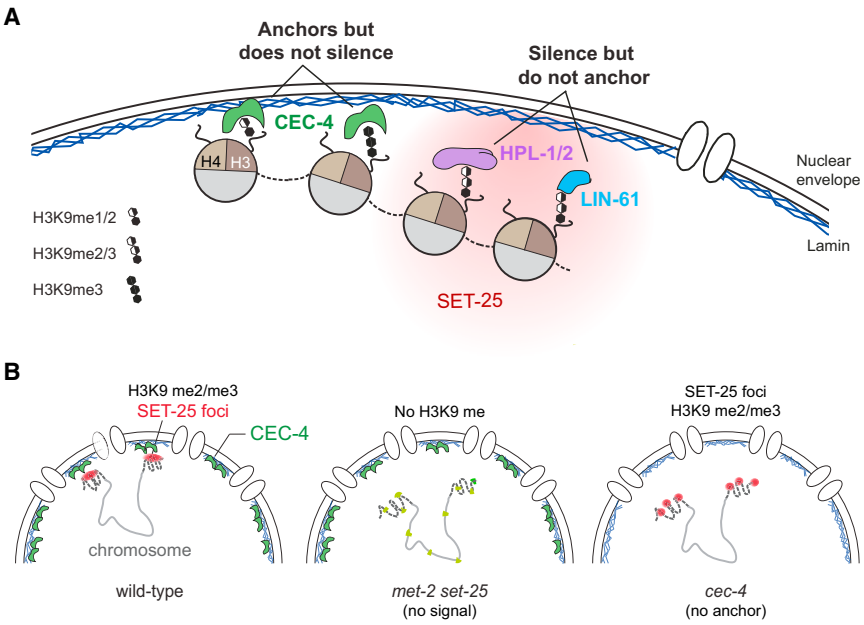

Figure 7. Different H3K9 me1, me2, and/or me3 Ligands Mediate Anchoring and Transcriptional Repression

(A) Model showing the split function of H3K9me for anchoring and repression thanks to different ligands.

(B) Summary of chromosome organization in early embryos in indicated genotypes. In WT embryos H3K9 methylation-enriched chromosome arms (dash lines) bind CEC-4 at the INM and are enriched for SET-25 (red foci). Lack of H3K9 methylation (*met-2 set-25* mutant) releases heterochromatin in embryos and derepresses genes (light green spots). Loss of CEC-4 compromises chromatin position, but does not induce gene expression.

We have not identified a direct homolog of CEC-4 in non-nematode species, and we suspect that this protein's two functions, INM-association and specific H3K9me-recognition, may be embodied in two separate polypeptides in mammals. As mentioned, an example of such split function may be the mammalian nuclear membrane-spanning protein PPR14, which can bind HP1. The interpretation that PPR14 anchors heterochromatin through this ligand is complicated, however, by the pleiotropic effects its loss has on nuclear shape (Poleshko et al., 2013). Similarly, the mammalian LBR may bind HP1 and carries a Tudor domain with a preference for H4K20me2 in vitro (Hirano et al., 2012; Ye and Worman, 1996). Whereas there is no compelling evidence that either H4K20me2 or HP1 mediate perinuclear anchoring in early development, LBR itself is implicated in the spatial organization of the genome in differentiated mammalian cells, particularly in cells that do not express Lamin A/C (Clowney et al., 2012; Solovei et al., 2013). Unfortunately, indirect effects again complicate the interpretation of LBR ablation, since this transmembrane protein has sterol reductase activity that regulates cholesterol metabolism and maintains appropriate spacing between inner and outer nuclear membranes (Holmer et al., 1998). Thus, both indirect effects and redundancy among anchors have made it difficult to characterize chromatin-tethering pathways in mammalian cells. Nonetheless, it is possible that these INM proteins function through chromatin binding proteins that resemble CEC-4. Separation of function mutations that uniquely compromise chromatin positioning will be needed to define these pathways unequivocally.

In other species, repressive epigenetic marks other than H3K9 methylation may contribute to the spatial sequestration of repressed chromatin. In mouse 3T3 embryonic fibroblasts (MEFs), the Polycomb mark H3K27me3 was reported to contribute to perinuclear positioning at the edges of LADs (Harr et al., 2015). In worms, the loss of Polycomb components MES-3 and MES-6 led to derepression of our heterochromatic reporter in embryos (Towbin et al., 2012), but did not trigger release from the nuclear periphery. Moreover, in most species, the H3K27me3-positive foci found in differentiating cells are not perinuclear (Eberhart et al., 2013). This, however, does not preclude the possibility that combinatorial epigenetic signatures target chromatin to the INM.

The relative simplicity of the *C. elegans* system and the conserved nature of its epigenetic and developmental programs has allowed us to dissect nuclear organization with a genetic approach. Given the conserved role H3K9me has in chromatin positioning, it is likely that factors with analogous functions as CEC-4 exist elsewhere. Functional screens in compromised backgrounds will be able to shed light on relevant anchors in differentiated cells. Disruption of specific anchors in differentiated tissues will extend our understanding of the function of heterochromatin sequestration.

(B) Quantitation of *hlh-1* and muscle specific *myo-3* expression by qRT-PCR in indicated genotypes, 40 min and 24 hr after HS relative to before HS; data normalized to *pmp-3* gene. Error bars = SEM of 3 biological replicas.

(C) Stereoscopic representative images of synchronized bean stage embryos before and 24 hr after HS. As control, *cec-4* null embryos lacking *HS::hlh-1* were treated similarly. Hatched larva-like worms highlighted with dashed white line and arrow. Scale bar, 20 μm.

(D) Average hatching ratio after HS according to genotype in bar plot. Error bars = SEM of six independent assays, n = total embryos tested.

(E) Muscle reporter pattern for indicated genotypes. Z-projections of bright field and fluorescent *myo-3p::RFP* (from *gwIs4*) imaging taken 18 hr after HS. Wild-type L1 imaged independently. Scale bars = 5 μm.

(F) Intestine reporter *nhx-2p::npp-9::GFP* pattern for indicated genotypes. Z-projections taken as in (E). n = 3, total number of embryos scored = 53 and 55 respectively. Scale bars,5 μm.

See also Figure S6.

EXPERIMENTAL PROCEDURES

RNAi Screen

RNAi was performed at 22.5°C by placing L1 worms on feeding plates as previously described (Timmons et al., 2001). For the list of genes used (Table S3) in the RNAi screen see Supplemental Experimental Procedures.

Microscopy

Microscopy was carried out on a spinning disc confocal microscope, using 2% agarose pads for live-microscopy or poly-lysine coated slides for fixed samples. Acquisition and analysis of array and nucleolus distribution, array spot volume, expression levels of GFP-LacI and CEC-4-mCh, and enrichment of CEC-4 over array are online, along with a description of super resolution-structured illumination microscopy (SR-SIM; Elyra S.1 [Carl Zeiss]).

AlphaScreen Direct Binding and In Vitro Assays

Purified recombinant His-tagged CEC-4 CD (200 nM) was screened for its binding to modified histone peptides with the ALTA Biosciences peptide array system (Alta Biosciences, UK) and the AlphaScreen assay. Details for protein purification, peptide pull down and ITC are in Supplemental Experimental Procedures.

LEM-2 ChIP-Seq and RNA-Seq

Early embryonic progeny was harvested after synchronization (60–65 hr depending on each strain) for WT, *met-2 set-25,* and *cec-4* mutant strains in two independent biological replicates. LEM-2 ChIP was performed as described (Ikegami et al., 2010). Total RNA was extracted by phenol/chloroform, further purified, and depleted for rRNA. Detailed information about library preparation and data analysis is described in Supplemental Experimental Procedures.

Heat-Shock Induced Muscle Differentiation

Two cell-stage embryos, of different genetic backgrounds containing the *HS::hlh-1* transgene, were allowed to develop until bean stage (300 min at 22.5°C). HS at 34°C for 10 min was performed either on 2% agarose pads or on liquid with a thermal cycler with in situ slide block. After recovery for 24 hr, evaluation of hatching larva-like worms was determined by stereomicroscopy, and reporter markers by spinning disc confocal microscopy. Details for qPCR of HS samples is described in Supplemental Experimental Procedures.

ACCESSION NUMBERS

The accession numbers for the ChIP-seq and RNA-seq data reported in this paper is NCBI Gene Expression Omnibus GEO: GSE74134.

SUPPLEMENTAL INFORMATION

Supplemental Information includes Supplemental Experimental Procedures, six figures, and seven tables and can be found with this article online at http://dx.doi.org/10.1016/j.cell.2015.10.066.

AUTHOR CONTRIBUTIONS

Conceptualization, A.G.-S., B.D.T., and S.M.G.; Methodology, A.G.-S., B.D.T., and D.S.C.; Validation, A.G.-S., V.K., D.S.C.; Formal Analysis, D.G., M.H.H; Investigation, A.G.-S., B.D.T., V.K., D.S.C., M.H.H, L.G., L.W., T.Y., X.W.; Resources, K.Z.; Writing – Review & Editing, A.G.-S., B.D.T., D.S.C., S.M.G.; Supervision, K.Z., S.M.G.; Funding Acquisition, S.G.M.

ACKNOWLEDGMENTS

Some strains were provided by the *Caenorhabditis* Genetics Center (CGC) of the NIH Office of Research Infrastructure Programs (P40 OD010440). We thank G-J. Hendriks, H. Grosshans, R. Thierry, P. Zeller, A. Peters, P. Hein, Y. Gruenbaum, and P. Askjaer for reagents and materials. We thank J. Lieb and K. Ikegami for training A.G.-S. in LEM-2 ChIP. We thank the FMI Worm, Genomics, Protein Structure, Protein Analysis, and Microscopy facilities for valuable advice and support. A.G.-S. was supported by FP7 Marie Curie Network Nucleosome 4D and the SNSF NCCR "Frontiers in Genetics." S.M.G. thanks the FMI and SNSF for support.

Received: July 1, 2015
Revised: October 7, 2015
Accepted: October 27, 2015
Published: November 19, 2015

REFERENCES

Barski, A., Cuddapah, S., Cui, K., Roh, T.-Y., Schones, D.E., Wang, Z., Wei, G., Chepelev, I., and Zhao, K. (2007). High-resolution profiling of histone methylations in the human genome. Cell *129*, 823–837.

Brachner, A., and Foisner, R. (2011). Evolvement of LEM proteins as chromatin tethers at the nuclear periphery. Biochem. Soc. Trans. *39*, 1735–1741.

Clowney, E.J., LeGros, M.A., Mosley, C.P., Clowney, F.G., Markenskoff-Papadimitriou, E.C., Myllys, M., Barnea, G., Larabell, C.A., and Lomvardas, S. (2012). Nuclear aggregation of olfactory receptor genes governs their monogenic expression. Cell *151*, 724–737.

Couteau, F., Guerry, F., Muller, F., and Palladino, F. (2002). A heterochromatin protein 1 homologue in Caenorhabditis elegans acts in germline and vulval development. EMBO Rep. *3*, 235–241.

Eberhart, A., Feodorova, Y., Song, C., Wanner, G., Kiseleva, E., Furukawa, T., Kimura, H., Schotta, G., Leonhardt, H., Joffe, B., and Solovei, I. (2013). Epigenetics of eu- and heterochromatin in inverted and conventional nuclei from mouse retina. Chromosome Res. *21*, 535–554.

Etchberger, J.F., Lorch, A., Sleumer, M.C., Zapf, R., Jones, S.J., Marra, M.A., Holt, R.A., Moerman, D.G., and Hobert, O. (2007). The molecular signature and cis-regulatory architecture of a C. elegans gustatory neuron. Genes Dev. *21*, 1653–1674.

Fischle, W., Wang, Y., and Allis, C.D. (2003a). Binary switches and modification cassettes in histone biology and beyond. Nature *425*, 475–479.

Fischle, W., Wang, Y., Jacobs, S.A., Kim, Y., Allis, C.D., and Khorasanizadeh, S. (2003b). Molecular basis for the discrimination of repressive methyl-lysine marks in histone H3 by Polycomb and HP1 chromodomains. Genes Dev. *17*, 1870–1881.

Fukushige, T., and Krause, M. (2005). The myogenic potency of HLH-1 reveals wide-spread developmental plasticity in early C. elegans embryos. Development *132*, 1795–1805.

Fussner, E., Ahmed, K., Dehghani, H., Strauss, M., and Bazett-Jones, D.P. (2010). Changes in chromatin fiber density as a marker for pluripotency. Cold Spring Harb. Symp. Quant. Biol. *75*, 245–249.

Gerstein, M.B., Lu, Z.J., Van Nostrand, E.L., Cheng, C., Arshinoff, B.I., Liu, T., Yip, K.Y., Robilotto, R., Rechtsteiner, A., Ikegami, K., et al.; modENCODE Consortium (2010). Integrative analysis of the Caenorhabditis elegans genome by the modENCODE project. Science *330*, 1775–1787.

González-Aguilera, C., Ikegami, K., Ayuso, C., de Luis, A., Íñiguez, M., Cabello, J., Lieb, J.D., and Askjaer, P. (2014). Genome-wide analysis links emerin to neuromuscular junction activity in Caenorhabditis elegans. Genome Biol. *15*, R21.

Greer, E.L., Beese-Sims, S.E., Brookes, E., Spadafora, R., Zhu, Y., Rothbart, S.B., Aristizábal-Corrales, D., Chen, S., Badeaux, A.I., Jin, Q., et al. (2014). A histone methylation network regulates transgenerational epigenetic memory in C. elegans. Cell Rep. *7*, 113–126.

Gudise, S., Figueroa, R.A., Lindberg, R., Larsson, V., and Hallberg, E. (2011). Samp1 is functionally associated with the LINC complex and A-type lamina networks. J. Cell Sci. *124*, 2077–2085.

Guelen, L., Pagie, L., Brasset, E., Meuleman, W., Faza, M.B., Talhout, W., Eussen, B.H., de Klein, A., Wessels, L., de Laat, W., and van Steensel, B. (2008). Domain organization of human chromosomes revealed by mapping of nuclear lamina interactions. Nature *453*, 948–951.

Harr, J.C., Luperchio, T.R., Wong, X., Cohen, E., Wheelan, S.J., and Reddy, K.L. (2015). Directed targeting of chromatin to the nuclear lamina is mediated by chromatin state and A-type lamins. J. Cell Biol. *208*, 33–52.

Hirano, Y., Hizume, K., Kimura, H., Takeyasu, K., Haraguchi, T., and Hiraoka, Y. (2012). Lamin B receptor recognizes specific modifications of histone H4 in heterochromatin formation. J. Biol. Chem. *287*, 42654–42663.

Hiratani, I., Ryba, T., Itoh, M., Yokochi, T., Schwaiger, M., Chang, C.W., Lyou, Y., Townes, T.M., Schübeler, D., and Gilbert, D.M. (2008). Global reorganization of replication domains during embryonic stem cell differentiation. PLoS Biol. *6*, e245.

Hiratani, I., Takebayashi, S., Lu, J., and Gilbert, D.M. (2009). Replication timing and transcriptional control: beyond cause and effect–part II. Curr. Opin. Genet. Dev. *19*, 142–149.

Holmer, L., Pezhman, A., and Worman, H.J. (1998). The human lamin B receptor/sterol reductase multigene family. Genomics *54*, 469–476.

Ikegami, K., Egelhofer, T.A., Strome, S., and Lieb, J.D. (2010). Caenorhabditis elegans chromosome arms are anchored to the nuclear membrane via discontinuous association with LEM-2. Genome Biol. *11*, R120.

Kind, J., Pagie, L., Ortabozkoyun, H., Boyle, S., de Vries, S.S., Janssen, H., Amendola, M., Nolen, L.D., Bickmore, W.A., and van Steensel, B. (2013). Single-cell dynamics of genome-nuclear lamina interactions. Cell *153*, 178–192.

Koester-Eiserfunke, N., and Fischle, W. (2011). H3K9me2/3 binding of the MBT domain protein LIN-61 is essential for Caenorhabditis elegans vulva development. PLoS Genet. *7*, e1002017.

Kubben, N., Adriaens, M., Meuleman, W., Voncken, J.W., van Steensel, B., and Misteli, T. (2012). Mapping of lamin A- and progerin-interacting genome regions. Chromosoma *121*, 447–464.

Mattout, A., Aaronson, Y., Sailaja, B.S., Raghu Ram, E.V., Harikumar, A., Mallm, J.P., Sim, K.H., Nissim-Rafinia, M., Supper, E., Singh, P.B., et al. (2015). Heterochromatin Protein 1β (HP1β) has distinct functions and distinct nuclear distribution in pluripotent versus differentiated cells. Genome Biol. *16*, 213.

Meister, P., Towbin, B.D., Pike, B.L., Ponti, A., and Gasser, S.M. (2010). The spatial dynamics of tissue-specific promoters during C. elegans development. Genes Dev. *24*, 766–782.

Meister, P., Mango, S.E., and Gasser, S.M. (2011). Locking the genome: nuclear organization and cell fate. Curr. Opin. Genet. Dev. *21*, 167–174.

Meuleman, W., Peric-Hupkes, D., Kind, J., Beaudry, J.B., Pagie, L., Kellis, M., Reinders, M., Wessels, L., and van Steensel, B. (2013). Constitutive nuclear lamina-genome interactions are highly conserved and associated with A/T-rich sequence. Genome Res. *23*, 270–280.

Minc, E., Allory, Y., Worman, H.J., Courvalin, J.C., and Buendia, B. (1999). Localization and phosphorylation of HP1 proteins during the cell cycle in mammalian cells. Chromosoma *108*, 220–234.

Nestorov, P., Tardat, M., and Peters, A.H. (2013). H3K9/HP1 and Polycomb: two key epigenetic silencing pathways for gene regulation and embryo development. Curr. Top. Dev. Biol. *104*, 243–291.

Nigg, E.A. (1992). Assembly and cell cycle dynamics of the nuclear lamina. Semin. Cell Biol. *3*, 245–253.

Padeken, J., and Heun, P. (2014). Nucleolus and nuclear periphery: velcro for heterochromatin. Curr. Opin. Cell Biol. *28*, 54–60.

Peric-Hupkes, D., Meuleman, W., Pagie, L., Bruggeman, S.W., Solovei, I., Brugman, W., Gräf, S., Flicek, P., Kerkhoven, R.M., van Lohuizen, M., et al. (2010). Molecular maps of the reorganization of genome-nuclear lamina interactions during differentiation. Mol. Cell *38*, 603–613.

Pickersgill, H., Kalverda, B., de Wit, E., Talhout, W., Fornerod, M., and van Steensel, B. (2006). Characterization of the Drosophila melanogaster genome at the nuclear lamina. Nat. Genet. *38*, 1005–1014.

Pinheiro, I., Margueron, R., Shukeir, N., Eisold, M., Fritzsch, C., Richter, F.M., Mittler, G., Genoud, C., Goyama, S., Kurokawa, M., et al. (2012). Prdm3 and Prdm16 are H3K9me1 methyltransferases required for mammalian heterochromatin integrity. Cell *150*, 948–960.

Poleshko, A., Mansfield, K.M., Burlingame, C.C., Andrake, M.D., Shah, N.R., and Katz, R.A. (2013). The human protein PRR14 tethers heterochromatin to the nuclear lamina during interphase and mitotic exit. Cell Rep. *5*, 292–301.

Solovei, I., Wang, A.S., Thanisch, K., Schmidt, C.S., Krebs, S., Zwerger, M., Cohen, T.V., Devys, D., Foisner, R., Peichl, L., et al. (2013). LBR and lamin A/C sequentially tether peripheral heterochromatin and inversely regulate differentiation. Cell *152*, 584–598.

Steffen, P.A., Fonseca, J.P., and Ringrose, L. (2012). Epigenetics meets mathematics: towards a quantitative understanding of chromatin biology. BioEssays *34*, 901–913.

Studencka, M., Konzer, A., Moneron, G., Wenzel, D., Opitz, L., Salinas-Riester, G., Bedet, C., Krüger, M., Hell, S.W., Wisniewski, J.R., et al. (2012a). Novel roles of Caenorhabditis elegans heterochromatin protein HP1 and linker histone in the regulation of innate immune gene expression. Mol. Cell. Biol. *32*, 251–265.

Studencka, M., Wesołowski, R., Opitz, L., Salinas-Riester, G., Wisniewski, J.R., and Jedrusik-Bode, M. (2012b). Transcriptional repression of Hox genes by C. elegans HP1/HPL and H1/HIS-24. PLoS Genet. *8*, e1002940.

Taddei, A., and Gasser, S.M. (2012). Structure and function in the budding yeast nucleus. Genetics *192*, 107–129.

Talamas, J.A., and Capelson, M. (2015). Nuclear envelope and genome interactions in cell fate. Front. Genet. *6*, 95.

Taouji, S., Dahan, S., Bossé, R., and Chevet, E. (2009). Current Screens Based on the AlphaScreen Technology for Deciphering Cell Signalling Pathways. Curr. Genomics *10*, 93–101.

Taverna, S.D., Li, H., Ruthenburg, A.J., Allis, C.D., and Patel, D.J. (2007). How chromatin-binding modules interpret histone modifications: lessons from professional pocket pickers. Nat. Struct. Mol. Biol. *14*, 1025–1040.

Timmons, L., Court, D.L., and Fire, A. (2001). Ingestion of bacterially expressed dsRNAs can produce specific and potent genetic interference in Caenorhabditis elegans. Gene *263*, 103–112.

Towbin, B.D., Meister, P., Pike, B.L., and Gasser, S.M. (2010). Repetitive transgenes in C. elegans accumulate heterochromatic marks and are sequestered at the nuclear envelope in a copy-number- and lamin-dependent manner. Cold Spring Harb. Symp. Quant. Biol. *75*, 555–565.

Towbin, B.D., González-Aguilera, C., Sack, R., Gaidatzis, D., Kalck, V., Meister, P., Askjaer, P., and Gasser, S.M. (2012). Step-wise methylation of histone H3K9 positions heterochromatin at the nuclear periphery. Cell *150*, 934–947.

Unnikrishnan, A., Gafken, P.R., and Tsukiyama, T. (2010). Dynamic changes in histone acetylation regulate origins of DNA replication. Nat. Struct. Mol. Biol. *17*, 430–437.

Wilson, K.L., and Foisner, R. (2010). Lamin-binding Proteins. Cold Spring Harb. Perspect. Biol. *2*, a000554.

Ye, Q., and Worman, H.J. (1996). Interaction between an integral protein of the nuclear envelope inner membrane and human chromodomain proteins homologous to *Drosophila* HP1. J. Biol. Chem. *271*, 14653–14656.

Zheng, C., Karimzadegan, S., Chiang, V., and Chalfie, M. (2013). Histone methylation restrains the expression of subtype-specific genes during terminal neuronal differentiation in Caenorhabditis elegans. PLoS Genet. *9*, e1004017.

Zullo, J.M., Demarco, I.A., Piqué-Regi, R., Gaffney, D.J., Epstein, C.B., Spooner, C.J., Luperchio, T.R., Bernstein, B.E., Pritchard, J.K., Reddy, K.L., and Singh, H. (2012). DNA sequence-dependent compartmentalization and silencing of chromatin at the nuclear lamina. Cell *149*, 1474–1487.

Cell

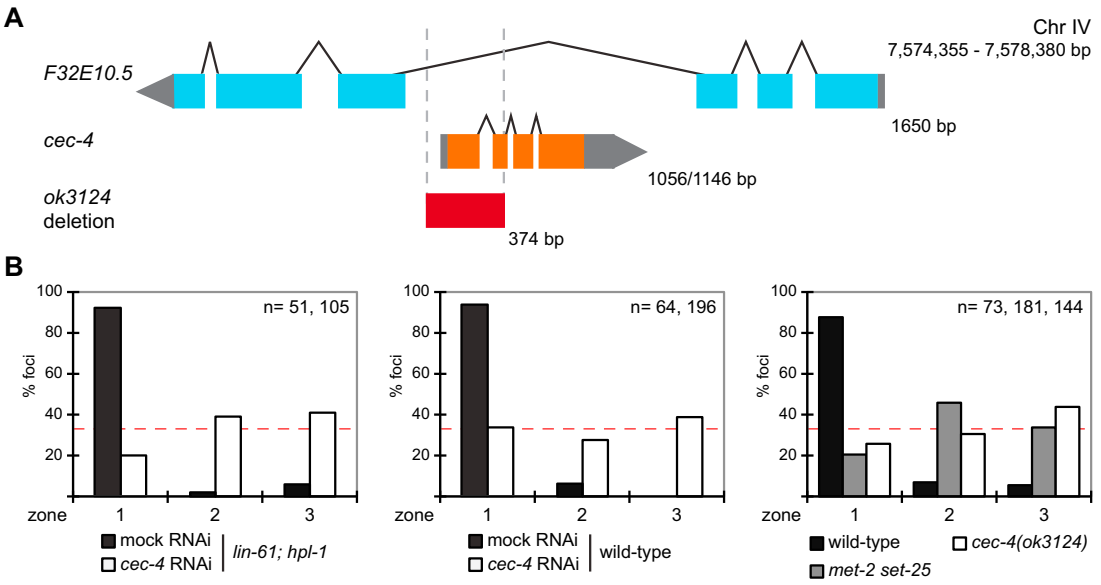

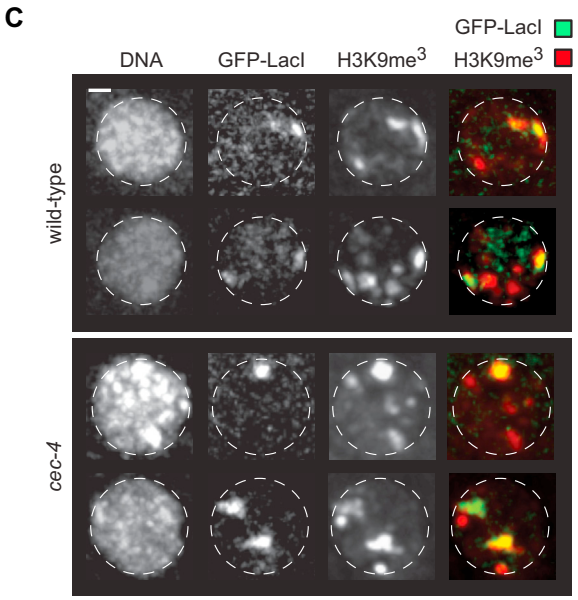

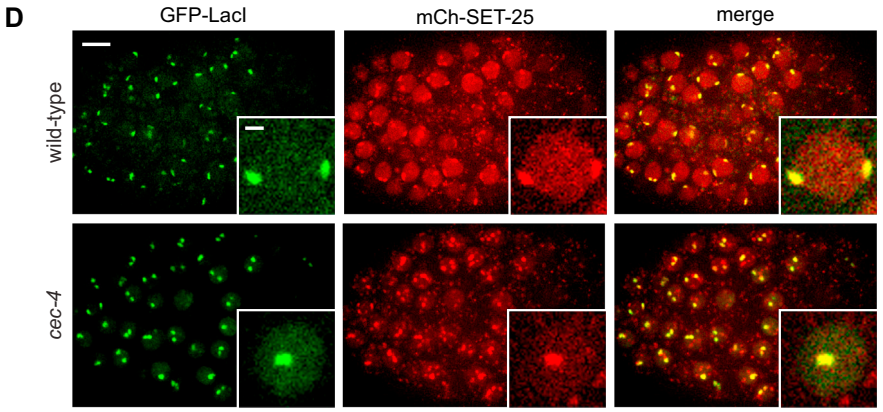

(legend on next page)

Figure S1. Genomic Context of *cec*-4 and Its Deletion Allele, Related to Figure 1

Heterochromatic array contains H3K9me3 and co-localizes with SET-25 even when it is away from nuclear periphery in *cec-4* mutant.

(A) Schematic representation (not to scale) of genomic region where *cec-4* gene is localized, and deletion allele coverage.

(B) Quantitation of array distribution in different experimental conditions as indicated, n: foci scored in presented order. Pair-wise comparisons of *mock RNAi* and WT conditions with the respective *cec-4 RNAi* and *cec-4* mutant show statistically significant differences with p-value < 0.001 in all comparisons, χ^2 test.

(C) Immunofluorescence (IF) of transgene *gwIs4* array (anti-GFP) and repressive histone mark H3K9me3 in WT and *cec-4* mutant strains. Z-projection of representative nuclei are shown, co-localization observed as yellow signal in merged panels. Scale bar, 2 μm.

(D) Live microscopy of N-terminally tagged SET-25 with mCherry (mCh-SET-25) together with array in indicated genotypes. Z-projection images of embryos in individual and merged colors. Insets: single nuclei. Scale bars, 5 and 2 μm for embryos and insets respectively.

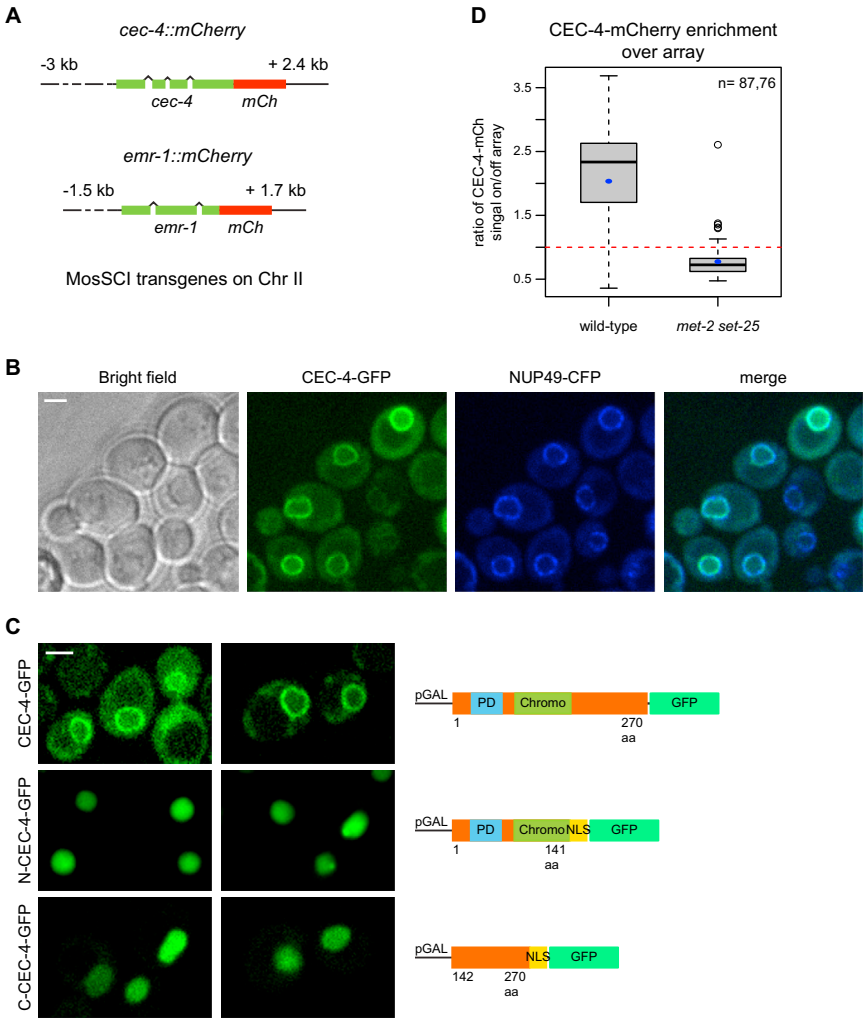

Figure S2. CEC-4 and EMR-1 Constructs Used for This Study, Related to Figures 2 and 4

CEC-4 forms a nuclear ring in *S. cerevisiae*, which is compromised by loss of full-length protein.

(A) Schematic representation of CEC-4 and EMR-1 fusion constructs to mCherry. Both constructs were integrated as single copy on Chr II by MosSCI. *cec-4::mCherry* transgene contains the endogenous promoter (upstream −3kb from transcription start site) and 3′UTR (542bp after stop codon) of *cec-4* gene. *emr-1::mCherry* was kindly provided by Askjer P. and contains the endogenous promoter (upstream −1.567kb from transcription start site) and 3′UTR (300bp after stop codon) of *emr-1* gene.

(B) Expression of intron-less full-length CEC-4 fused C-terminally to GFP in *S. cerevisiae*. Bright field, CEC-4-GFP, NUP-49-CFP (as perinuclear marker) and merged single plane images are shown.

(C) Full-length, N-term and C-term fragments of CEC-4 fused to GFP expressed in yeast. Schematic representation of each construct is presented, in which the GAL1-10 promoter (pGAL) drives CEC-4-mCherry and corresponding fragment fusions. Single plane images of representative patterns are shown. Scale bars on (B) and (C) panel, 2 μm.

(D) Quantitation of CEC-4-mCherry intensity level on array-bound region in contrast to a non-array perinuclear region, as described in Supplemental Experimental Procedures for WT and *met-2 set-25* mutant embryos. Whiskers: 1st and 3rd quartiles, black circles: outliers, black lines: median, blue dots: mean, red dashed line: baseline set as no difference in enrichment, n: total number of arrays per nuclei measured of each genotype.

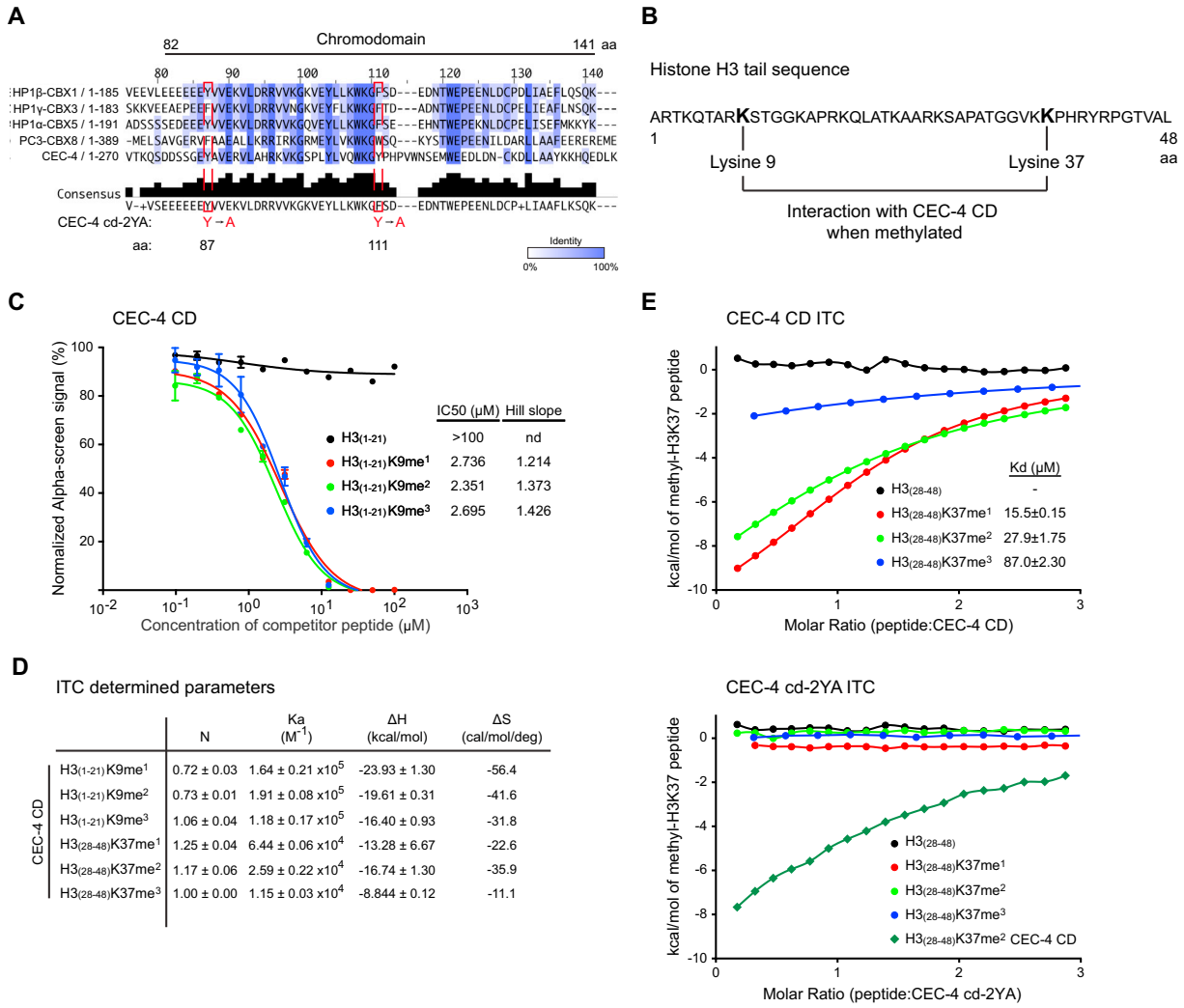

Figure S3. CEC-4 Chromodomain Is Conserved and Binds to All Methylated Forms of H3K9 and to H3K37me with Lower Affinity, Related to Figure 3

CD point mutations impair binding to all substrates tested.

(A) ClustalW multiple sequence alignment of CEC-4's CD (82-141 aa) with different *H. sapiens* CBX proteins as indicated. Blue color range represents percentage of identity, and consensus sequence is displayed. The two highlighted lysines (dashed red boxes) replaced by alanines in the CEC-4 cd 2YA construct.

(B) Histone H3 tail sequence for visualization of amino acid context of lysines 9 and 37, to which CEC-4 CD showed positive.

(C) IC_{50} (half maximal inhibitory concentration) of H3K9 peptides binding to CEC-4 CD measured by AlphaScreen peptide displacement assay. Non-biotinylated H3K9 peptides were used to compete with the binding of CEC-4 CD and biotin-H3K9me2 peptide in AlphaScreen binding assay.

(D) Table showing parameters measured for association of CEC-4 CD and the different methylated states of indicated H3 peptides. N (stoichiometry), K (association constant), ΔH (enthalpic change) and ΔS (entropy change) in Isothermal Titration Calorimetry (ITC) assay.

(E) Quantitation of binding affinities of methylated H3K37 peptides to CEC-4 CD and mutant cd-2YA, determined by ITC. For all graphs solid lines represent a nonlinear least-square fit using one-site fitting equation.

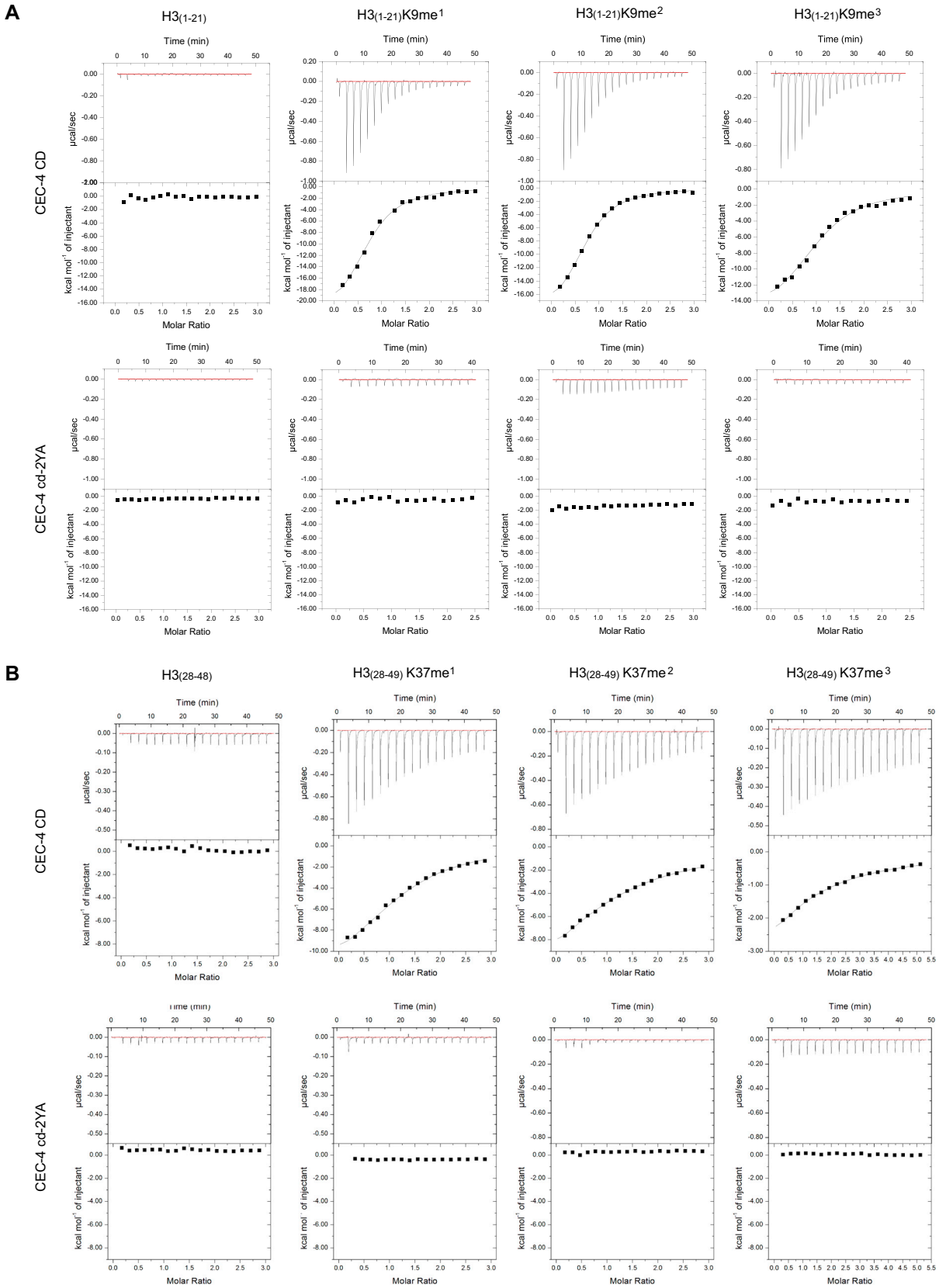

(legend on next page)

Figure S4. Intact CEC-4 CD Binds Preferentially to All Methylated Forms of H3K9 and with Less Affinity for H3K37 (me1 > me2 > me3) as Monitored by ITC, Related to Figure 3

(A) Raw binding data of ITC injections of all methylated forms of H3K9 for both CEC-4 CD and CEC-4cd-2YA is shown. Dissociation constants (Kd) determined are shown in Fig 2E. Kd's with CEC-4cd-2YA were unable to be determined.

(B) Same as in (A) except that the peptides are related to methylation of H3K37. Kd's are shown in Fig S2E.

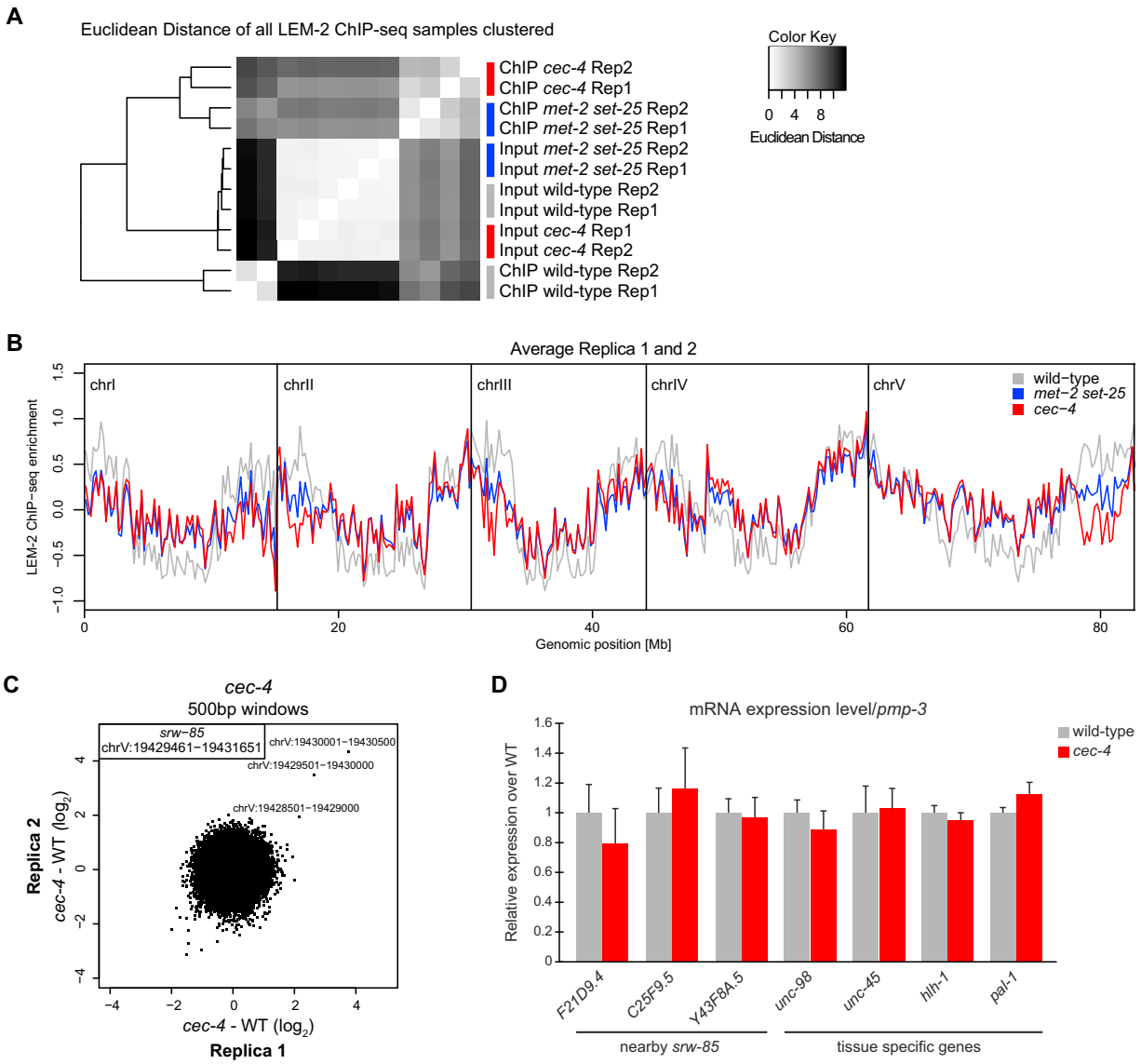

Figure S5. LEM-2 ChIP Enrichment Signals of *met-2 set-25* and *cec-4* Mutants Cluster and Are Different from WT, with a Less Polarized Pattern, Related to Figure 5

Genes *srw-85* and *C18D4.6* are depleted for H3K9me in *cec-4* embryos, while only *srw-85* is derepressed.

(A) Heat-map of hierarchical clustered Euclidean distances of LEM-2 ChIP and Input (total chromatin extracted) normalized reads of WT, *met2 set-25,* and *cec-4* mutants in duplicate.

(B) Average of duplicates of LEM-2 ChIP enrichment plotted over chromosomes. Tracks are shown only for autosomal chromosomes. Averaged signals (*Z* scores of IP – input) are shown in 200 kb windows.

(C) Relative expression profiles in windows of 500 bp (not strand assigned) for the whole genome of cec-*4* mutants to WT levels in early embryos. Scatter plots compare replicas of indicated genotypes.

(D) qRT-PCR mRNA level quantitation for indicated genes in WT and *cec-4* mutant background. Data shown normalized to *pmp-3* gene and relative to the expression in WT. Error bars = SEM of five biological replicas of early embryo extracts.

A

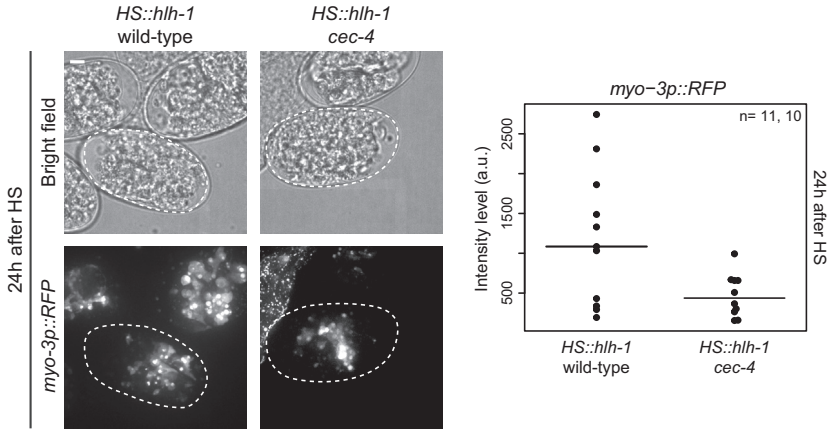

B

Genotype	Embryos	Hatched larva-like worms
HS::hlh-1 CEC-4-mCherry cec-4	33	0
HS::hlh-1 CEC-4cd2YA-mCherry cec-4	32	3
HS::hlh-1 cec-4	63	15
HS::hlh-1	58	0

Figure S6. Muscle-Specific myo3-RFP Expression Occurs in Both Genotypes after HS, Albeit at Higher Levels in WT, Related to Figure 6

Restoration by expression of CEC-4-mCherry, but not the CEC-4 CD-2YA mutant.

(A) Muscle specific *myo-3p::RFP* reporter (contained in *gwIs4* array) for indicated genotypes 24 hr after HS. Z-projection images of bright field and *myo-3p::RFP* are shown. Scale bar, 5 μm. Quantitation of RFP intensity signal 24 hr after HS for indicated genotypes. Intensity levels are plotted in a.u., black line: median, n: number of embryos of respective genotype.

(B) Table showing number of hatched larva-like worms for different strains tested.

CHAPTER 3: ADDITIONAL CHARACTERIZATION OF CEC-4

Adriana Gonzalez-Sandoval,[1,2] Benjamin D. Towbin,[1,3] Peter Zeller,[1,2] Veronique Kalck,[1] and Susan M. Gasser[1,2]

[1]Friedrich Miescher Institute for Biomedical Research, Maulbeerstrasse 66, CH-4058 Basel, Switzerland
[2]Faculty of Natural Sciences, University of Basel, Klingelbergstrasse 50/70, CH-4056 Basel, Switzerland
[3]Present address: Department of Molecular Cell Biology, The Weizmann Institute of Science, Rehovot 76100, Israel

Preliminary unpublished data. A. G.-S. together with B.D.T. and P. Z. contributed to the experiments presented on the first section. V. K. generated the results of the other sections with direct supervision and collaboration of A. G.-S.; S.M.G. functioned as supervisor for all sections.

SUMMARY

This chapter describes unpublished experiments that did not fit into the scope of the paper published, but were performed for the purpose of further characterization of *cec-4*. The first section is related to the phenotypic characterization of homozygous *cec-4* mutant worms. We find that these worms show no differences in comparison to wild-type worms in relation to H3K9 distribution, embryonic developmental timing, brood-size, embryonic lethality and male induction. The second section contains experiments related to the targeting of CEC-4 at the nuclear periphery. CEC-4 has an intrinsic localization to the nuclear periphery, which appears to be independent of lamin or known INM proteins. The third section presents a pilot experiment for genetic interactions of *cec-4* with other readers of H3K9 in relation to the levels of expression of our GFP-LacI reporter contained in *gwIs4* array. Quite unexpectedly *cec-4* mutant shows a suppressive effect on *hpl-2* and *met-2 set-25* mutants, suggesting an active role of *cec-4* in the higher levels of expression of our reporter when these genes are missing. This last section is a potentially interesting direction to continue the study of perinuclear anchoring of chromatin.

PHENOTYPIC CHARACTERIZATION OF CEC-4 MUTANT

The mutant allele of *cec-4* was not previously characterized. When we identified *cec-4* as a factor required for chromatin anchoring in embryos, we sought to test whether its loss had any physiological impact.

Since CEC-4 contains a chromodomain that recognizes H3K9 methylation (Gonzalez-Sandoval et al., 2015), we determined if the distribution of these mark was altered in the absence of it. We used two approaches: (1) Immunofluorescence and measurement of radial distribution (Figure 3.1) and (2) Chromatin Immunoprecipitation followed by deep-sequencing (Figure 3.2). In the absence of CEC-4 the levels and distribution of H3K9me2 and me3 were not significantly altered on a chromosomal level, but there seems to be a slight shift inwards of chromatin marked by H3K9me3, when scored by fluorescence microscopy.

The mislocalization effect of *cec-4* mutant occurs only in early embryonic stages, afterwards compensatory mechanisms again anchor our heterochromatic reporter (Gonzalez-Sandoval et al., 2015). Therefore we wanted to first address the effects in these early embryonic stages and thought that developmental timing could be an immediate phenotype to score. We saw no change in embryonic development scored by two different means (Figure 3.3).

A more general characterization of phenotypes in worms is to measure brood-size, embryonic lethality and male induction. In comparison to wild-type worms, *cec-4* mutants do not change brood-size nor embryonic lethality scores, but they do have a very slight difference in male induction (Figure 3.4). Differences in male induction suggest possible issues in X chromosome segregation and gonad function, but further experiments need to be done to properly understand the involvement of CEC-4 and chromatin organization in this phenomenon.

In each following section we described the experiments in more detail and suggest possible directions in which these studies could continue.

H3K9 me2/me3 radial distribution

Immunofluorescence of H3K9me2 and me3 as well as nuclear pores or lamin, as indicated in Figure 3.1, were performed to score the radial distribution of chromatin marked by these two epigenetic marks. CEC-4 is a chromodomain protein that reads all methylated forms of H3K9 with similar affinities (Gonzalez-Sandoval et al., 2015). Therefore, we wanted to monitor whether or not their nuclear distribution changes due to the lack of this reader.

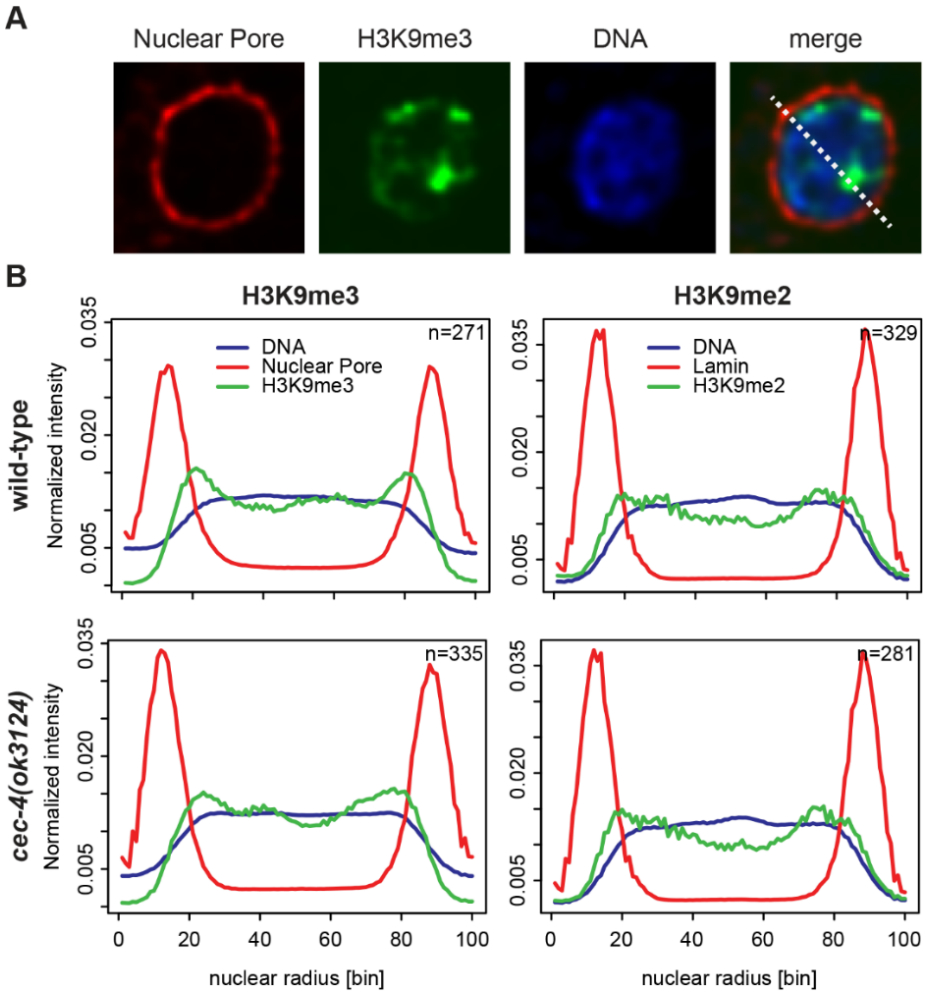

Figure 3.1. H3K9me2 chromatin is enriched at the INM independent of *cec-4*. H3K9me3 partially requires *cec-4*. N=1. (A) Representative nuclear central focal plane of *cec-4* mutant embryo stained for H3K9me3 and nuclear pore. Dotted line on merge panel represents line profile used for quantification. (B) Quantification of radial intensity of wild-type and *cec-4* mutant embryos. Embryos were stained for the indicated histone modification (green), DNA (blue), and LMN-1 or nuclear pore (red). For each panel, the indicated number (n) of radial line profiles was scaled and polled into 100 binds, normalized, and averaged.

There is a difference in the global distribution of H3K9me3 as monitored by immunostaining in the *cec-4* mutant, but no obvious change of H3K9me2. CEC-4 has a slightly higher affinity for H3K9me2, which seems not to be affected, in contrast to H3K9me3. This difference may reflect alternative modes of INM association, such as the tethering of telomeres (which are also H3K9me-enriched) to SUN-1, which we previously showed to be independent of all forms of H3K9 methylation (Ferreira et al., 2013). Nonetheless, we know from LEM-2 ChIP that the perinuclear localization of chromosome arms is compromised in the *cec-4* mutant. Is the global pattern of H3K9me3 staining a reflection of the shift of endogenous chromatin away from LEM-2? This is a likely hypothesis. More interesting is the question why H3K9me2 does not shift away. Are there additional and distinct ligands that recognize these marks, and are they INM associated? Or does it reflect the kind of loci that contain the marks, e.g. H3K9me3-

enriched promoters might be more likely to shift away due to transcription, while H3K9me2-enriched repetitive elements may not shift, since they may not be transcriptionally active. A high-resolution correlation of histone modification and positioning by CEC-4 ChIP-seq would be one way to pursue this. One would expect that CEC-4 correlates better with the pattern of H3K9me3, since its radial distribution seems to change in the absence of *cec-4*.

Another way to continue this study would be to do Electron Microscopy (EM) negative staining in order to visualize endogenous heterochromatin and score if there is a difference in the global distribution of heterochromatin in the *cec-4* mutant embryos. One caveat may be that perinuclear heterochromatin is less pronounced in embryos, thus it might be difficult to see a significant difference. Nonetheless, it could be tested.

H3K9 me2/me3 distribution by chromosome

Chromatin Immunoprecipitation followed by deep-sequencing (ChIP-seq) of H3K9me0, H3K9me2 and H3K9me3 was performed in wild-type and *cec-4* mutant embryos, and was compared to Input chromatin, to score differences in the levels and distribution of these marks throughout the genome.

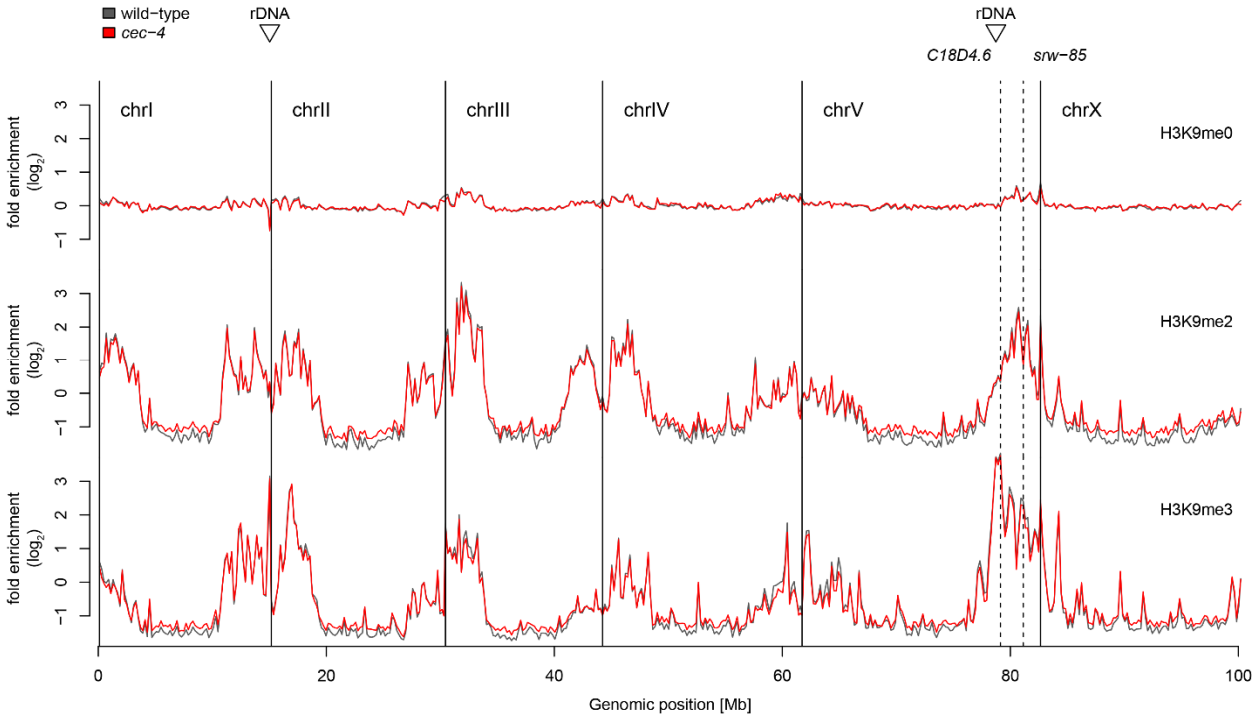

Figure 3.2. Lack of anchoring by *cec-4* mutant does not seem to alter enrichment of H3K9me2 and me3 globally. N=1. H3K9me0, H3K9me2 and H3K9me3 ChIP-seq profiles over chromosomes of early embryos of wild-type (dark gray) and *cec-4* (red) mutants. Dashed line shows *srw-85* and *C18D4.6* genes, and triangles show rDNA clusters.

There are no dramatic changes in the distribution of H3K9 along the chromosomes in the *cec-4* mutant. However, as reported in (Gonzalez-Sandoval et al., 2015) there is a change in compaction of the heterochromatic reporter array. This change in compaction may be

independent of H3K9, at least at the level of resolution obtained by ChIP-seq, since we score no major changes in the enrichment and distribution of this mark. This further confirms the absence of change in gene expression profiles. Compaction and transcription can be uncoupled (Therizols et al., 2014), and our results confirms this statement in *C. elegans* embryos for the heterochromatic reporter. Still we need to test if there is decompaction of endogenous chromatin in *cec-4* mutant and what effects this may have on genome function.

What is the mechanism of compaction at the nuclear periphery? It may be that the spatial distribution of CEC-4 along the INM physically constrains or compacts chromatin that contains methylated H3K9. To test this, one needs a quantitative means to monitor chromatin compaction. One approach would be to integrate differential fluorescent probe binding sites (or to do FISH), for loci that are 50kb or 100kb apart, in a zone containing H3K9me3. If the distance between the two probes increase in a *cec-4* mutant, but the H3K9me pattern does not change, one can attribute the compaction to CEC-4 itself. One could test chromatin also by monitoring accessibility to Micrococcal nuclease (MNase) and subsequence deep-sequencing of the accessible sites (Zhang and Pugh, 2011), in the presence and absence of CEC-4. The relative accessibility of linker DNA to MNase is generally thought to correlate with decompaction, thus MNAse sensitivity may allow us to score the decompaction of the endogenous genome when it is released from the INM. One would expect differences mostly in chromosome arms, whose localization at the nuclear periphery is compromised in *cec-4* mutants. If this is the case, one means to confirm the correlation would be to target the enrichment of H3K9 methylation to a specific locus that is not normally localized at the periphery, and to see if it becomes compacted and localizes at the nuclear periphery. We cannot exclude the possibility of factors or elements, other than CEC-4 or those that are independent of H3K9 methylation, which could mediate compaction at the nuclear periphery.

Embryonic Developmental Timing

To score effects of lack of anchoring specifically in embryonic stages, we decided to compare the time of development in *cec-4* mutant and wild-type embryos. We first recorded a time-lapse of embryonic development every 15 minutes over 6 hours. We started imaging embryos from 2-cell stage to assure that the comparison between stages and timing was accurate. In the second approach we picked 2-cell stage embryos in pools of approximately 10 embryos, of each genotype, and let them develop for 5 hours at 22.5 °C (bean-stage). Then we made a stringent categorization of embryos reaching bean stage by eye, to see if there was a difference in the proportion of embryos reaching the specific stage.

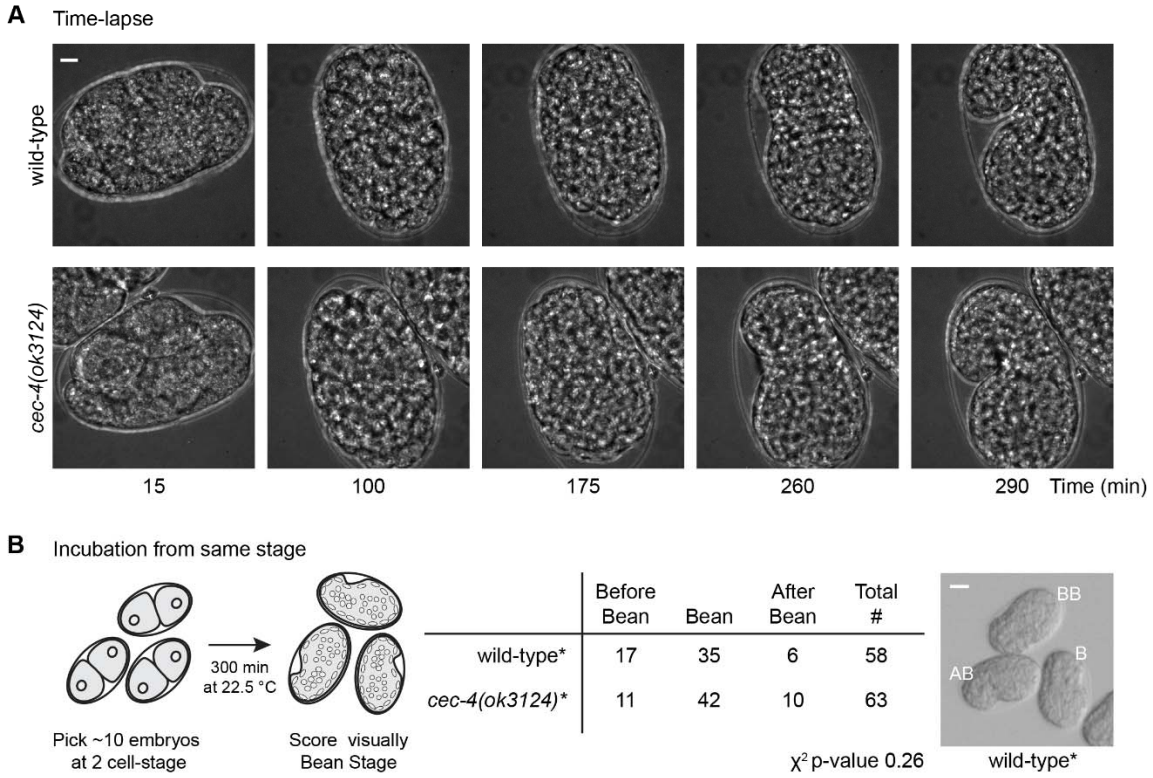

Figure 3.3. Lack of anchoring by *cec-4* mutant does not alter timing of embryonic development. N=1 for each experiment. (A) Bright light microscopy of synchronized wild-type and *cec-4* mutant embryos at specific time points as indicated. Scale bar = 5µm (B) Schematic representation of experimental procedure. Table shows classification of embryos before/after and at bean stage. Chi² test shows no significant differences for both genotypes. Genotypes are mark with stars because both also contain the *HS::hlh-1* and *gwIs4* transgenes. Representative image of wild-type embryos which shows embryos of each classification: BB – Before Bean stage, B – Bean stage, AB – After Bean stage. Scale bar = 20µm.

No significant difference in the timing of embryonic development, between wild-type and *cec-4* mutant genotypes, was seen by time-lapse nor by synchronization when picking 2 cell-stage embryos. These experiments demonstrate no visual phenotypic difference in embryos that lack chromatin anchored to the nuclear periphery. Perhaps the differences are occurring at the molecular level and changes in early and late replicating origins could be an option to analyze further.

The *cec-4* dependent phenotype reported in (Gonzalez-Sandoval et al., 2015) occurred only with the condition of forced muscle differentiation. Altering cell cycle timing in embryos is another approach to assay the importance of anchoring that may become more evident under stress conditions. The experiment proposed here is to block replication in embryos by Hydroxyurea (HU) or another chemical treatment and then release them from it. If chromatin anchoring is important for proper replication control, one would expect that *cec-4* mutant embryos would have a deficit in recovery after the release of HU. Temperature stress or hypoxia stress would be another set of environmental perturbations to test in this assay. It is possible that the spatial organization of heterochromatin in the embryo is only there to

dampen effects of environmental or stochastic perturbation of the normal developmental program.

Brood-size, Embryonic lethality and Male Induction at 26°C

A common phenotypic experiment performed on mutants of *C. elegans* is to score brood-size, embryonic lethality and male induction, at regular (15-22.5°C) and heat-stress temperatures. We decided to score these phenotypes at elevated temperature, i.e. 26°C. We grew the worms at 26°C for two generations, in order to allow them to adjust to the temperature. In the third generation we singled 20 L4-stage worms per genotype. Over 3 consecutive days we passed each singled worm to a new plate and counted the total number of embryos laid, the number of larvae progeny produced and the number of males. Brood-size refers to the total number of larvae hatched on plates. Embryonic lethality is the ratio of larvae hatched by the total number of embryos counted. Male induction refers to the proportion of larvae that are males.

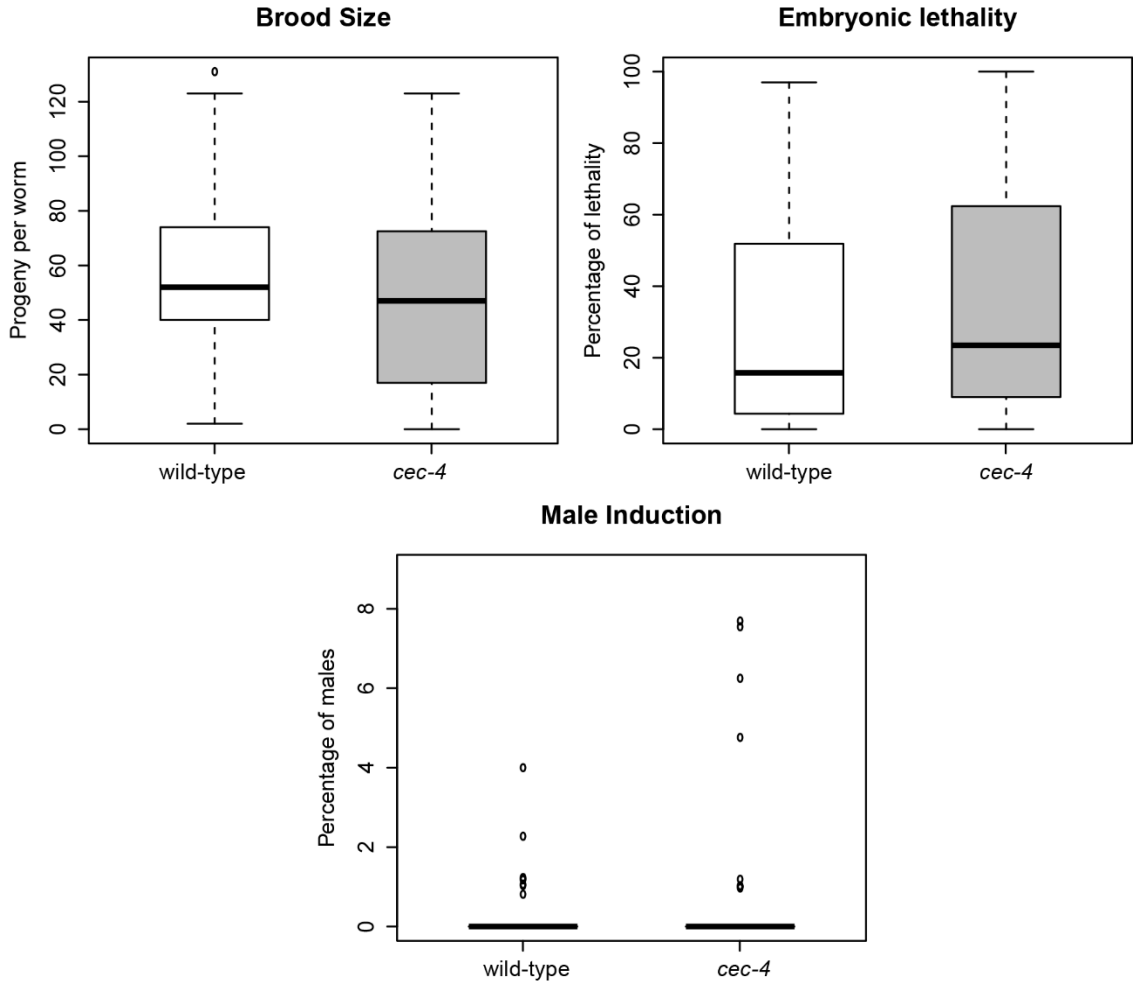

Figure 3.4. At 26°C, *cec-4* mutant worms have a similar brood-size and embryonic lethality as wild-type, with a slight increase of males. N=1. Boxplots representing brood-size, embryonic lethality and male induction as indicated for each genotype; whiskers = 1st and 3rd quartiles, black lines: median, number of worms scored = 20 for each condition.

At the stress temperature of 26°C, the mutant of *cec-4* behaves similar to wild-type worms in relation to brood-size, embryonic lethality and male induction. There is a very slight increase in the proportion of males in *cec-4* mutant, which is not statistically significant. Nonetheless, we observe, anecdotally, that it is easier to find males on growing plates and to induce male production for crosses with the *cec-4* mutant strain. A change in male induction rates can be associated with issues in X chromosome segregation. Preliminary observations of *cec-4* mutant embryos did not show striking differences in chromosome segregation, although this conclusion is again qualitative and anecdotal. Careful quantification of chromosome segregation in a large number of embryos would be needed to significantly identify differences, since the increment in male induction seems to be very low.

If we consider the difference in male induction as meaningful, does this mean that *cec-4* has a role specifically on the X chromosome? The X chromosome is not enriched for H3K9 methylation, except for the left arm (Ikegami et al., 2010). Recently it was reported that the X chromosome on males is located closer to the nuclear periphery due to association with the nuclear pore (Sharma et al., 2014). No additional interactions of the X chromosome and nuclear lamina have been reported. Perhaps the effect of *cec-4* is indirect or independent of its function in recognizing H3K9 methylation. The CEC-4 chromodomain can also bind to H3K37me1/2 although with a lower affinity (Gonzalez-Sandoval et al., 2015), but this unusual modification has not been reported to exist in *C. elegans*. It is possible that CEC-4 has an alternate role in gonads, specifically for the segregation of chromosome X. This could be identified using CEC-4 ChIP-seq to show an unexpected enrichment of CEC-4 on the sex chromosome. Additionally, using chromosome paints for the X chromosome, in males and hermaphrodites in both wild-type and *cec-4* mutant backgrounds would help us to understand if CEC-4 affects the nuclear organization of the X chromosome.

CEC-4 LOCALIZATION TO THE NUCLEAR PERIPHERY

CEC-4 has no transmembrane domain and no obvious CAAX motif as is found in mammalian Lamin A. Therefore we wanted to characterize how CEC-4 is localized at the INM. We used three approaches to study the localization of CEC-4: (1) downregulation or deletion of known NE proteins in worms and yeast respectively, (2) yeast two hybrid screen of interactor partners followed by RNAi test in worms and (3) we scored the localization of fluorescently tagged fragments of the CEC-4 protein, in both worms and budding yeast.

In worms, we performed RNAi against known NE components, with no successful candidates leading to the loss of CEC-4 perinuclear localization (Figure 3.5). In yeast, ectopically expressed, fluorescently tagged CEC-4 also localizes at the nuclear periphery, as it does in worms (Gonzalez-Sandoval et al., 2015). Deletion alleles of INM components and nuclear pore proteins were tested for the mislocalization of CEC-4 and no positive candidate was found (Figure 3.6).

We also tried to identify interactors of CEC-4 by a yeast two hybrid (Y2H) screening. The four screens performed yielded several hits, but some of them were false positives (Table 1). Hits from the first screen were tested by RNAi for delocalization of CEC-4, but none had an effect (Figure 3.7).

Finally, as it was reported in (Gonzalez-Sandoval et al., 2015) for yeast, we expressed complementary N- and C-terminal fragments of CEC-4 in worms, to identify the domain of CEC-4 required for its position at the nuclear periphery. Neither truncated form was enriched at the nuclear periphery, in contrast to the intact protein, suggesting that both the N- and C-termini are important (Figure 3.8). Additionally, we know that a two-point mutated chromodomain of CEC-4 does not perturb its localization (Gonzalez-Sandoval et al., 2015).

In each section below, we described these experiments in more detail and give possible ways to continue these studies.

RNAi of known NE proteins in worms

To identify factors at the nuclear periphery required for the perinuclear localization of CEC-4, we utilized RNAi to silence known NE components. We silenced each candiate gene individually and in pair-wise combinations, and scored the localization of CEC-4-mCherry fusion in embryos. Here we show one example of the RNAi results.

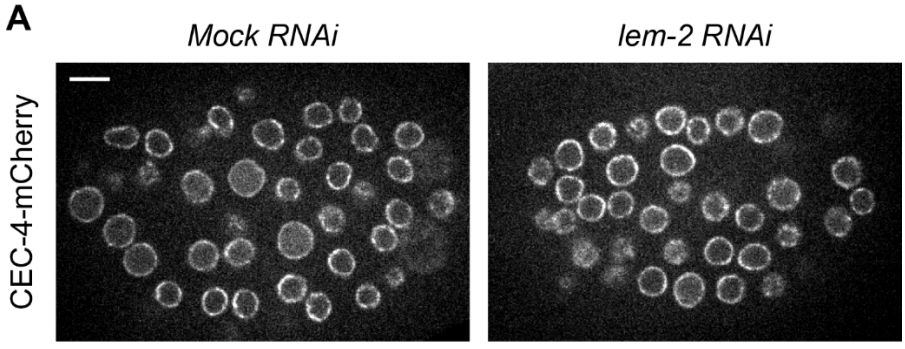

Figure 3.5. Localization of CEC-4 is not disrupted when known NE components are depleted. N=2. (A) Single plane images of representative embryos treated by RNAi as indicated. Worm strain carries a fusion version of CEC-4 (CEC-4-mCherry). Scale bar = 5 μm. (B) List of NE components silenced by RNAi, single or in pair-wise combination of all of them.

There was no change in the localization of CEC-4 by silencing, individually or in combination, known NE components. Three explanations can be given: (1) CEC-4 localization is independent of other INM proteins, but since it does not contain a predicted transmembrane domain this is unlikely; (2) there is an unknown protein required to anchor or (3) there are multiple factors that aid in CEC-4 peripheral localization. We predict more than two known proteins would be involved since we tested known INM proteins pair-wise.

An additional screen will need to be performed to identify possible factors involved in the perinuclear localization of CEC-4. The experiment proposed is a mutagenesis screen with Ethyl methanesulfonate (EMS) for the delocalization of CEC-4-mCherry in embryos. This

experiment can be done in a mutant background or in wild-type worms. This may allow us to identify potential mutations within CEC-4 or other uncharacterized factor required for the proper localization of CEC-4.

CEC-4 expressed in yeast – mutants of NE components

In budding yeast, an inducible plasmid carrying a fused version of CEC-4 with GFP is localized at the nuclear periphery, similarly as in worms. This experiment confirmed that the localization of CEC-4 is independent of lamin, since yeast do not have intermediate filament proteins nor a distant homologue of lamin (Gonzalez-Sandoval et al., 2015). To screen for the mislocalization of CEC-4, the CEC-4-GFP plasmid was transformed into different yeast mutant backgrounds related to NE components

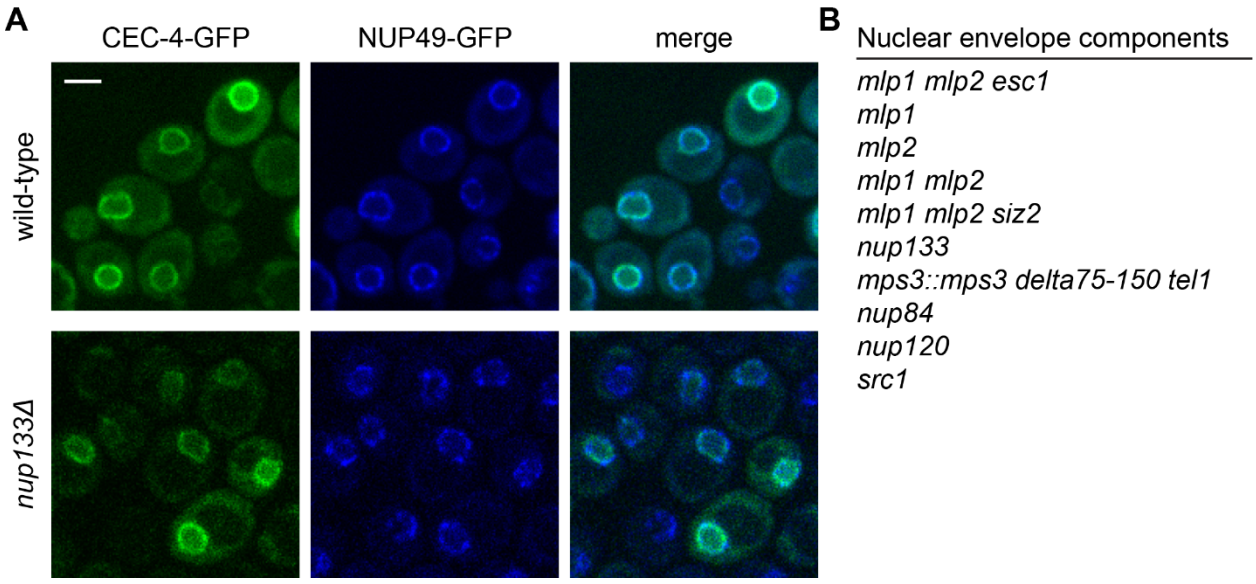

Figure 3.6. Deletion of nuclear envelop components in yeast does not disrupt the perinuclear localization of CEC-4-GFP. N=2. (A) Expression of intron-less full-length CEC-4 fused C-terminally to GFP in *S. cerevisiae*. CEC-4-GFP, NUP-49-CFP (as perinuclear marker) and merged channels, single plane images, are shown for two different genotypes. Scale bar = 2 µm. (B) List of yeast mutant strains used for experiments, all related to NE components. Since *mlp1* deletion also perturbs sumoylation, this modification is also unlikely to be involved in CEC-4 localization, even though SUMO plays a role in heterochromatin localization in yeast.

The exogenously expressed CEC-4-GFP formed rings in all NE yeast mutants tested. In other words no NE tested is involved in CEC-4's perinuclear distribution. To identify how CEC-4 is localized to the nuclear periphery, a straightforward experiment would be random mutagenesis of the CEC-4-GFP fusion on a yeast expression plasmid, followed by fluorescence microscopy to identify the localization of each mutant form. Plasmid transformation is much faster in yeast than in worms, therefore the screening will be more

efficient and any hits can be flowed up with studies in worms. This may allow us to identify the domain or core amino-acids important for the perinuclear localization of CEC-4.

CEC-4 interaction partners by Y2H screen

We used Hybrigenics Services© to screen by Y2H, potential interactors of CEC-4 that would be later tested for the localization of CEC-4 in worms. Four independent screens were performed, using the same Prey library (*C. elegans* embryo_RP1) which contains all proteins reported to be expressed during embryogenesis. As a bait a C-terminal fragment (162-270 aa) of CEC-4 and full length were used, both with two different promoters (LexA and Gal4-inducible). Two different promoters were tested preventing potential issues that may arise due to expression of CEC-4 in yeast, which is not endogenous. Two versions of CEC-4 were tested with the expectation that differences in the interactors identified may arise (more are expected with the full length protein than with the C-terminal fragment). Since the chromodomain of CEC-4 is on the N-terminal region, we hypothesized that the C-terminal portion would be more likely to interact with nuclear periphery. Experiments expressing complementary fragments (N- and C- terminal) in worms and yeast, led to the conclusion that the holoprotein is necessary for CEC-4's perinuclear localization (Figure 3.8 and Gonzalez-Sandoval et al., 2015). The hits obtained in the first screen (Screen 1) were further tested for the interaction with CEC-4 by Y2H in our laboratory.

Using confirmed RNAi clones of Screen 1 hit genes, we depleted each independently in worms to score for the localization of CEC-4-mCherry in embryos. Two genotypes were used: wild-type background and *met-2 set-25* mutant, where heterochromatin is localized away from the periphery. The mutant was used as a sensitized background, thinking this would facilitate CEC-4 displacement from the periphery.

Table 1. Summary of results derived from Y2H screens. In house, Y2H confirmation led to four reproducible hits. However, when tested independently by RNAi, none altered CEC-4 perinuclear localization. N=1.

Screen 1	Screen 2	Screen 3	Screen 4	Confidence*	Y2H confirmation	RNAi	Gen 1	Gen 2
ncam-1	*ncam-1*			Very high	positive	Yes	No	No
B0024.11	*B0024.11*			Moderate	positive	Yes	No	No
ceh-37	*ceh-37*	*ceh-37*	*ceh-37*	Low	false positive	Yes	No	No
	C06E1.1			Good	not tested	No		
	C09F9.2			Good	not tested	No		
C15H9.4				Moderate	positive	Yes	No	No
	apl-1			Good	not tested	No		
	atad-3			Moderate	not tested	No		
	cpna-2			Moderate	not tested	No		
	csn-5			Low	not tested	No		
	egl-9			Moderate	not tested	No		
	myo-3			Moderate	not tested	No		
let-607				Moderate	positive	Yes	No	No
	ret-1			Moderate	not tested	No		
ttx-1			*ttx-1*	Low	false positive	Yes	No	No
		ztf-13	*ztf-13*	Very high	not tested	No		

C08H9.16	*C08H9.16*	Moderate	not tested	No
	hecd-1	Moderate	not tested	No
	unc-53	High	not tested	No
	vab-3	non specific	not tested	No

Screen 1 – LexA promoter, C-term-CEC-4
Screen 2 – Gal4 promoter, C-term-CEC-4
Screen 3 – LexA promoter, CEC-4
Screen 4 – Gal4 promoter, CEC-4
Confidence* - PBS® value, Hybrigenics Services©
Y2H confirmation – In house, see Figure 3.7
RNAi – RNAi test in worms for delocalization of CEC-4 in embryos in two different genetic backgrounds
Gen1 – wild-type worms with integrated CEC-4-mCherry
Gen2 – *met-2 set-25* mutant worms with integrated CEC-4-mCherry

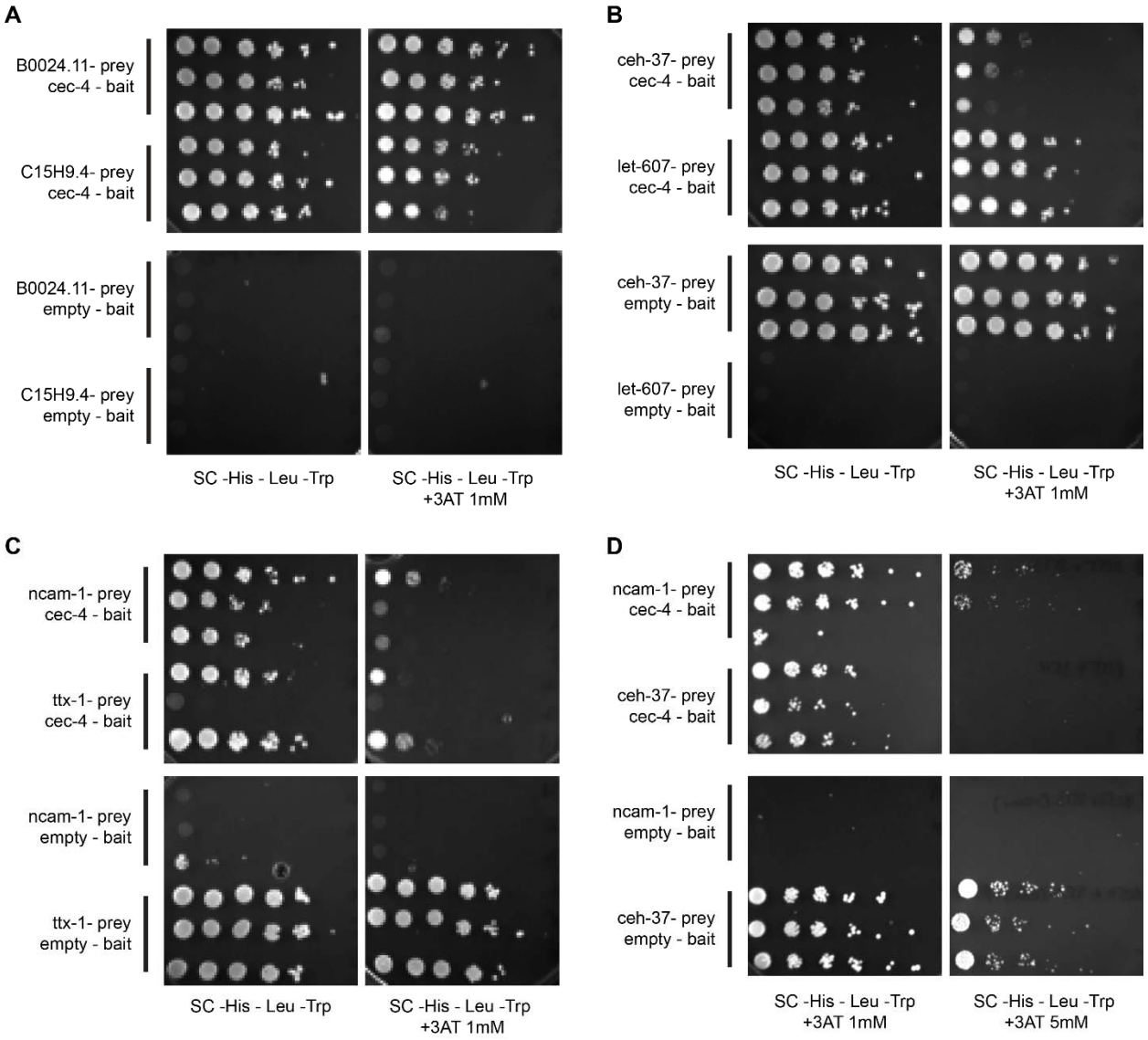

Figure 3.7. Y2H confirmation in house of Screen 1 hits, 4 out of 6 hits are true positives. N=1. (A) Assays were performed by mating the two yeast strains transformed with the B0024.11-prey or C15H9.4-prey and cec-4-bait or empty-bait plasmids as indicated. Diploid yeasts expressing both

proteins were selected on SC media lacking histidine, leucine and tryptophan (SC –His –Leu –Trp) and on media with additional 3AT drug in indicated concentrations (SC –His –Leu –Trp +3AT) to ensure positive interactors. (B) Same as in A but with different prey plasmids: ceh-37-prey and let-607-prey. (C) Same as in A but with different prey plasmids: ncam-1-prey and ttx-1-prey. (D) Same as in A but with different prey plasmids: ncam-1-prey and ceh-37-prey and let-607-prey. SC –His –Leu –Trp +3AT selection media only.

In the Y2H confirmation experiment only diploid yeast bearing the two interacting proteins can grow on the selective media. Confirmation of the specificity of the result happens when prey plasmids are co-transformed with the empty-bait vector and cells do not grow. For ceh-37-prey and ttx-1-prey plasmids, these interaction was not specific, meaning it was a false positive result. Higher concentrations of 3AT drug were used for two preys, to increase stringency of the selection and confirm the interaction of ncam-1-prey. In worms *ncam-1* (neuronal cell adhesion molecule homolog -1) is reported to have a transmembrane domain and localize at the cell membrane of neuronal cells and pharynx, but CEC-4 is expressed in all cell-types in all life stages, therefore is unlikely that this interactor is involved in the global localization of CEC-4. The other confirmed positive hits are not well characterized, making it difficult to address a proper connection with CEC-4 and the nuclear periphery at this time. *B0024.11* is an orthologue of PUS7 (pseudouridylate synthase 7 (putative)) related to RNA processing. *C15H9.4* is an orthologue of human TMCC1/2/3 (transmembrane and coiled-coil domain family 1/2/3) and TEX28 (testis expressed 28), but nothing more has been reported about this gene. *let-607* is an orthologue of CREB (Cyclic AMP-responsive Element-Binding) family of transcription factors and its deletion is lethal (WormBase Version:WS251).

In worms we depleted by RNAi the hits from Screen 1 and found no effect on the localization of CEC-4 in any of the two genotypes used.

Since 33% of the hits from Screen 1 turned out to be false positives, further Y2H confirmation of hits from Screens 2-4 is needed. A similar RNAi strategy can be carried out for true hits, but if none are positive it is likely that Y2H will not lead to the identification of a CEC-4 nuclear periphery interactor. As suggested above, an EMS screen in worms or random mutagenesis of CEC-4 in yeast could be used to answer the question of the perinuclear localization of CEC-4.

CEC-4 domains in worms

In order to map the domain required to direct CEC-4 to the INM, we reported in (Gonzalez-Sandoval et al., 2015) the expression and localization of complementary, N- and C-terminal, fragments of CEC-4 in yeast. The N-terminal fragment contains CEC-4 chromodomain (82-141 aa) and a second conserved motif - PD (putative domain, 25-76 aa), found in other CD-containing proteins. The C-terminal fragment does not contain an identifiable domain and is predicted to be disordered by secondary structure analysis. Both fragments yield a diffuse nuclear distribution in yeast (see Chapter 2, Figure S2C), suggesting that the integrity of the holoprotein is necessary for its enrichment to the nuclear periphery. We also tested N- and C- complementary fragments in worms, with expression of extrachromosomal and integrated plasmids.

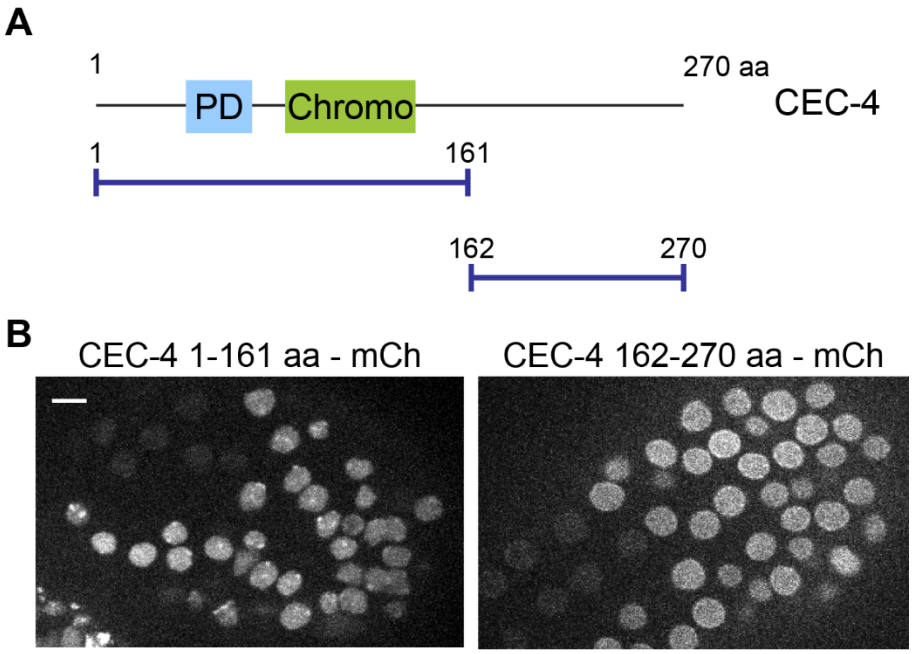

Figure 3.8. Complementary N- and C- fragments of CEC-4 have a dispersed signal inside the nucleus. As expected, the CD labels foci of heterochromatin, while the C-terminal domain does not (only in extrachromosomal injections) N=2. (A) Schematic representation of CEC-4 full length and complementary fragments expressed in worms. PD – putative domain (blue), Chromo – chromodomain (green). (B) CEC-4 fragments fused to mCherry were injected into worms extra-chromosomally. Single plane images of representative embryos of each fragment are shown.

Similar to the expression in yeast, N- (1-161 aa) and C- (162-270 aa) fragments of CEC-4 are dispersed inside the nucleus of *C. elegans* embryos, suggesting that the integrity of the whole protein is required for perinuclear localization. It was extremely difficult to identify embryos expressing the extra-chromosomal fragments and integrated versions were expressed at even lower levels. Perhaps fragmentation of the protein is not a strategy that should be followed for CEC-4. Rather mutagenesis of the holoprotein may yield more promising results.

GENETIC INTERACTIONS BETWEEN H3K9 RELATED FACTORS

What are the dynamics between readers/writers of H3K9 methylation? We know that HPL-1 and CEC-4 accumulate on the heterochromatic reporter (Gonzalez-Sandoval et al., 2015; Towbin et al., 2012). HPL-1 appears to bind all methylated forms of H3K9 (Fischle W., unpublished data), while HPL-2 and LIN-61 recognize H3K9me2/3. We do not have convincing data on enrichment of HLP-2 and LIN-61 on the array, although ChIP for HPL-2 does indeed detect the array (Meister et al., 2011).

In embryos, CEC-4 has little involvement in gene expression, in contrast to HPL-2 and LIN-61. In relation to anchoring, the scenario is reverese, CEC-4 plays a role and the other two H3K9 readers do not. We were curious to explore if the changes in gene expression that occur in *hpl-2* and *lin-61* mutants would be enchanced or reduced when there is a lack of anchoring (i.e. when *cec-4* is deleted). In addition, MET-2 and SET-25 act redundantly for the anchoring

of heterochromatin and each has a role in gene expression. We next asked if there is epistasis between these two factors and CEC-4 with respect to silencing, given they are all required for anchoring.

Gene expression changes in cec-4 mutant combined with other H3K9 related proteins

We made strains combining wild-type, *hpl-1, hpl-2, lin-61* and *met-2 set-25* mutants with the mutant allele of *cec-4,* to addreess genetic interactions between these factors in relation to gene expression. We measured the intensity levels of the GFP-LacI protein expression from a housekeepin promoter (*baf-1p*) in the *gwIs4* heterochromatic reporter in early embryos. All the strains were imaged under identical conditions in order to direcly compare the fluorescent signals.

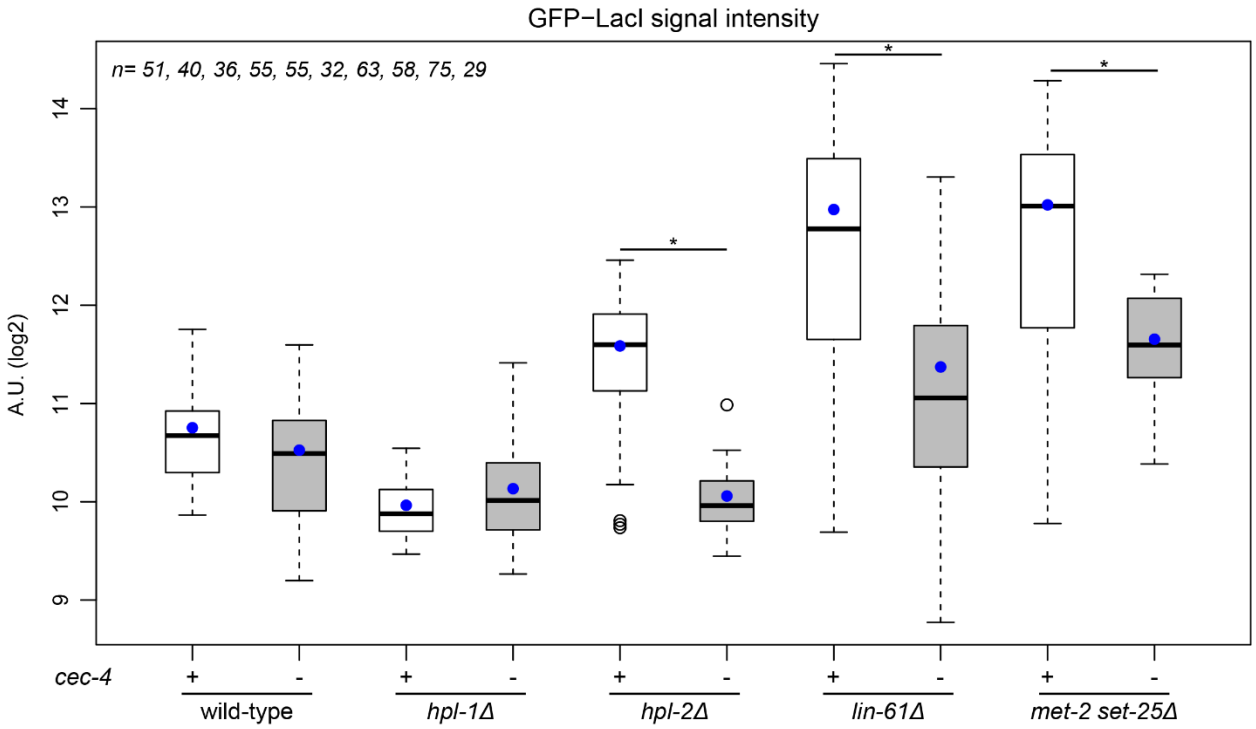

Figure 3.9. Suppressive effect of *cec-4* mutant in combination with *hpl-2, lin-61*** and *met-2 set-25* mutants in relation to expression of GFP-LacI heterochromatic reporter. N=3. Quantified signal intensity displayed as box plot in log2 scale, whiskers = 1st and 3rd quartiles. Black lines: median, blue dots: mean, n = embryos scored per strain in given order, pair-wise comparison for * p-value < 0.001 in Wilcoxon test. ** The effect related to *lin-61* was not observed in the other two replicas of this experiment.

Quite unexpectedly, there is a suppressor effect when *cec-4* is combined with *hpl-2, lin-61* or the *met-2 set-25* double mutant. The effect with *lin-61* although shown here, was not reproducible in experimental replicates, so perhaps it does not have an effect as strong as the other mutants.

We conclude that CEC-4 has an activating role at the nuclear periphery in the absence of *hpl-2* and *lin-61*. Interestingly, there is no suppressor effect with the *hpl-1* mutant, suggesting that the activating role of CEC-4 can only be seen in the presence of active transcription. It is important to consider that we are limited by the ability to image GFP-LacI by microscopy and cannot measure minimal levels of GFP-LacI expression. In order to properly assign this last conclusion other mutants non-related to H3K9 that alter the expression of the array need to be screened in combination with *cec-4* mutant. One possibility is that the activating role of CEC-4 is indirect and there is an unidentified 'activating' factor (Factor A) that interacts with CEC-4 at the nuclear periphery. In a wild-type situation, competition between Factor A and HPL-2/LIN-61 for binding sites on the array favors the later, and the array will be kept silent. When HPL-2/LIN-61 is deleted, the array remains at the periphery thanks to CEC-4 and Factor A can help in the activation of array expression. When CEC-4 is deleted, the interaction of the array with Factor A is lost, and the array does not change its expression as dramatically as it does it at the nuclear periphery.

In relation to the *met-2 set-25* mutant where there is no H3K9 methylation present, the explanation has to be different. In this double mutant the array is already away from the nuclear periphery and the additional removal of *cec-4* does not change its position. The first conclusion is that *met-2 set-25* and *cec-4* mutants are not entirely epistatic, not with respect to gene expression. Although, they are likely to be epistatic for chromatin positioning because the two point chromodomain mutant mimics *cec-4* null for array positioning (Gonzalez-Sandoval et al., 2015). This suggest that CEC-4 has an additional role independent of anchoring heterochromatin at the nuclear periphery. We note that CEC-4 can also bind to H3K37me1/me2 *in vitro* (Gonzalez-Sandoval et al., 2015), perhaps the unknown function of CEC-4 is through the recognition of this mark. This is highly speculative, since this modification has not been reported to exist outside of *S. ceverisiae* and was not detected in our analysis of *C. elegans* methylated peptides. Interestingly, there is a striking and additive brood-size reduction of the *met-2 set-25; cec-4* triple mutant under normal laboratory conditions, qualitatively assessed. Is this reduction related to the other function of CEC-4 that becomes more prominent when H3K9 methylation is not present? Or is it an indirect effect due to genes that remain upregulated when worms lack H3K9 methylation and CEC-4? Further experiments are required to further to understand this phenotype.

The first experiment proposed to address these questions is qPCR or RNA-seq analysis of the mutants, which show this suppressive effect on the array. This would confirm whether endogenous genes are similarly (or oppositely) affected. In addition, a careful quantification of brood-size, embryonic lethality and male induction should be done for all these mutants.

In order to further understand the genetic interaction effects identified, we need to discover physical interactor factors for all the proteins related to H3K9 methylation. We know that HPL-1 and CEC-4 sit on the heterochromatic reporter array, but we do not know if this is the case for LIN-61 or how significant is the enrichment of HPL-2 (assessed by ChIP-qPCR). There is still missing data on the binding affinity of some of these factors to H3K9 methylation, which would help in concluding remarks about binding competition. We propose to do Bio-ID (proximity-dependent biotin identification), which is a relatively recent method for screening protein-protein interactions in living cells (Roux et al., 2012). Knowing about physical interactor partners of CEC-4 will help us to elucidate its other functions independent of anchoring.

EXPERIMENTAL PROCEDURES

Strains and Constructs

All worm and yeast strains used are listed in Table S1 and S2 respectively. Plasmids are listed in Table S3.

For CEC-4 domain constructs, the whole gene was first amplified from N2 worms genomic DNA, and fragments were further amplified with specific primers for each position. All plasmid constructs were generated by MultiSite Gateway® cloning (Invitrogen). Transformation of plasmids into worms was done by injection, using the MosSCI technique (Frokjaer-Jensen et al., 2008). We used two different types of transformed worms, either with plasmids not integrated, or the integrated version.

Worms for microscopy and developmental (Figure 3.3B) experiments were grown at 22.5˚C. H3K9 ChIP sequencing strains were grown at 20˚C. Brood-size, embryonic lethality and male induction worms were starved at 22.5°C and then shifted to 26°C.

For yeast experiments, CEC-4 full length (1-270 aa – plasmid #3582) was cloned into Advanced Gateway destination vector plasmid #14193 (pAG415GAL-ccdB-EGFP). All plasmids were transformed using standard transformation protocol in GA-3628 (wild-type with nuclear pore fluorescently labeled) or strains listed in Table S2. Yeast were grown at 30°C.

Immunofluorescence (IF)

IF was done as described in (Towbin et al., 2012). Antibodies used in pairs: monoclonal anti-H3K9me2 (Abcam, ab1220) and Alexa-568 anti-mouse; polyclonal anti-H3K9me3 (Cell Signalling Technology, #9754S) and Alexa-568 anti-rabbit; for nuclear pores: monoclonal mAB414 (Abcam, ab24609) and Alexa-555 anti-mouse; for lamin: anti-CeLMN-1 (a gift from Y. Gruenbaum, The Hebrew University of Jerusalem, Jerusalem, Israel) and Alexa-488 anti-rabbit.

Microscopy

Except Figure 3.3B, microscopy was carried out on spinning disk multipoint confocal microscopes: (1) AxioImager M1 [Carl Zeiss] + Yokogawa CSU-22 scan head, Plan-Neofluar 100×/1.45 NA oil objective, EM-CCD camera [Cascade II; Photometrics], and MetaMorph 7.7.2 software or (2) Olympus IX81 + Yokogawa CSU-X1 scan head, PlanApo 100x/1.45 TIRFM or 60x/1.45 NA oil objectives, 2X Back-illuminated EM-CCD EvolveDelta (Photometrics), and VisiView 2.1.4 software. Live microscopy embryo samples were prepared as previously described in (Meister et al., 2010). Figure 3.1 images were de-convolved with Huygens Pro software. Single plane images and analysis were generated using Fiji/ImageJ software (Schindelin et al., 2012).

For radial quantitation of H3K9me (Figure 3.1), more than 120 independent manually selected line profiles (5 pixels wide) were used at the central nuclear plane, lines were extended laterally by 12.5% of the nuclear diameter, and signal intensities were extracted

and pooled into 100 bins. Individual profiles were normalized, averaged, and plotted by using R.

Embryonic development bright-light images (Figure 3.3A) were recorded as time-lapse microscopy, one image every 5 minutes for 5 hours (61 frames total). Embryos were selected at 2-cell stage as starting point of recording. Specific time-points were selected for illustrating purposes.

For Figure 3.3B, microscopy was carried out on fluorescence stereomicroscope (Leica MZ FL III, PlanApo 2x/0.07 NA, Leica DFC350 FX camera 0.63x lens, and Imagic ims Client V14Q4_p3 software).

Quantitation of GFP signal intensity on focal stack images (Figure 3.9) was done by selecting the plane at the embryo middle section and then subtracting the average background of each corresponding image. Box-plots were created using R.

For yeast experiments, cells were cultured overnight at 30°C in a synthetic medium containing 2% raffinose, 0.1% sucrose and lacking the leucine amino acid to prevent the loss of the CEC-4-GFP plasmid. Next day cultures were diluted in the same medium containing raffinose and imaged when cells are at a concentration of 0.2-0.4 $x10^7$ cells/ml, live yeast cells were mounted on pad of agarose (1.4%) containing raffinose or galactose.

H3K9 ChIP-seq

Early embryo extracts, ChIP, library preparation and analysis was performed as described in (Gonzalez-Sandoval et al., 2015) with some modifications. ChIP was performed with 3-6 ug of each antibody coupled with Dynabeads Sheep Anti-mouse IgG (Invitrogen). Antibodies used: H3 (Abcam, ab10799), H3K9me2 (MBL, MABI0317) and H3K9me3 (MBL, MABI0318). Chromatin concentration used for over-night incubation: 10ug for H3 and 20ug for H3K9me2/3 ChIP. Finally, ChIP-seq signals are displayed as z-scores of IP – input for both wild-type and *cec-4* mutant samples.

Brood-size, Embryonic lethality and Male Induction scoring

Worms of corresponding genotypes were starved at 22.5°C, and shifted to 26°C on new plates with food for two generations. L4-stage worms of F3 were placed on individual plates and after 24hrs worms were removed from each plate into a new plate. This process was repeated over 3 consecutive days. Embryos, larvae and males were counted from each plate where the singled worms were placed. Brood-size is equal to the total number of larvae per worm. Embryo lethality is the ratio of total number of larvae by total number of embryos. Male induction is the total number of males divided by the total number of larvae.

RNAi

RNAi was performed by placing larval stage 1 (L1) worms on feeding plates as previously described (Timmons et al., 2001). Table S4 lists genes tested for CEC-4-mCherry localization experiments. All RNAi clones used were sequenced first to confirm target. As a mock RNAi control, the L4440 vector (Fire vector library) was modified by removing an *EcoRV* fragment containing 25bp identical to GFP-LacI.

Hybrigenic Services©

ULTImate Y2H™ is an optimized version of Y2H in the cell-to-cell mating process, patented by the company. Screen parameters: Nature – cDNA, Reference bait fragments – Caenorhabditis elegans-cec-4 (aa 162-270) & (aa 1-270), Prey library – Caenorhabditis elegans embryo_RP1, Vectors – pB27 (N-LexA-bait-C fusion) & pB35 (N-GAL4-bait-C fusion, inducible). Analyzed Interactions – 61, 62.3, 69, 64.8 millions in each screen respectively.

Y2H drop assay

Bait and prey vectors (all constitutively expressed under ADH promotor) (Table S3) provided by Hybrigenics Services© and an in-house positive control, were transformed in specific combinations (Table S5) in the yeast strain GA-6307. For drop assay 3 independent colonies were tested. The cultures were done in liquid medium lacking leucine (Leu) and tryptophan (Trp) to be sure to keep both plasmids. The Histidine (His) reporter gene was used to monitor the possible protein-protein interactions. Cultures were spotted on the appropriate synthetic medium (SC-Leu-Trp-His with or without 3AT) with highest concentration of 10^5 cells and a serial dilution of 5 fold. Plates after incubation for 2 days at 30^o C were analyzed for interaction. The assay was performed in presence or absence of 3AT at indicated concentrations, as inhibitor of HIS3 to reduce possible false positives interactions.

Table S1. List of worm strains used

Strain	**Genotype**	**Reference**
N2	wild-type, Bristol isolate	
GW105	*gwIs4 [baf-1p::GFP-lacI::let-858 3'UTR; myo-3p::RFP] X; gvIs[hsp-16.2::hlh-1 rol6(su1006)]*	(Meister et al., 2010)
GW211	*hpl-1(tm1624) gwIs4 [baf-1p::GFP-lacI::let-858 3'UTR; myo-3p::RFP] X*	(Gonzalez-Sandoval et al., 2015)
GW215	*hpl-2(tm1489) III; gwIs4 [baf-1p::GFP-lacI::let-858 3'UTR; myo-3p::RFP] X*	(Gonzalez-Sandoval et al., 2015)
GW631	*lin-61(n3809) I; gwIs4 [baf-1p::GFP-lacI::let-858 3'UTR; myo-3p::RFP] X*	(Towbin et al., 2012)
GW637	*met-2(n4256) set-25(n5021) III; gwIs4 [baf-1p::GFP-lacI::let-858 3'UTR; myo-3p::RFP] X*	(Towbin et al., 2012)
GW828	*cec-4(ok3124) IV*	(Gonzalez-Sandoval et al., 2015)
GW833	*cec-4(ok3124) IV; gwIs4 [baf-1p::GFP-lacI::let-858 3'UTR; myo-3p::RFP] X*	(Gonzalez-Sandoval et al., 2015)
GW849	*gwSi17 [cec-4p::cec-4::WmCherry::cec-4 3'UTR] II*	(Gonzalez-Sandoval et al., 2015)

GW860	*gwSi17 [cec-4p::cec-4::WmCherry::cec-4 3'UTR] II; gwIs4 [baf-1p::GFP-lacI::let-858 3'UTR; myo-3p::RFP] X*	(Gonzalez-Sandoval et al., 2015)
GW871	*gwSi17 [cec-4p::cec-4::WmCherry::cec-4 3'UTR] II; met-2(n4256) set-25(n5021) III; gwIs4 [baf-1p::GFP-lacI::let-858 3'UTR; myo-3p::RFP] X*	(Gonzalez-Sandoval et al., 2015)
GW964	*gwEx80[cec4p::cec4_161-270::Wmcherry-NLS-3'UTR]*	This study
GW977	*cec-4(ok3124) IV; hpl-1(tm1624) X ; gwIs4 [baf-1p::GFP-lacI::let-858 3'UTR; myo-3p::RFP] X*	This study
GW978	*hpl-2(tm1489) III; cec-4(ok3124) IV; gwIs4 [baf-1p::GFP-lacI::let-858 3'UTR; myo-3p::RFP] X*	This study
GW979	*lin-61(n3809) I; cec-4(ok3124) IV; gwIs4 [baf-1p::GFP-lacI::let-858 3'UTR; myo-3p::RFP] X*	This study
GW984	*met-2(n4256) set-25(n5021) III; cec-4(ok3124) IV; gwIs4 [baf-1p::GFP-lacI::let-858 3'UTR; myo-3p::RFP] X*	This study
GW1017	*cec-4(ok3124) IV; gwIs4 [baf-1p::GFP-lacI::let-858 3'UTR; myo-3p::RFP] X; gvIs [hsp-16.2::hlh-1 rol6(su1006)]*	(Gonzalez-Sandoval et al., 2015)
GW1153	*gwSi25[cec4p::cec4_161-270::Wmcherry-NLS-3'UTR]II*	This study
GW1174	*gwSi26[cec4p::cec4_1-161::Wmcherry-NLS-3'UTR]II*	This study
No stock	*cec4p::cec4_1-161::Wmcherry-NLS-3'UTR*	This study

Table S2. List of yeast strain used

Strain	**Background**	**Genotype**	**Reference**
GA-1340	W303	*can1-100* ***mlp1****::URA3* ***mlp2****::HIS3* ***esc1****::KanMx4*	(Andrulis et al., 2002)
GA-1469	W303	***mlp1****::TRP1*	(Hediger et al., 2002)
GA-1470	W303	***mlp2****::HIS3*	(Hediger et al., 2002)
GA-1526	W303	***mlp1****::TRP1,* ***mlp2****::HIS3*	(Hediger et al., 2002)
GA-2470	W303	***nup133****::HIS3*	(Bucci and Wente, 1998)
GA-3628	W303	*can1-100 NUP49::CFP-NUP49 URA3*	(Taddei et al., 2006)
GA-4887	W303	***mps3::mps3 delta75-150****KanMx6 tel1::URA*	(Schober et al., 2009)
GA-5306	W303	*can1-100* ***nup84****::His3*	(Nagai et al., 2008)
GA-5307	W303	*can1-100* ***nup120****::His3*	(Nagai et al., 2008)
GA-5545	W303	***src1****::hygro NUP49-GFP*	(Ferreira et al., 2011)
GA-5670	W303	***mlp1****::URA3* ***mlp2****::HIS3* ***siz2****::cloNAT*	(Ferreira et al., 2011)

GA-6307	L40	*MATa his3-Δ200 ade2 leu2-3, 112 trp1-901 lys2-801am LYS2::(lexApo)4-HIS3 URA3::(lexAop)8-LacZ*	(Horigome et al., 2011)

Table S3. List of plasmids used

Plasmid	**Description**
#1741	pFN3 pLexA-GAD4
#3488	pIK37_cec4p_cec4-D3(161-270)Wmcherry
#3508	pB27 cec-4 fusion N-lexA-cec-4-D3-C
#3509	pP6 Prey, fusion N-Gal4-AD-B0024.11-C
#3510	pP6 Prey, fusion N-Gal4-AD-C15H9.4-C
#3511	pP6 Prey, fusion N-Gal4-AD-ceh-37-C
#3512	pP6 Prey, fusion N-Gal4-AD-let-607-C
#3513	pP6 Prey, fusion N-Gal4-AD-ncam-1-C
#3514	pP6 Prey, fusion N-Gal4-AD-ttx-1-C
#3515	pB27 Fusion N-LexA-C
#3516	pP6 fusion N-Gal4_AD_C
#3582	pAG415GAL_cec4-GFP
#3677	pIK37_cec4p_cec4-D4(1-161)Wmcherry

Table S4. List of genes silenced by RNAi

Genes silenced by RNAi
anc-1
B0024.11
baf-1
C15H9.4
ceh-37
emr-1
lem-2
let-607
lmn-1
ncam-1

Genes silenced by RNAi
sun-1
ttx-1
unc-83
unc-84
zyg-12

Table S5. Combination of plasmids for Y2H interaction test

Bait	Prey	Clone name	Interaction
		no-prey	
#3508	no	cec-4-bait	negative control
		empty-prey	
#3508	#3516	cec-4-bait	negative control
		B0024.1-prey	
#3508	#3509	cec-4-bait	interaction test
		C15H9.4-prey	
#3508	#3510	cec-4-bait	interaction test
		ceh-37-prey	
#3508	#3511	cec-4-bait	interaction test
		let-607-prey	
#3508	#3512	cec-4-bait	interaction test
		ncam-1-prey	
#3508	#3513	cec-4-bait	interaction test
		ttx-1-prey	
#3508	#3514	cec-4-bait	interaction test
		no-prey	
#3515	no	empty-bait	negative control
		empty-prey	
#3515	#3516	empty-bait	negative control
		B0024.11-prey	
#3515	#3509	empty-bait	interaction test
		C15H9.4-prey	
#3515	#3510	empty-bait	interaction test
		ceh-37-prey	
#3515	#3511	empty-bait	interaction test
		let-607-prey	
#3515	#3512	empty-bait	interaction test
		ncam-1-prey	
#3515	#3513	empty-bait	interaction test
		ttx-1-prey	
#3515	#3514	empty-bait	interaction test
#1741	no	LexA-AD-fusion	positive control

REFERENCES

Andrulis, E.D., Zappulla, D.C., Ansari, A., Perrod, S., Laiosa, C.V., Gartenberg, M.R., and Sternglanz, R. (2002). Esc1, a Nuclear Periphery Protein Required for Sir4-Based Plasmid Anchoring and Partitioning. Mol Cell Biol *22*, 8292-8301.

Bucci, M., and Wente, S.R. (1998). A novel fluorescence-based genetic strategy identifies mutants of Saccharomyces cerevisiae defective for nuclear pore complex assembly. Mol Biol Cell *9*, 2439-2461.

Ferreira, H.C., Luke, B., Schober, H., Kalck, V., Lingner, J., and Gasser, S.M. (2011). The PIAS homologue Siz2 regulates perinuclear telomere position and telomerase activity in budding yeast. Nat Cell Biol *13*, 867-874.

Ferreira, H.C., Towbin, B.D., Jegou, T., and Gasser, S.M. (2013). The shelterin protein POT-1 anchors Caenorhabditis elegans telomeres through SUN-1 at the nuclear periphery. J Cell Biol *203*, 727-735.

Frokjaer-Jensen, C., Wayne Davis, M., Hopkins, C.E., Newman, B.J., Thummel, J.M., Olesen, S.-P., Grunnet, M., and Jorgensen, E.M. (2008). Single-copy insertion of transgenes in *Caenorhabditis elegans*. Nat Genet *40*, 1375-1383.

Gonzalez-Sandoval, A., Towbin, B.D., Kalck, V., Cabianca, D.S., Gaidatzis, D., Hauer, M.H., Geng, L., Wang, L., Yang, T., Wang, X.*, et al.* (2015). Perinuclear Anchoring of H3K9-Methylated Chromatin Stabilizes Induced Cell Fate in C. elegans Embryos. Cell *163*, 1333-1347.

Hediger, F., Dubrana, K., and Gasser, S.M. (2002). Myosin-like proteins 1 and 2 are not required for silencing or telomere anchoring, but act in the Tel1 pathway of telomere length control. J Struct Biol *140*, 79-91.

Horigome, C., Okada, T., Shimazu, K., Gasser, S.M., and Mizuta, K. (2011). Ribosome biogenesis factors bind a nuclear envelope SUN domain protein to cluster yeast telomeres. EMBO J *30*, 3799-3811.

Ikegami, K., Egelhofer, T.A., Strome, S., and Lieb, J.D. (2010). Caenorhabditis elegans chromosome arms are anchored to the nuclear membrane via discontinuous association with LEM-2. Genome biology *11*, R120.

Meister, P., Schott, S., Bedet, C., Xiao, Y., Rohner, S., Bodennec, S., Hudry, B., Molin, L., Solari, F., Gasser, S.M.*, et al.* (2011). Caenorhabditis elegans Heterochromatin protein 1 (HPL-2) links developmental plasticity, longevity and lipid metabolism. Genome biology *12*, R123.

Meister, P., Towbin, B.D., Pike, B.L., Ponti, A., and Gasser, S.M. (2010). The spatial dynamics of tissue-specific promoters during C. elegans development. Genes & Development *24*, 766-782.

Nagai, S., Dubrana, K., Tsai-Pflugfelder, M., Davidson, M.B., Roberts, T.M., Brown, G.W., Varela, E., Hediger, F., Gasser, S.M., and Krogan, N.J. (2008). Functional Targeting of DNA Damage to a Nuclear Pore-Associated SUMO-Dependent Ubiquitin Ligase. Science *322*, 597-602.

Roux, K.J., Kim, D.I., Raida, M., and Burke, B. (2012). A promiscuous biotin ligase fusion protein identifies proximal and interacting proteins in mammalian cells. Journal of Cell Biology *196*, 801-810.

Schindelin, J., Arganda-Carreras, I., Frise, E., Kaynig, V., Longair, M., Pietzsch, T., Preibisch, S., Rueden, C., Saalfeld, S., Schmid, B.*, et al.* (2012). Fiji: an open-source platform for biological-image analysis. Nat Methods *9*, 676-682.

Schober, H., Ferreira, H., Kalck, V., Gehlen, L.R., and Gasser, S.M. (2009). Yeast telomerase and the SUN domain protein Mps3 anchor telomeres and repress subtelomeric recombination. Genes Dev *23*, 928-938.

Sharma, R., Jost, D., Kind, J., Gomez-Saldivar, G., van Steensel, B., Askjaer, P., Vaillant, C., and Meister, P. (2014). Differential spatial and structural organization of the X chromosome underlies dosage compensation in C. elegans. Genes Dev *28*, 2591-2596.
Taddei, A., Van Houwe, G., Hediger, F., Kalck, V., Cubizolles, F., Schober, H., and Gasser, S.M. (2006). Nuclear pore association confers optimal expression levels for an inducible yeast gene. Nature *441*, 774-778.
Therizols, P., Illingworth, R.S., Courilleau, C., Boyle, S., Wood, A.J., and Bickmore, W.A. (2014). Chromatin decondensation is sufficient to alter nuclear organization in embryonic stem cells. Science *346*, 1238-1242.
Timmons, L., Court, D.L., and Fire, A. (2001). Ingestion of bacterially expressed dsRNAs can produce specific and potent genetic interference in *Caenorhabditis elegans*. Gene *263*, 103-112.
Towbin, Benjamin D., González-Aguilera, C., Sack, R., Gaidatzis, D., Kalck, V., Meister, P., Askjaer, P., and Gasser, Susan M. (2012). Step-Wise Methylation of Histone H3K9 Positions Heterochromatin at the Nuclear Periphery. Cell *150*, 934-947.
Zhang, Z., and Pugh, B.F. (2011). High-resolution genome-wide mapping of the primary structure of chromatin. Cell *144*, 175-186.

CHAPTER 4: CONCLUDING REMARKS AND FUTURE PROSPECTS

In this thesis I have investigated a mechanism through which chromatin is associated to the nuclear periphery in *C. elegans* embryos.

Using an established transgene-based reporter of heterochromatin, we have identified CEC-4, and H3K9me1/2/3 binding protein that is localized at the nuclear periphery for chromatin anchoring purposes. We confirmed the majority of the effects seen with the heterochromatic reporter to occur in endogenous chromatin. Thanks to the characteristics of CEC-4, further experiments identified a functional role of perinuclear chromatin anchoring in an induced muscle differentiation developmental program.

CEC-4 is a chromodomain protein with an intrinsic localization at the nuclear envelope. CEC-4 recognizes all three methylated forms of H3K9, a signal required for the perinuclear sequestration of chromatin. Therefore, it functions as a chromatin anchor protein. Anchoring by CEC-4 in embryos supports full commitment to an induced muscle differentiation program (Chapter 2). Work by Dr. D. Cabianca has shown that CEC-4 also has a partially redundant role in nuclei of some differentiated tissues, though CEC-4 is only essential for anchoring in embryos. Extensive characterization of CEC-4, shows that CEC-4 contributes to the perinuclear distribution of H3K9me3 marked chromatin, although distribution of H3K9me2 or me3 along the chromosomes is independent of CEC-4. Additionally, anchoring of chromatin by CEC-4 is not involved in timing of embryonic development under standard laboratory conditions nor brood-size or embryonic viability under stress temperature (26°C). Only a very slight increase in male induction is seen in *cec-4* mutant worms at 26°C, but further experiments are needed to confirm this result. While CEC-4 does not have a putative transmembrane domain, we attempted to identify an additional protein interactor that would anchor CEC-4 at the nuclear periphery. Several experiments were performed in both *C. elegans* and *S. cerevisiae* to screen for potential INM factors and none were identified. Finally, CEC-4 seems to have an activating role on gene expression under sensitized conditions (i.e. lack of other readers of H3K9) (Chapter 3) that is independent of its role in anchoring through H3K9 methylation.

The major conclusion drawn from the work presented on this thesis and potential future research are discussed here.

Perinuclear localization of chromatin is not necessary for gene silencing nor for cell differentiation under normal developmental conditions

There is a striking enrichment of dense staining, silent chromatin at the nuclear periphery (Comings, 1980). This nuclear sub-compartmentalization is gained over time during differentiation and several studies have presented the nuclear lamina as a repressive gene environment (reviewed in Akhtar and Gasser, 2007; Ciabrelli and Cavalli, 2015; Fadloun et al., 2013; Gibcus and Dekker, 2013; Kind and van Steensel, 2010; Mattout et al., 2015; Mattout and Meshorer, 2010; Towbin et al., 2009). Tethering experiments of genes towards

the nuclear lamina led to the ambiguous conclusion that for some genes it has a silencing effect, but for others it does not (Kumaran and Spector, 2008; Reddy et al., 2008). Several components of the nuclear lamina have been implicated in the tethering of chromatin to the nuclear periphery and only some of these components have an effect on gene expression. Unfortunately, many of thesenuclear envelope components have other important functions in the cell, making it difficult to conclude that changes in gene expression stem from changes in chromatin anchoring. Moreover, it has been described that tissue specific nuclear envelope proteins are required for the perinuclear position of whole chromosomes, yet no changes in gene expression were reported (reviewed in Talamas and Capelson, 2015).

We are beginning to understand the importance of histone and DNA modifications, and the enzymes that deposit or remove them, in both transcription and the formation of transcription-correlated compartments. Still we know little about what regulates epigenetic changes in chromatin structure and whether nuclear sub-compartments are a result or an active participant in epigenetic control. A greater understanding of the mechanisms involved in chromatin localization will allow us to address the cross-talk between spatial distribution and chromatin structure, and how they influence nuclear function.

Histone H3K9 methylation is essential for the sequestration of chromatin at the nuclear lamina in *C. elegans* (Towbin et al., 2012), and most likely this is a conserved phenomenon (Kind et al., 2013; Pinheiro et al., 2012). In this thesis we show that CEC-4 recognizes the methylation of H3K9 on chromatin for anchoring purposes (Gonzalez-Sandoval et al., 2015). Strikingly, gene expression profiles are not altered in embryos where anchoring is disrupted. This argues that anchoring of heterochromatin is not an essential driving force for silencing. In other words, gene silencing can occur without the need of nuclear periphery localization. Although many studies have reported the nuclear lamina as a repressive environment, additional studies are required to determine whether the sequestration of chromatin at the nuclear periphery (or its release) is a result or a cause of gene regulation. At least, in *C. elegans* early embryonic development, chromatin anchoring is not necessary for proper gene expression under normal conditions, scored on a mix-stage embryonic population level. Under the experimental conditions performed, we cannot exclude stochastic changes or cell to cell variations. Additionally, since chromatin at the periphery accumulates over time, we cannot exclude that at later stages anchoring does play a role in maintaining proper gene expression.

Moreover, H3K9 methylated chromatin anchoring does not play a significant role in cell differentiation. In both conditions where chromatin is detached in *C. elegans* embryos (lack of H3K9 methylation or of CEC-4), development continues without any dramatic difference in cell differentiation. This can also be seen in mouse, where it has been described an LBR and Lamin A/C dependent tethering of chromatin. Mice that lack both of these proteins present major issues in cell structure and nuclear organization and die immediately after birth. Yet ablation of both proteins does not prevent cell differentiation (Solovei et al., 2013).

Genome-wide analysis of DNA replication domain distribution correlates with the 3D organization of chromatin domains (Pope et al., 2014; Ryba et al., 2010). Chromatin associated with the nuclear lamina (LADs) correlate with late replicating domains (Rao et al., 2014). Upon neuronal differentiation, 20% of the genome changes replication timing concomitant with changes in gene expression of intermediate/low CpG-containing promoters and radial positioning towards the nuclear periphery for the specific loci tested (Hiratani et

al., 2008). Perhaps perinuclear localization of chromatin plays a more important role in relation to replication, than in the control of gene expression *per se*. In order to prove a causal link between subnuclear position and altered genome function, it is necessary to show genetically that the mechanism that mediates positioning also mediates late replication.

Chromatin anchoring can be involved in gene silencing, supporting the commitment to an induced differentiation program

The *cec-4* mutant worms proliferate like wild-type worms with no difference in brood-size or embryonic lethality at 20°C or 26°C (heat stress). We observed no obvious developmental delay nor other defect in embryonic stages in which we see delocalization of heterochromatin (Chapter 3). At later stages of worm development compensatory anchorage mechanisms act even in the *cec-4* mutant (Gonzalez-Sandoval et al., 2015) and perhaps masks the impact of mislocalization. This is also observed in the absence H3K9 methylation in worms (Towbin et al., 2012). Therefore, we sought a method to test the functionality of anchoring specifically during embryonic stages. Embryos lacking anchoring by deletion of *cec-4* do not have a reproducibly altered gene expression profile (except for one gene). This characteristic helped us directly address the effects of a lack of anchoring, since there would not be any indirect effects due to misexpressed genes. We examined the effect of *cec-4* mutation on an induced differentiation program, by the heat-shock inducible expression of the muscle master regulator HLH-1 (MyoD). In wild-type embryos, induction of HLH-1 forces cells into the muscle specification pathway, resulting in 100% conversion of embryos into muscle bodies. In contrast, about 25% of the *cec-4* mutant embryos manage to develop for the subsequent 24 hours to the point of hatching from the eggshell. Our interpretation is that the loss of heterochromatin anchoring impedes the proper commitment of cells to muscle, allowing cells to continue expressing other developmental programs, which lead to a larva-like state. Thus under this forced condition, anchoring of heterochromatin supports gene expression silencing, but unfortunately we do not understand how. It may influence events that prepare genes for tissue-restricted patterns of expression, such as early or late replication.

In mammalian cells a mechanism of oscillatory expression of the PARD3 circadian hub, through association with the nuclear lamina has been described (Zhao et al., 2015). PARD3 interacts with LADs and this contact is regulated by CTCF-PARP1. When cells are starved by serum shock and then released, the circadian rhythms are synchronized in HCT116 cells, allowing examination of the interactions of the PARD3 locus over time. Transcriptional activity of PARD3 remains high at the peak of recruitment to the nuclear lamina, and attenuation of transcription occurred after several hours concomitant with the addition of H3K9me2. The mechanism is not very well understood, but this study highlights that reposition of circadian genes towards the nuclear periphery is part of their regulation, but that association with the nuclear periphery does not lead to immediate transcriptional repression. Could the nuclear lamina function only to fine-tune gene regulation? The nuclear periphery seems to be influencing events related to silencing and depending on the case by case gene regulation, certain factors will retain silencing more efficiently at this location. The role of CEC-4 in such mechanisms remains to be discovered.

Worms have proven to be an invaluable tool for the study of nuclear organization, and further experiments may find conditions of physiological stress in which perinuclear anchoring plays

a role. In addition, identification and ablation of other anchors that function at later stages of development, will help us further understand the function of this nuclear subcompartment.

REFERENCES

Akhtar, A., and Gasser, S.M. (2007). The nuclear envelope and transcriptional control. Nat Rev Genet *8*, 507-517.

Ciabrelli, F., and Cavalli, G. (2015). Chromatin-driven behavior of topologically associating domains. J Mol Biol *427*, 608-625.

Comings, D.E. (1980). Arrangement of chromatin in the nucleus. Human Genetics *53*.

Fadloun, A., Eid, A., and Torres-Padilla, M.E. (2013). Mechanisms and dynamics of heterochromatin formation during mammalian development: closed paths and open questions. Curr Top Dev Biol *104*, 1-45.

Gibcus, J.H., and Dekker, J. (2013). The hierarchy of the 3D genome. Mol Cell *49*, 773-782.

Gonzalez-Sandoval, A., Towbin, B.D., Kalck, V., Cabianca, D.S., Gaidatzis, D., Hauer, M.H., Geng, L., Wang, L., Yang, T., Wang, X., *et al.* (2015). Perinuclear Anchoring of H3K9-Methylated Chromatin Stabilizes Induced Cell Fate in C. elegans Embryos. Cell *163*, 1333-1347.

Hiratani, I., Ryba, T., Itoh, M., Yokochi, T., Schwaiger, M., Chang, C.W., Lyou, Y., Townes, T.M., Schubeler, D., and Gilbert, D.M. (2008). Global reorganization of replication domains during embryonic stem cell differentiation. PLoS Biol *6*, e245.

Kind, J., Pagie, L., Ortabozkoyun, H., Boyle, S., de Vries, S.S., Janssen, H., Amendola, M., Nolen, L.D., Bickmore, W.A., and van Steensel, B. (2013). Single-cell dynamics of genome-nuclear lamina interactions. Cell *153*, 178-192.

Kind, J., and van Steensel, B. (2010). Genome-nuclear lamina interactions and gene regulation. Curr Opin Cell Biol *22*, 320-325.

Kumaran, R.I., and Spector, D.L. (2008). A genetic locus targeted to the nuclear periphery in living cells maintains its transcriptional competence. J Cell Biol *180*, 51-65.

Mattout, A., Cabianca, D.S., and Gasser, S.M. (2015). Chromatin states and nuclear organization in development--a view from the nuclear lamina. Genome biology *16*, 174.

Mattout, A., and Meshorer, E. (2010). Chromatin plasticity and genome organization in pluripotent embryonic stem cells. Curr Opin Cell Biol *22*, 334-341.

Pinheiro, I., Margueron, R., Shukeir, N., Eisold, M., Fritzsch, C., Richter, F.M., Mittler, G., Genoud, C., Goyama, S., Kurokawa, M., *et al.* (2012). Prdm3 and Prdm16 are H3K9me1 methyltransferases required for mammalian heterochromatin integrity. Cell *150*, 948-960.

Pope, B.D., Ryba, T., Dileep, V., Yue, F., Wu, W., Denas, O., Vera, D.L., Wang, Y., Hansen, R.S., Canfield, T.K., *et al.* (2014). Topologically associating domains are stable units of replication-timing regulation. Nature *515*, 402-405.

Rao, S.S., Huntley, M.H., Durand, N.C., Stamenova, E.K., Bochkov, I.D., Robinson, J.T., Sanborn, A.L., Machol, I., Omer, A.D., Lander, E.S., *et al.* (2014). A 3D map of the human genome at kilobase resolution reveals principles of chromatin looping. Cell *159*, 1665-1680.

Reddy, K.L., Zullo, J.M., Bertolino, E., and Singh, H. (2008). Transcriptional repression mediated by repositioning of genes to the nuclear lamina. Nature *452*, 243-247.

Ryba, T., Hiratani, I., Lu, J., Itoh, M., Kulik, M., Zhang, J., Schulz, T.C., Robins, A.J., Dalton, S., and Gilbert, D.M. (2010). Evolutionarily conserved replication timing profiles predict long-range chromatin interactions and distinguish closely related cell types. Genome Res *20*, 761-770.

Solovei, I., Wang, A.S., Thanisch, K., Schmidt, C.S., Krebs, S., Zwerger, M., Cohen, T.V., Devys, D., Foisner, R., Peichl, L.*, et al.* (2013). LBR and lamin A/C sequentially tether peripheral heterochromatin and inversely regulate differentiation. Cell *152*, 584-598.
Talamas, J.A., and Capelson, M. (2015). Nuclear envelope and genome interactions in cell fate. Front Genet *6*, 95.
Towbin, Benjamin D., González-Aguilera, C., Sack, R., Gaidatzis, D., Kalck, V., Meister, P., Askjaer, P., and Gasser, Susan M. (2012). Step-Wise Methylation of Histone H3K9 Positions Heterochromatin at the Nuclear Periphery. Cell *150*, 934-947.
Towbin, B.D., Meister, P., and Gasser, S.M. (2009). The nuclear envelope -- a scaffold for silencing? Current Opinion in Genetics & Development *19*, 180-186.
Zhao, H., Sifakis, E.G., Sumida, N., Millan-Arino, L., Scholz, B.A., Svensson, J.P., Chen, X., Ronnegren, A.L., Mallet de Lima, C.D., Varnoosfaderani, F.S.*, et al.* (2015). PARP1- and CTCF-Mediated Interactions between Active and Repressed Chromatin at the Lamina Promote Oscillating Transcription. Mol Cell *59*, 984-997.

APPENDIX

Supplemental Material (related to Chapter 2):

- Supplemental Experiments Procedures
- Supplemental Tables
- Supplemental References

Cell

Supplemental Information

Perinuclear Anchoring of H3K9-Methylated Chromatin Stabilizes Induced Cell Fate in *C. elegans* Embryos

Adriana Gonzalez-Sandoval, Benjamin D. Towbin, Veronique Kalck, Daphne S. Cabianca, Dimos Gaidatzis, Michael H. Hauer, Liqing Geng, Li Wang, Teddy Yang, Xinghao Wang, Kehao Zhao, and Susan M. Gasser

Supplemental Experimental Procedures:

Constructs and Strains

Gene synthesis of *cec-4* for protein expression and yeast constructs were from GenScript USA Inc. For the CEC-4 tagged construct, the gene was amplified from N2 worm genomic DNA. All plasmid constructs were generated by MultiSite Gateway® cloning (Invitrogen). The Y87A and Y111A point mutations in the *cec-4* gene, referred to as 2YA, were introduced by multi-site-directed mutagenesis (Agilent Technologies) for both *in vivo* and *in vitro* experiments. All worm and yeast strains used are listed in Table S1 and S2, respectively. The *cec-4(ok3124)* strain received from CGC was out-crossed six times to N2 wild-type strain. CEC-4 tagged wild-type and mutant cd2YA versions, were made using the MosSCI technique (Frokjaer-Jensen et al., 2008). The MosSCI strains were out-crossed twice to N2 wild-type strain. The EMR-1-mCherry strain was kindly provided by P. Askjer; the intestine specific marker strain (*nhx-2p::npp-9::GFP*) in Fig. 6F by Hendricks G.J. and H. Grosshans (Friedrich Miescher Institute for Biomedical Research, Basel, Switzerland, personal communication). Worms for microscopy experiments were grown at 22.5˚C; RNA and LEM-2 ChIP sequencing strains were grown at 20˚C; qPCR strains were grown at 20˚C except for Fig. 6B at 22.5˚C. For yeast experiments, CEC-4 full length (1-270 aa), CEC-4N (1-144 aa) and CEC-4C (142-270 aa) were cloned into Advanced Gateway Destination vector plasmid 14193 (pAG415GAL-ccdB-EGFP); plasmids were transformed using standard transformation protocol in GA-1981 or GA-3628 strains (see Table S2 for strain details). Yeast were grown at 30°C.

RNAi

RNAi was performed by placing larval stage 1 (L1) worms on feeding plates as previously described (Timmons et al., 2001). Table S3 and S6 lists genes tested in RNAi screen and CEC-4-

mCherry localization experiments. All RNAi clones used were sequenced first to confirm target. As a mock RNAi control, the L4440 vector (Fire vector library) was modified by removing an *EcoRV* fragment containing 25bp identical to GFP-LacI.

Immunofluorescence (IF)

IF for Fig. S1C was done as described in (Meister et al., 2010), and for Fig. 2B and 5C IF as described in (Rohner et al., 2013). Antibodies used in pairs: for *gwIs4:* monoclonal anti-GFP (MBL-D153-3) and Alexa-488 anti-rat; for H3K9 methylation: monoclonal anti-H3K9me3 (Wako #303-34832) and Alexa-568 anti-mouse; for nuclear pores: monoclonal mAB414 (Abcam ab24609) and Alexa-555 anti-mouse; for lamin: anti-CeLMN-1 (a gift from Y. Gruenbaum, The Hebrew University of Jerusalem, Jerusalem, Israel) and Alexa-488, -555 or -647 anti-rabbit; for CEC-4-mCherry: monoclonal anti-mCherry (Life technologies M11217) and Alexa-488 anti-rat; for nucleolus: anti-Fibrillarin (kindly provided by P. Heun, Welcome Trust Center for Cell Biology, Edinburgh, UK) and Alexa-555 anti-human.

Microscopy

Except for Fig. 2B and 6C, microscopy was carried out on spinning disk multipoint confocal microscopes: (1) AxioImager M1 [Carl Zeiss] + Yokogawa CSU-22 scan head, Plan-Neofluar 100×/1.45 NA oil objective, EM-CCD camera [Cascade II; Photometrics], and MetaMorph 7.7.2 software or (2) Olympus IX81 + Yokogawa CSU-X1 scan head, PlanApo 100x/1.45 TIRFM or 60x/1.45 NA oil objectives, 2X Back-illuminated EM-CCD EvolveDelta (Photometrics), and VisiView 2.1.4 software. Live microscopy samples were prepared as previously described (Meister et al., 2010). Figs. 1E, 1F, 5C and S1C were de-convolved with Huygens Pro software. Single plane and 3D reconstruction (maximum intensity Z-projections) images and analysis were generated using Fiji/ImageJ software (Schindelin et al., 2012). Quantitation of array and

nucleolus distribution on focal stacks of images was done with plugin PointPicker (http://bigwww.epfl.ch/ thevenaz/pointpicker/) as described (Meister et al., 2010); for proper quantitation in *cec-4(ok3124)* mutant, we used a strain with an additional copy of a lacO free *baf-1p::GFP-LacI* transgene (*gwIs39*), to enhance the GFP signal and be able to identify nuclear periphery.

Quantitation of GFP/RFP signal intensity on focal stack images was done selecting the plane at the embryo middle section and subtracting the average background of corresponding image. In Fig. 1F all strains were compared to average wild-type signal intensity. In Fig. S2D, quantitation of CEC-4-mCherry enrichment over array on focal stacks of images was done measuring, for each nucleus, the mCherry intensity in the nuclear volume occupied by the array and divided by the mCherry intensity in an equivalent region outside the array at the nuclear periphery. In Fig. 2D, quantitation of CEC-4-mCherry and EMR-1-mCherry fluorescent intensity in various tissues of L1 worms was performed on single nuclei, selecting a middle nuclear section plane; the obtained intensity values were normalized on the average background fluorescence of the corresponding image. Zoning assay graphs were done in Microsoft Excel and Intensity signal box-plots in R.

For Fig. 1F Fiji ImageJ was used to change de dynamic range of deconvolved images, giving more value to low intense pixels (same settings applied to all images). Pixel classification in Ilastik 1.1.5 image analysis and classification software (Sommer, 2011)was used to segment the greyscale images in 3D space. With all Ilastik features selected, three individual labels were trained for detecting (1) the background, (2) the nuclei and (3) the GFP foci. A Matlab based function was used analyze the Ilastik probability maps and calculate different nuclei and foci parameters. Spot volume describes the 3D foci dimensions in voxels and Spot distance is

calculated by measuring the minimal 3D distance from the Spot centroid to the nuclear periphery.

For Fig. 2B, high-resolution imaging was performed with a super resolution-structured illumination (SR-SIM) microscope (Elyra S.1 [Carl Zeiss], Plan-Apochromat 63x/1.4 NA objective lens, EM-CCD camera [iXon 885; Andor Technology], and ZEN Blue 2010D software [Carl Zeiss]). Processing was performed with Zen software [Carl Zeiss]. For Fig. 6C, microscopy was carried out on fluorescence stereomicroscope (Leica MZ FL III, PlanApo 2x/0.07 NA, Leica DFC350 FX camera 0.63x lens, and Imagic ims Client V14Q4_p3 software).

For yeast experiments (Fig. S2B and C), cells were cultured overnight at 30°C in a synthetic medium containing 2% raffinose, 0.1% glucose and lacking leucine to prevent the loss of the plasmid. The next day cultures were diluted in the same medium containing raffinose only, and were imaged when cells reached a concentration of 0.2-0.4 $x10^7$ cells/ml. Live yeast cells were mounted on pad of agarose (1.4%) containing raffinose or galactose for imaging.

Multiple sequence alignment

CEC-4 and *H. sapiens* CBX protein sequences were aligned with ClustalW (www.ebi.ac.uk), and visualized by Jalview (Waterhouse et al., 2009).

Recombinant protein purification

The CEC-4 CD (aa 25-141) and CEC-4 cd-2YA (aa 25-141, Y87A-Y111A) constructs were cloned into pOPINF vector using the In-Fusion system (Clontech) (Berrow et al., 2007), proteins were expressed in the *E. coli* strain BL21 Rosetta pLysS and affinity purified through the His tag binding to ProBond Ni-NTA resin (Invitrogen) according to manufacturer's instructions. For ITC experiments His tag was removed by HRV 3C protease digestion (Novagen) and proteins were

further purified by gel filtration on a HiLoad 16/60 Superdex 75 column in 20 mM Tris pH 7.5, 200 mM NaCl, 0.02% NaN3 and 1 mM TCEP. Purity was confirmed by SDS–PAGE and Coomassie blue staining. Protein concentration was measured by UV absorbance (280 nm).

Binding Assay SulfoLink

H3K9me0 and H3K9me3 peptides (aa 1-20 + Cys) (gift from A. Peters, Friedrich Miescher Institute for Biomedical Research, Basel, Switzerland) were reduced and coupled to SulfoLink beads (Thermo scientific) according to manufacturer's instructions. 25µM of recombinant His tagged CEC-4 CD and CEC-4 cd-2YA were incubated with the peptide-beads slurry (7µM peptide concentration) for 2 h at 4ºC on a rotator. After washing three times with 20mM Tris-HCl pH 7.5, 0.2M NaCl and 0.05% Triton X-100 for 1min-5min-1min, respectively, bound proteins were released from the beads, run on an SDS-PAGE gel, and stained by SYPRO® Ruby.

Peptide array library and AlphaScreen direct binding

AlphaScreen direct binding assays were performed in 384-well plate (ProxiPlate^{TM}-384 Plus, Perkin Elmer) with AlphaScreen Histidine Detection kit (Nickel Chelate, PerkinElmer #6760619) in optimized assay buffer (25mM HEPES, 100mM NaCl, 0.1% BSA, 0.05% Tween20, pH=7.5). The binding of CEC-4 CD to histone peptides was performed by AlphaScreen assay with ALTA Biosciences peptide array system (Alta Biosciences, UK). Three different peptide concentrations (62.5, 125 and 250nM) were used to screen histone peptides binding to CEC-4 CD (200nM). Quantitation was based on the intensity readout. The peptides with an intensity of 50-fold more than the control (assay condition without protein) were considered as hits. Table S4 shows raw data generated from AlphaScreen.

AlphaScreen direct binding was further used for confirmation of methylated H3K9 binding to CEC-4 CD. 3µl of 2-fold serial dilutions of N-terminal biotinylated histone $H3_{1-21}$K9 peptides, final concentration 0.5-500nM, were plated in a 384-well plate followed by adding 3µl of N-terminal His-tagged CEC-4 CD (final 200nM). After incubation at room temperature for 1 hour, 3µl of streptavidin-coated donor beads (20ug/ml) and 3µl of nickel chelate acceptor beads (20ug/ml) were then added under low light conditions. The plates were sealed and incubated at room temperature for 1 h, then read on an EnVision multilabel Plate Reader (Perkin Elmer).

Peptide displacement assay

IC50 (half maximal inhibitory concentration) for H3K9 peptides to CEC-4 CD were measured by AlphaScreen peptide displacement assay and done in duplicate. 2-fold series dilution of non-biotinylated H3K9 peptides starting from 100µM were used for competing with the binding of biotin-H3K9me2 (50nM) to CEC-4 CD (25nM). After incubation at room temperature for 1 hour, streptavidin-coated donor beads (20ug/ml) and nickel chelate acceptor beads (20ug/ml) were then added under low light conditions. The plate was then read on the EnVision using the AlphaScreen protocol after 1 hour incubation.

Isothermal Titration Calorimetry (ITC)

ITC was carried out on a MicroCal iTC200 calorimeter (GE Healthcare) at 25°C in 20 mM Tris-HCl pH7.5, 100 mM NaCl. 30 µM recombinant-cleaved CEC-4 CD and CEC-4 cd-2YA proteins were loaded into sample cell, 450µM histone $H3_{1-21}$K9 or $H3_{28-48}$K37 peptide solution was sequentially injected into sample cell; with exception of 800µM for $H3_{28-48}$K37me3 . Thermodynamic parameters N (stoichiometry), Ka (association constant), ΔH (enthalpic change) and ΔS (entropy change) were obtained by nonlinear least-square fitting using Origin software. ITC experiments were performed twice.

LEM-2 Chromatin Immuno-precipitation followed by deep sequ encing (ChIP-seq)

Wild-type, *met-2 set-25* and *cec-4* mutant strains were grown in parallel and in two independent biological replicas. For each strain, 400,000 L1 worms were grown synchronously in 500 ml S-medium containing HB101 *E. coli* strain, as food source, under continuous agitation (180 rpm) at 20ºC until gravid adults with early embryos were observed (between 60-65 hours depending on strain). Embryonic progeny was harvested using hypochlorite treatment. Embryos were cross-linked with 2.16% formaldehyde in M9 buffer for 30 minutes at room temperature, washed twice with M9 and once with FA buffer (50mM HEPES-KOH pH7.5, 1mM EDTA, 1% Triton X-100, 0.1% sodium deoxycholate, 150mM NaCl). LEM-2 ChIP was performed as described (Ikegami et al., 2010) with anti-LEM-2 (Novus Biologicals #48540002). Libraries were prepared from chromatin IP (1.7 -7.4 ng) and input (10 ng) samples using the NEBNext ultra DNA library prep kit for Illumina (NEB # 7370) and the NEBNext Multiplex Oligos for Illumina (NEB # E7335), according to the manufacturer's recommendations. No size selection was performed during sample preparation and the libraries were indexed and amplified using 15 PCR cycles, using the recommended conditions. After a final cleanup with Agencourt AmPure XP beads (Beckman # A63881), the library size distribution and concentrations were determined using a BioAnalyzer 2100 (Agilent technologies) and Qubit (Invitrogen) instrument, respectively. The final pools were prepared by mixing equimolar amounts of all individually indexed libraries and then sequenced on a HiSeq 2500 (Illumina) in Rapid mode (Paired-End 50). Processing of the LEM-2 ChIP-seq data, all paired-end ChIP-seq data (2x50bp) were mapped to the *C. elegans* genome (ce6) with the R package QuasR (Gaidatzis et al., 2015) (http://www.bioconductor.org/packages/3.1/bioc/html/QuasR.html) using the included aligner bowtie (Langmead et al., 2009) allowing only for uniquely mapping read pairs. The command

used to do the alignments was "proj<- qAlign("samples.txt","BSgenome.Celegans.UCSC.ce6")" which instructs bowtie to align using the parameters "--fr -m 1 --best --strata --maxins 500 --phred33-quals". Read density along the genome was calculated by tiling the genome into 200kb windows (non-overlapping) and counting the number of sequence fragments within each window. The command used to create the window count table was qCount(proj,regions,useRead="first"). This instructs QuasR to position each read at the middle of its respective fragment (determined by the two reads) and to only consider the first read (on any strand) for quantitation in order to avoid double counting. To compensate for differences in the read depths of the various libraries, we divided each sample by the total number of mapped reads and multiplied by the average library size. Log2 expression levels were calculated after adding a pseudocount of 1 (y=log2(x+1)). Finally, ChIP-seq signals are displayed as z-scores of IP – input.

RNA followed by deep sequencing (RNA-seq)

Wild-type, *met-2 set-25*, *cec-4* mutant strains were grown in two independent biological replicas. For each strain, 100,000 - 200,000 L1 worms were grown synchronously in 250 ml S-medium containing HB101 *E. coli* strain under continuous agitation (180 rpm) at 20ºC until gravid adults with early embryos were observed (between 60-65 hours depending on strain). Embryonic progeny was harvested using hypochlorite treatment, re-suspended in 500µl Trizol® and snap-freeze in liquid nitrogen. Extraction of RNA was performed according to the WormBook protocol (Stiernagle, 2006). Total RNA was purified using RNeasy kit (QIAGEN 74104) including DNase treatment. Depletion of ribosomal RNA was done for 5 µg of total RNA with Ribo-Zero™ Margnetic Gold Kit (Epicentre MRGZG12324) and further concentrated with RNA Clean & Concentrator™ kit (Zymo Research R1015) according to corresponding manufacturer's

instructions. From the depleted RNA 50ng were used for library preparation with the ScriptSeq v2 RNA-seq Library preparation kit (Epicentre). Equimolar pools of 3 samples were created and loaded on an Illumina HiSeq v3 flowcell using a cBot. Sequencing was performed on a HiSeq 2500 sequencer for 51 cycles running RTA 1.17.21.3. Samples were demultiplexed and FastQ files were generated using blc2fastq-1.8.4. Processing of the RNA-seq data, gene expression levels from RNA-seq data were quantified as described previously (Hendriks et al., 2014) using WormBase (WS190) annotation for coding transcripts and in windows of 500bp (unstranded) for the whole genome, in order to track non-genic changes.

Real-Time Quantitative PCR (RT-qPCR)

For gene expression levels in Fig. 5F same initial RNA extracts were used as for RNA-seq with addition of parallel grown and extracted cultures of *met-2* and *set-25* single mutant strains. For Fig. 6B three independent replicas of mixed stage embryo extracts were collected as described below in the Heat-shock induced muscle differentiation section. For Fig. S5C five independent early embryo extracts were used: starting from 25, 000 synchronized L1 worms of wild-type and *cec-4* mutant grown on peptone-rich (PR) plates with OP50 *E.coli* for 60-65 hours until gravid adults with early embryos were observed; RNA extraction was performed by 4 rounds of freeze cracking, treat with chloroform and transfer aqueous phase to Direct-zol™ column and follow manufacturer's instructions (30 minutes DNase I digestion included). For all RNA extracts cDNA synthesis was done with SuperScript® III First-Strand Synthesis System (Thermo Fisher Scientific 18080-051) according to manufacturer's instructions, starting from 1-2 µg of total RNA and using $(dT)_{20}$ oligos; RNase H treatment was included.

LEM-2 ChIP qPCR samples of corresponding genotypes were produced as described above for LEM-2 Chromatin Immuno-precipitation followed by deep sequencing.

All RT-qPCR reactions were done in 10µl volume, using diluted cDNA to 500ng or total volume of ChIPed and Input (10% of total material used) samples, with SYBR® Green PCR Master Mix (Life technologies 4309155) for Fig. 6B and 5F mRNA or GoTaq® Green Master Mix (Promega M712) for Fig. 5E and S5C according to manufacturer's instructions. Gene-specific primers (see Table S5) were used in 300nM concentration. StepOnePlus™ System (Life technologies 4376600) was used for qPCR run and data collection. Further analysis was done in Microsoft Excel.

All primer pairs were tested and selected for amplification efficiencies ranging from 90-100%, except for *unc-98* with 83%, *C18D6.4* with 73% and *myo-3* with 68%. For gene expression analysis $\Delta\Delta C_T$ method was used, *pmp-3* carried as housekeeping gene for sample normalization. For ChIP-qPCR ChIP sample data was normalized to corresponding input chromatin (reported as percentage input on figures).

Heat-shock induced muscle differentiation

Except for Fig. 6B, two cell stage embryos were isolated from transgenic gravid adults containing heat-shock (HS) expression construct *gvIs[hsp-16.2::hlh-1 rol6(su1006)]* and *gwIs4 [baf-1p::GFP-lacI::let-858 3'UTR; myo-3p::RFP]* or *[nhx-2p::npp-9::BLRP:GFP:3xHA-unc-54 3'UTR]* and different genetic backgrounds as stated in each figure; in Fig. 6C an extra *cec-4* mutant alone was carried as control for HS induction. Isolated embryos were incubated for 300 min at 22.5°C, either directly on agarose slides or in liquid inside humid chamber. All working genotypes reach embryonic bean stage after this incubation period. Embryos were shifted to 34°C for 10 min in a thermal cycler with a In-Situ slide block. Recovery from HS induction was done at 22.5°C in humid chamber and assessment of hatched larva-like worms was done in between 18 to 24 h after HS. Images were taken on stereomicroscope and/or spinning disk

confocal microscope, as appropriate. As controls for myogenic conversion we observed twitching and fluorescent reporter *myo-3p::RFP* bared in *gwIs4* array. For Fig. 6B, synchronized L1 worms of corresponding genotypes were plated on PR-plates with OP50 bacteria, and incubated for 2 days at 22.5°C until gravid adulthood. Embryonic progeny was harvested using hypochlorite treatment. Mixed stage embryos were split into three 1.5ml tubes with equal volumes: one tube was re-suspended in 500µl Trizol® and snap-frozen in liquid nitrogen (before HS condition), the rest were heat-shocked in a thermal cycler for 10 min at 34°C. They recovered at room temperature, one tube for 40 min (40' after HS) and second tube 24 h (24h after HS). Both tubes were re-suspended in Trizol® and snap-frozen like the "before HS" sample.

Table S1. List of worm strains used in this study. Related to Experimental Procedures

Strain	Genotype	Reference
N2	wild-type, Bristol isolate	
GW76	*gwIs4 [baf-1p::GFP-lacI::let-858 3'UTR; myo-3p::RFP] X*	(Meister et al., 2010)
GW105	*gwIs4 [baf-1p::GFP-lacI::let-858 3'UTR; myo-3p::RFP] X; gvIs[hsp-16.2::hlh-1 rol6(su1006)]*	(Meister et al., 2010)
GW211	*hpl-1(tm1624) gwIs4 [baf-1p::GFP-lacI::let-858 3'UTR; myo-3p::RFP] X*	This study
GW215	*hpl-2(tm1489) III; gwIs4 [baf-1p::GFP-lacI::let-858 3'UTR; myo-3p::RFP] X*	This study
GW566	*gwIs39 [baf-1p::GFP-LacI::let-858 3'UTR; vit-5p::GFP] III; gwIs4 [baf-1p::GFP-lacI::let-858 3'UTR; myo-3p::RFP] X*	(Towbin et al., 2012)
GW631	*lin-61(n3809) I; gwIs4 [baf-1p::GFP-lacI::let-858 3'UTR; myo-3p::RFP] X*	(Towbin et al., 2012)
GW637	*met-2(n4256) set-25(n5021) III; gwIs4 [baf-1p::GFP-lacI::let-858 3'UTR; myo-3p::RFP] X*	(Towbin et al., 2012)
GW638	*met-2(n4256) set-25(n5021) III*	(Towbin et al., 2012)
GW641	*set-25(n5021) III*	(Towbin et al., 2012)
GW793	*lin-61(n3809) I; hpl-1(tm1624) gwIs4 [baf-1p::GFP-lacI::let-858 3'UTR; myo-3p::RFP] X*	This study
GW796	*lin-61(n3809) I; hpl-2(tm1489) III; hpl-1(tm1624) gwIs4 [baf-1p::GFP-lacI::let-858 3'UTR; myo-3p::RFP] X*	(Towbin et al., 2012)
GW828	*cec-4(ok3124) IV*	This study
GW829	*gwIs39 [baf-1p::GFP-LacI::let-858 3'UTR; vit-5p::GFP] III; cec-4(ok3124) IV; gwIs4 [baf-1p::GFP-lacI::let-858 3'UTR; myo-3p::RFP] X*	This study
GW833	*cec-4(ok3124) IV; gwIs4 [baf-1p::GFP-lacI::let-858 3'UTR; myo-3p::RFP] X*	This study
BN142	*bqSi142 [pBN20 Pemr-1::emr-1::mCherry)] II*	(Morales-Martinez et al., 2015)
GW835	*ttTi5605 II?; unc-119(?) gwIs39 [baf-1p::GFP-LacI::let-858 3'UTR; vit-5p::GFP] III; gwIs4 [baf-1p::GFP-lacI::let-858 3'UTR; myo-3p::RFP] X ; gwIs85 [his-72p::mcherry-set-25::his-72 3'UTR; unc-119(+)]*	This study
GW836	*ttTi5605 II?; unc-119(?) gwIs39 [baf-1p::GFP-LacI::let-858 3'UTR; vit-5p::GFP] III; cec-4(ok3124) IV; gwIs4 [baf-1p::GFP-lacI::let-858 3'UTR; myo-3p::RFP] X ; gwIs85 [his-72p::mcherry-set-25::his-72 3'UTR; unc-119(+)]*	This study
GW849	*gwSi17 [cec-4p::cec-4::WmCherry::cec-4 3'UTR] II*	This study
GW860	*gwSi17 [cec-4p::cec-4::WmCherry::cec-4 3'UTR] II; gwIs4 [baf-1p::GFP-lacI::let-858 3'UTR; myo-3p::RFP] X*	This study
GW862	*gwSi17 [cec-4p::cec-4::WmCherry::cec-4 3'UTR] II; cec-4(ok3124) IV; gwIs4 [baf-1p::GFP-lacI::let-858 3'UTR; myo-3p::RFP] X*	This study
GW871	*gwSi17 [cec-4p::cec-4::WmCherry::cec-4 3'UTR] II; met-2(n4256) set-25(n5021) III; gwIs4 [baf-1p::GFP-lacI::let-858 3'UTR; myo-3p::RFP] X*	This study
GW905	*gwSi18 [cec-4p::cec-4cd2YA::WmCherry::cec-4 3'UTR] II; cec-4(ok3124) IV; gwIs4 [baf-1p::GFP-lacI::let-858 3'UTR; myo-3p::RFP] X*	This study
GW907	*met-2(n4256) III*	This study
GW1017	*cec-4(ok3124) IV; gwIs4 [baf-1p::GFP-lacI::let-858 3'UTR; myo-3p::RFP] X; gvIs [hsp-16.2::hlh-1 rol6(su1006)]*	This study
GW1041	*bqSi142 [pBN20 Pemr-1::emr-1::mCherry)] II; gwIs39 [baf-1::GFP-LacI::let-858 3'UTR; vit-5::GFP] III; cec-4(ok3124) IV; gwIs4 [baf-1p::GFP-lacI::let-858 3'UTR; myo-3p::RFP] X*	This study
GW1056	*bqSi142 [pBN20(unc-119(+) Pemr-1::emr-1::mCherry)] II; gwIs39 [baf-1::GFP-LacI::let-858 3'UTR; vit-5::GFP] III; gwIs4 [baf-1p::GFP-lacI::let-858 3'UTR; myo-3p::RFP] X*	This study
GW1160	*met-2(n4256)set-25(n5021) III; gwIs4 [baf-1p::GFP-lacI::let-858 3'UTR; myo-3p::RFP] X; gvIs [hsp-16.2::hlh-1 rol6(su1006)]*	This study
GW1192	*gwSi17 [cec-4p::CEC-4-WmCherry::cec-4 3'UTR] II; cec-4(ok3124) IV; gwIs4 [baf-1p::GFP-lacI::let-858 3'UTR; myo-3p::RFP] X; gvIs [hsp-16.2::hlh-1 rol6(su1006)]*	This study
GW1193	*gwSi18 [cec-4p::CEC-4_Y87A_Y111A-WmCherry::cec-4 3'UTR] ttTi5605 II; cec-4(ok3124) IV; gwIs4 [baf-1p::GFP-lacI::let-858 3'UTR; myo-3p::RFP] X; gvIs [hsp-16.2::hlh-1 rol6(su1006)]*	This study
GW1262	*[nhx-2p::npp-9::GFP] II; gvIs [hsp-16.2::hlh-1 rol6(su1006)]*	Unpublished
GW1263	*[nhx-2p::npp-9::GFP] II; cec-4(ok3124) IV; gvIs [hsp-16.2::hlh-1 rol6(su1006)]*	Unpublished
RB2301	*cec-4(ok3124) IV*	Obtained from CGC*

*CGC: Caenorhabditis Genetics Center
Alleles marked with a question mark (?) were not genotyped after genetic crosses

Supplemental Tables:

Table S2. List of yeast strains. Related to Experimental Procedures

Strain	Background	Genotype	Reference
GA-1340	W303	*can1-100* ***mlp1****::URA3* ***mlp2****::HIS3* ***esc1****::KanMx4*	(Andrulis et al., 2002)
GA-1469	W303	***mlp1****::TRP1*	(Hediger et al., 2002)
GA-1470	W303	***mlp2****::HIS3*	(Hediger et al., 2002)
GA-1526	W303	***mlp1****::TRP1,* ***mlp2****::HIS3*	(Hediger et al., 2002)
GA-1981	W303	*MATa/MATα, leu2-3,112/leu2-3,112, his3-11,15/his3-11,15, trp1-1/trp1-1, can1-100/can1-100, ade2-1/ade2-1, ura3-1/ura3-1 = W303 diploid*	(Thomas and Rothstein, 1989)
GA-2470	W303	***nup133****::HIS3*	(Bucci and Wente, 1998)
GA-3628	W303	*can1-100 NUP49::CFP-NUP49 URA3*	(Taddei et al., 2009)
GA-4887	W303	***mps3::mps3 delta75-150****KanMx6 tel1::URA*	(Schober et al., 2009)
GA-5306	W303	*can1-100* ***nup84****::His3*	(Nagai et al., 2008)
GA-5307	W303	*can1-100* ***nup120****::His3*	(Nagai et al., 2008)
GA-5545	W303	***src1****::hygro NUP49-GFP*	(Ferreira et al., 2011)
GA-5670	W303	***mlp1****::URA3* ***mlp2****::HIS3* ***siz2****::cloNAT*	(Ferreira et al., 2011)

Table S3. Potential me-K ligands screened for anchoring function. Related to Fig 1

Screened by	Gene Public Name	Sequence Name	Domain Title
mutant*	*hpl-1*	*K08H2.6*	Chromo
mutant*	*hpl-2*	*K01G5.2*	Chromo
RNAi	*cec-1*	*ZK1236.2*	Chromo
RNAi	*cec-2*	*C50A2.2*	Chromo
RNAi	*cec-3*	*T09A5.8*	Chromo
RNAi	*cec-4*	*F32E10.2*	Chromo
RNAi	*cec-5*	*F32E10.6*	Chromo
RNAi	*cec-6*	*T12E12.2*	Chromo
RNAi	*cec-7*	*Y37D8A.11*	Chromo
RNAi	*cec-8*	*Y55B1BR.3*	Chromo
RNAi	*cec-9*	*C29H12.5*	Chromo
RNAi	*cec-10*	*ZK973.2*	Chromo
RNAi	*chd-1*	*H06O01.2*	Chromo
RNAi	*chd-3*	*T14G8.1*	Chromo & PHD
RNAi	*let-418*	*F26F12.7*	Chromo & PHD
RNAi	*mrg-1*	*Y37D8A.9*	Chromo
RNAi	*mys-1*	*VC5.4*	Chromo
RNAi	*mys-2*	*K03D10.3*	Chromo
RNAi	*set-31*	*C15H11.5*	Chromo
NA	*tag-192*	*T04D1.4*	Chromo
mutant*	*lin-61*	*R06C7.7*	MBT repeat
RNAi	*mbtr-1*	*Y48G1A.6*	MBT repeat
RNAi	*athp-1*	*C44B9.4*	PHD
RNAi	*athp-3*	*Y116A8C.22*	PHD
RNAi	*dpff-1*	*C28H8.9*	PHD
RNAi	*F53H1.4*	*F53H1.4*	PHD
RNAi	*flt-1*	*ZK783.4*	PHD
RNAi	*ing-3*	*Y51H1A.4*	PHD
RNAi	*jmjd-1.1*	*F43G6.6*	PHD
RNAi	*jmjd-1.2*	*F29B9.2*	PHD
RNAi	*jmjd-2*	*Y48B6A.11*	PHD
RNAi	*lin-49*	*F42A9.2*	PHD
RNAi	*lsy-13*	*T06A10.4*	PHD
RNAi	*nra-3*	*C17G1.4*	PHD
RNAi	*phf-31*	*F13E6.3*	PHD
RNAi	*phf-32*	*F17A2.3*	PHD
RNAi	*phf-33*	*K09A11.5*	PHD
RNAi	*rpy-1*	*C18H9.7*	PHD
RNAi	*set-16*	*T12D8.1*	PHD
RNAi	*set-8*	*F02D10.7*	PHD
RNAi	*set-9*	*F15E6.1*	PHD
RNAi	*slx-1*	*F56A3.2*	PHD
RNAi	*W03H9.1*	*W03H9.1*	PHD

RNAi	*Y52E8A.2*	*Y52E8A.2*	PHD
RNAi	*zfp-1*	*F54F2.2*	PHD
NA	*athp-2*	*H20J04.2*	PHD
NA	*C11G6.3*	*C11G6.3*	PHD
NA	*dgk-1*	*C09E10.2*	PHD
NA	*lin-59*	*T12F5.4*	PHD
NA	*mys-4*	*C34B7.4*	PHD
NA	*nurf-1*	*F26H11.2*	PHD
NA	*phf-10*	*F33E11.6*	PHD
NA	*phf-14*	*Y59A8A.2*	PHD
NA	*phf-15*	*Y53G8AR.2*	PHD
NA	*phf-30*	*T23B12.1*	PHD
NA	*phf-34*	*F21G4.4*	PHD
NA	*rbr-2*	*ZK593.4*	PHD
NA	*set-26*	*Y51H4A.12*	PHD
RNAi	*C56G2.1*	*C56G2.1*	Tudor
RNAi	*ekl-1*	*F22D6.6*	Tudor
RNAi	*F32E10.5*	*F32E10.5*	Tudor
RNAi	*rsd-6*	*F16D3.2*	Tudor
RNAi	*smn-1*	*C41G7.1*	Tudor
RNAi	*tag-250*	*C29E4.5*	Tudor
RNAi	*tsn-1*	*F10G7.2*	Tudor

* Studied in (Towbin et al., 2012)

NA – Not available in Vidal or Ahringer RNAi libraries or not confirmed after sequencing clone

Table S4. AlphaScreen raw data with ALTA Biosciences Peptides. Related to Fig 3

Peptide name	Spacer-Biotin	Sequence	Peptide concentration		
			62.5nM	125nM	250nM
$H3_{1-21}$	N-term	ARTKQTARKSTGGKAPRKQLA	1860	4708	15808
$H3_{1-21}R2me^1$	N-term	AΞTKQTARKSTGGKAPRKQLA	1516	6560	15248
$H3_{1-21}R2me^2a$	N-term	AΨTKQTARKSTGGKAPRKQLA	1392	2976	11752
$H3_{1-21}R2me^2aT3p$	N-term	AΨΩKQTARKSTGGKAPRKQLA	1384	1364	2492
$H3_{1-21}R2me^2aT3pK4me^3$	N-term	AΨΩΘQTARKSTGGKAPRKQLA	1400	1480	3172
$H3_{1-21}R2me^2aK4me^3$	N-term	AΨTΘQTARKSTGGKAPRKQLA	1440	1964	13780
$H3_{1-21}T3p$	N-term	ARΩKQTARKSTGGKAPRKQLA	1520	1672	5552
$H3_{1-21}T3pK4me^3$	N-term	ARΩΘQTARKSTGGKAPRKQLA	1400	2188	8048
$H3_{1-21}K4me^1$	N-term	ARTΦQTARKSTGGKAPRKQLA	1684	6840	16040
$H3_{1-21}K4me^2$	N-term	ARTΠQTARKSTGGKAPRKQLA	2084	11680	14632
$H3_{1-21}K4me^3$	N-term	ARTΘQTARKSTGGKAPRKQLA	1468	4796	14120
$H3_{1-21}K4me^3K9ac$	N-term	ARTΘQTARΛSTGGKAPRKQLA	2144	1948	3972
$H3_{1-21}K4me^3K9me^3$	N-term	ARTΘQTARΘSTGGKAPRKQLA	1147000	1118404	1091920
$H3_{1-21}K9ac$	N-term	ARTKQTARΛSTGGKAPRKQLA	2636	2996	8060
$H3_{1-21}K9acS10p$	N-term	ARTKQTARΛΣTGGKAPRKQLA	1480	1372	2272
$H3_{1-21}K9acT11p$	N-term	ARTKQTARΛSΩGGKAPRKQLA	1304	1304	1480
$H3_{1-21}K9acS10pT11p$	N-term	ARTKQTARΛΣΩGGKAPRKQLA	1816	1768	1852
$H3_{1-21}K9me^1$	N-term	ARTKQTARΦSTGGKAPRKQLA	1071532	1048212	1067344
$H3_{1-21}K9me^2$	N-term	ARTKQTARΠSTGGKAPRKQLA	1174624	1158512	1155104
$H3_{1-21}K9me^3$	N-term	ARTKQTARΘSTGGKAPRKQLA	1153844	1140156	1119316
$H3_{1-21}K9me^3T11p$	N-term	ARTKQTARΘSΩGGKAPRKQLA	899188	811312	898040
$H3_{1-21}K9me^3S10p$	N-term	ARTKQTARΘΣTGGKAPRKQLA	960912	969700	927200
$H3_{1-21}K9me^3S10pT11p$	N-term	ARTKQTARΘΣΩGGKAPRKQLA	2620	2860	3140
$H3_{1-21}S10p$	N-term	ARTKQTARKΣTGGKAPRKQLA	1508	1852	4808
$H3_{1-21}T11p$	N-term	ARTKQTARKSΩGGKAPRKQLA	1752	5004	7804
$H3_{1-21}S10pT11p$	N-term	ARTKQTARKΣΩGGKAPRKQLA	1556	1972	1772
$H3_{1-21}S10pT11pK14ac$	N-term	ARTKQTARKΣΩGGΛAPRKQLA	1280	1344	1588
$H3_{1-21}S10pT11pK14me^3$	N-term	ARTKQTARKΣΩGGΘAPRKQLA	1192	1324	1404
$H3_{1-21}T11pK14ac$	N-term	ARTKQTARKSΩGGΛAPRKQLA	1296	1668	2872
$H3_{1-21}T11pK14me^3$	N-term	ARTKQTARKSΩGGΘAPRKQLA	1736	1748	5080
$H3_{1-21}K14ac$	N-term	ARTKQTARKSTGGΛAPRKQLA	1888	2336	8732
$H3_{1-21}K14acR17me^2a$	N-term	ARTKQTARKSTGGΛAPΨKQLA	1884	2040	3348
$H3_{1-21}K14me^1$	N-term	ARTKQTARKSTGGΦAPRKQLA	1864	3144	13728
$H3_{1-21}K14me^2$	N-term	ARTKQTARKSTGGΠAPRKQLA	1808	2268	9724
$H3_{1-21}K14me^3$	N-term	ARTKQTARKSTGGΘAPRKQLA	1468	1560	3496
$H3_{1-21}K14me^3R17me^2a$	N-term	ARTKQTARKSTGGΘAPΨKQLA	1176	1232	1212
$H3_{1-21}R17me^1$	N-term	ARTKQTARKSTGGKAPΞKQLA	2036	13696	12868
$H3_{1-21}R17me^2a$	N-term	ARTKQTARKSTGGKAPΨKQLA	1324	1396	2440
$H3_{14-34}$	N-term	KAPRKQLATKAARKSAPATGG	1268	9568	10812
$H3_{14-34}R17me^2aK18ac$	N-term	KAPΨΛQLATKAARKSAPATGG	1320	1344	2548
$H3_{14-34}K18ac$	N-term	KAPRΛQLATKAARKSAPATGG	1212	5252	6032
$H3_{14-34}K18acK23me^3$	N-term	KAPRΛQLATΘAARKSAPATGG	1268	1356	2784
$H3_{14-34}K18acK23me^1$	N-term	KAPRΛQLATΦAARKSAPATGG	1300	1372	1756
$H3_{14-34}K18acK23ac$	N-term	KAPRΛQLATΛAARKSAPATGG	1244	1464	1540
$H3_{14-34}K23ac$	N-term	KAPRKQLATΛAARKSAPATGG	1264	2972	5236
$H3_{14-34}K23acR26me^2a$	N-term	KAPRKQLATΛAAΨKSAPATGG	1224	1192	1584
$H3_{14-34}K23acR26me^2aK27_{ac}$	N-term	KAPRKQLATΛAAΨΛSAPATGG	1156	1276	1260
$H3_{14-34}K23me^1$	N-term	KAPRKQLATΦAARKSAPATGG	1388	1628	9924
$H3_{14-34}K23me^2$	N-term	KAPRKQLATΠAARKSAPATGG	1608	3308	12672
$H3_{14-34}K23me^3$	N-term	KAPRKQLATΘAARKSAPATGG	1332	2472	9180
$H3_{14-34}K23me^3R26me^2a$	N-term	KAPRKQLATΘAAΨKSAPATGG	1440	1516	2552
$H3_{14}$-34K23me3R26me^2aK27$_{ac}$	N-term	KAPRKQLATΘAAΨΛSAPATGG	1464	1288	1928
$H3_{14-34}R26me^1$	N-term	KAPRKQLATKAAΞKSAPATGG	2380	10000	11668

$H3_{14-34}R26me^2a$	N-term	KAPRKQLATKAAΨKSAPATGG	1440	2036	4144
$H3_{14-34}R26me^2aK27ac$	N-term	KAPRKQLATKAAΨΛSAPATGG	1348	1308	2988
$H3_{14-34}R26me^2aK27acS28p$	N-term	KAPRKQLATKAAΨΛΣAPATGG	1248	1440	1548
$H3_{14-34}R26me^2aS28p$	N-term	KAPRKQLATKAAΨKΣAPATGG	1380	1520	4604
$H3_{14-34}K27ac$	N-term	KAPRKQLATKAARΛSAPATGG	1348	5832	7692
$H3_{14-34}K27acS28p$	N-term	KAPRKQLATKAARΛΣAPATGG	1248	1280	1564
$H3_{14-34}K27me^1$	N-term	KAPRKQLATKAARΦSAPATGG	1272	3120	8008
$H3_{14-34}K27me^2$	N-term	KAPRKQLATKAARΠSAPATGG	1400	1724	6760
$H3_{14-34}K27me^3$	N-term	KAPRKQLATKAARΘSAPATGG	1384	2268	1856
$H3_{14-34}R26me^2aK27me^3$	N-term	KAPRKQLATKAAΨΘSAPATGG	1304	1412	1324
$H3_{14-34}K27me^3S28p$	N-term	KAPRKQLATKAARΘΣAPATGG	1252	1252	1732
$H3_{14-34}R26me^2aK27me^3S28p$	N-term	KAPRKQLATKAAΨΘΣAPATGG	1788	1328	1296
$H3_{14-34}S28p$	N-term	KAPRKQLATKAARKΣAPATGG	1208	1368	2180
$H3_{18-38}S28pT32p$	N-term	KQLATKAARKΣAPAΩGGVKKP	1308	1328	1248
$H3_{28-48}$	N-term	SAPATGGVKKPHRYRPGTVAL	1484	2720	3088
$H3_{28-48}T32p$	N-term	SAPAΩGGVKKPHRYRPGTVAL	1384	1472	1548
$H3_{28-48}K36me^1$	N-term	SAPATGGVΦKPHRYRPGTVAL	3052	2504	3904
$H3_{28-48}K36me^2$	N-term	SAPATGGVΠKPHRYRPGTVAL	1264	1692	3532
$H3_{28-48}K36me^3$	N-term	SAPATGGVΘKPHRYRPGTVAL	1204	1344	1584
$H3_{28-48}T32pK36me^3$	N-term	SAPAΩGGVΘKPHRYRPGTVAL	1824	1840	1848
$H3_{28-48}K37me^1$	N-term	SAPATGGVKΦPHRYRPGTVAL	1188136	1171004	1112992
$H3_{28-48}K37me^2$	N-term	SAPATGGVKΠPHRYRPGTVAL	128376	1222320	1124428
$H3_{28-48}K37me^3$	N-term	SAPATGGVKΘPHRYRPGTVAL	1404	3056	6148
$H3_{28-48}T32pK37me^3$	N-term	SAPAΩGGVKΘPHRYRPGTVAL	1300	1364	1512
$H3_{28-48}K36me^3K37me^3$	N-term	SAPATGGVΘΘPHRYRPGTVAL	1284	1516	2500
$H3_{28-48}T32pK36me^3K37me^3$	N-term	SAPAΩGGVΘΘPHRYRPGTVAL	1204	1364	1360
$H3_{71-91}$	N-term	VREIAQDFKTDLRFQSSAVMA	1260	1456	1208
$H3_{71-91}K79me^1$	N-term	VREIAQDFΦTDLRFQSSAVMA	1172	1208	1184
$H3_{71-91}K79me^2$	N-term	VREIAQDFΠTDLRFQSSAVMA	1320	1196	1280
$H3_{71-91}K79me^3$	N-term	VREIAQDFΘTDLRFQSSAVMA	1268	1328	1196
$H3_{110-130}$	N-term	CAIHAKRVTIMPKDIQLARRI	1296	1400	1184
$H3_{110-130}K115ac$	N-term	CAIHAΛRVTIMPKDIQLARRI	1328	1496	1944
$H3_{110-130}K115acT118p$	N-term	CAIHAΛRVΩIMPKDIQLARRI	1772	1816	1968
$H3_{110-130}T118p$	N-term	CAIHAKRVΩIMPKDIQLARRI	1508	1988	1776
$H3_{110-130}K122ac$	N-term	CAIHAKRVTIMPΛDIQLARRI	1256	1504	1404
$H3_{110-130}T118pK122ac$	N-term	CAIHAKRVΩIMPΛDIQLARRI	1240	1268	1204
$H3_{110-130}K115acT118pK122ac$	N-term	CAIHAΛRVΩIMPΛDIQLARRI	1236	1336	1280
$H3_{115-135}$	N-term	KRVTIMPKDIQLARRIRGERA-acid	1256	1444	2940
$H3_{115-135}R128me^1$	N-term	KRVTIMPKDIQLAΞRIRGERA-acid	1204	1836	1620
$H3_{115-135}R128me^2a$	N-term	KRVTIMPKDIQLAΨRIRGERA-acid	1284	2196	1252
$H3_{115-135}K122acR128me^2a$	N-term	KRVTIMPΛDIQLAΨRIRGERA-acid	1208	1288	1216
$H3_{1-21}$	C-term	ARTKQTARKSTGGKAPRKQLA	4076	3604	2976
$H3_{1-21}R2me^1$	C-term	AΞTKQTARKSTGGKAPRKQLA	4164	3376	2944
$H3_{1-21}R2me^2a$	C-term	AΨTKQTARKSTGGKAPRKQLA	3620	3316	2804
$H3_{1-21}R2me^2aT3p$	C-term	AΨΩKQTARKSTGGKAPRKQLA	2452	2352	1952
$H3_{1-21}R2me^2aT3pK4me^3$	C-term	AΨΩΘQTARKSTGGKAPRKQLA	2468	2260	1792
$H3_{1-21}R2me^2aK4me^3$	C-term	AΨTΘQTARKSTGGKAPRKQLA	4764	4104	2968
$H3_{1-21}T3p$	C-term	ARΩKQTARKSTGGKAPRKQLA	3980	3404	2540
$H3_{1-21}T3pK4me^3$	C-term	ARΩΘQTARKSTGGKAPRKQLA	3772	3220	2628
$H3_{1-21}K4me^1$	C-term	ARTΦQTARKSTGGKAPRKQLA	4736	4160	3332
$H3_{1-21}K4me^2$	C-term	ARTΠQTARKSTGGKAPRKQLA	5208	4804	3972
$H3_{1-21}K4me^3$	C-term	ARTΘQTARKSTGGKAPRKQLA	5440	4836	3540
$H3_{1-21}K4me^3K9ac$	C-term	ARTΘQTARΛSTGGKAPRKQLA	3320	2656	2084
$H3_{1-21}K4me^3K9me^3$	C-term	ARTΘQTARΘSTGGKAPRKQLA	594572	702360	587016
$H3_{1-21}K9ac$	C-term	ARTKQTARΛSTGGKAPRKQLA	3508	3412	2684
$H3_{1-21}K9acS10p$	C-term	ARTKQTARΛΣTGGKAPRKQLA	1648	1472	1352

$H3_{1-21}$K9acT11p	C-term	ARTKQTARΛSΩGGKAPRKQLA	2064	1744	1476
$H3_{1-21}$K9acS10pT11p	C-term	ARTKQTARΛΣΩGGKAPRKQLA	1636	1576	1576
$H3_{1-21}$K9me^{1}	C-term	ARTKQTARΦSTGGKAPRKQLA	580476	471332	420048
$H3_{1-21}$K9me^{2}	C-term	ARTKQTARΠSTGGKAPRKQLA	840592	793300	729364
$H3_{1-21}$K9me^{3}	C-term	ARTKQTARΘSTGGKAPRKQLA	530060	592652	551024
$H3_{1-21}$K9me^{3}T11p	C-term	ARTKQTARΘSΩGGKAPRKQLA	5044	4104	3260
$H3_{1-21}$K9me^{3}S10p	C-term	ARTKQTARΘΣTGGKAPRKQLA	6996	4384	3428
$H3_{1-21}$K9me^{3}S10pT11p	C-term	ARTKQTARΘΣΩGGKAPRKQLA	1920	1828	1488
$H3_{1-21}$S10p	C-term	ARTKQTARKΣTGGKAPRKQLA	2248	1920	1784
$H3_{1-21}$T11p	C-term	ARTKQTARKSΩGGKAPRKQLA	2864	2856	2264
$H3_{1-21}$S10pT11p	C-term	ARTKQTARKΣΩGGKAPRKQLA	1592	1712	1612
$H3_{4-24}$S10pT11pK14ac	C-term	Ac-KQTARKΣΩGGΛAPRKQLATKA	1208	1460	1260
$H3_{4-24}$S10pT11pK14me^{3}	C-term	Ac-KQTARKΣΩGGΘAPRKQLATKA	1196	1256	1212
$H3_{4-24}$T11pK14ac	C-term	Ac-KQTARKSΩGGΛAPRKQLATKA	1248	1216	1248
$H3_{4-24}$T11pK14me^{3}	C-term	Ac-KQTARKSΩGGΘAPRKQLATKA	1696	1624	1668
$H3_{4-24}$K9acK14ac	C-term	Ac-KQTARΛSTGGΛAPRKQLATKA	1536	1712	1552
$H3_{8-28}$K14ac	C-term	Ac-RKSTGGΛAPRKQLATKAARKS	3140	2980	2556
$H3_{8-28}$K14acR17me^{2}a	C-term	Ac-RKSTGGΛAPΨKQLATKAARKS	1980	1740	1592
$H3_{8-28}$K14me^{1}	C-term	Ac-RKSTGGΦAPRKQLATKAARKS	4456	3664	3052
$H3_{8-28}$K14me^{2}	C-term	Ac-RKSTGGΠAPRKQLATKAARKS	3832	3564	2864
$H3_{8-28}$K14me^{3}	C-term	Ac-RKSTGGΘAPRKQLATKAARKS	4616	4452	3256
$H3_{8-28}$K14me^{3}R17me^{2}a	C-term	Ac-RKSTGGΘAPΨKQLATKAARKS	3324	3164	2232
$H3_{8-28}$R17me^{1}	C-term	Ac-RKSTGGKAPΞKQLATKAARKS	5228	5024	3508
$H3_{8-28}$R17me^{2}a	C-term	Ac-RKSTGGKAPΨKQLATKAARKS	2172	3424	2368
$H3_{8-28}$K14acK18ac	C-term	Ac-RKSTGGΛAPRΛQLATKAARKS	2168	1940	1700
$H3_{12-32}$R17me^{2}aK18ac	C-term	Ac-GGKAPΨΛQLATKAARKSAPAT	1204	1200	1228
$H3_{12-32}$K18ac	C-term	Ac-GGKAPRΛQLATKAARKSAPAT	1176	1248	1076
$H3_{12-32}$K18acK23me^{3}	C-term	Ac-GGKAPRΛQLATΘAARKSAPAT	1188	1180	1188
$H3_{12-32}$K18acK23ac	C-term	Ac-GGKAPRΛQLATΛAARKSAPAT	1232	1192	1148
$H3_{18-38}$K23ac	C-term	Ac-KQLATΛAARKSAPATGGVKKP	1180	1388	1324
$H3_{18-38}$K23acR26me^{2}a	C-term	Ac-KQLATΛAAΨKSAPATGGVKKP	1148	1192	1428
$H3_{18-38}$K23acR26me^{2}aK27ac	C-term	Ac-KQLATΛAAΨΛSAPATGGVKKP	1236	1260	1220
$H3_{18-38}$K23me^{1}	C-term	Ac-KQLATΦAARKSAPATGGVKKP	1924	1952	1304
$H3_{18-38}$K23me^{2}	C-term	Ac-KQLATΠAARKSAPATGGVKKP	1860	1636	1448
$H3_{18-38}$K23me^{3}	C-term	Ac-KQLATΘAARKSAPATGGVKKP	1460	1376	1392
$H3_{18-38}$K23me^{3}R26me^{2}a	C-term	Ac-KQLATΘAAΨKSAPATGGVKKP	1228	1220	1172
$H3_{18-38}$K23me$_{3}$R26me^{2}aK27ac	C-term	Ac-KQLATΘAAΨΛSAPATGGVKKP	1144	1232	1260
$H3_{20-40}$	C-term	Ac-LATKAARKSAPATGGVKKPHR	4764	1920	2340
$H3_{20-40}$R26me^{1}	C-term	Ac-LATKAAΞKSAPATGGVKKPHR	2880	2072	1648
$H3_{20-40}$R26me^{2}a	C-term	Ac-LATKAAΨKSAPATGGVKKPHR	2032	1752	1772
$H3_{20-40}$R26me^{2}aK27ac	C-term	Ac-LATKAAΨΛSAPATGGVKKPHR	1388	1304	1228
$H3_{20-40}$R26me^{2}aK27acS28p	C-term	Ac-LATKAAΨΛΣAPATGGVKKPHR	1252	1308	1548
$H3_{20-40}$R26me^{2}aS28p	C-term	Ac-LATKAAΨKΣAPATGGVKKPHR	1488	1648	1068
$H3_{20-40}$K27ac	C-term	Ac-LATKAARΛSAPATGGVKKPHR	1608	1712	1620
$H3_{20-40}$K27acS28p	C-term	Ac-LATKAARΛΣAPATGGVKKPHR	1368	1112	1092
$H3_{20-40}$K27me^{1}	C-term	Ac-LATKAARΦSAPATGGVKKPHR	2940	2896	1908
$H3_{20-40}$K27me^{2}	C-term	Ac-LATKAARΠSAPATGGVKKPHR	2176	2544	1808
$H3_{20-40}$K27me$_{3}$	C-term	Ac-LATKAARΘSAPATGGVKKPHR	2588	2564	2100
$H3_{20-40}$R26me^{2}aK27me^{3}	C-term	Ac-LATKAAΨΘSAPATGGVKKPHR	2636	2560	1624
$H3_{20-40}$K27me^{3}S28p	C-term	Ac-LATKAARΘΣAPATGGVKKPHR	1520	1344	1220
$H3_{20-40}$R26me^{2}aK27me^{3}S28p	C-term	Ac-LATKAAΨΘΣAPATGGVKKPHR	1416	1356	1152
$H3_{20-40}$S28p	C-term	Ac-LATKAARKΣAPATGGVKKPHR	1528	1404	1224
$H4_{1-21}$	C-term	SGRGKGGKGLGKGGAKRHRKV	6232	5768	7256
$H4_{1-21}$S1p	C-term	ΣGRGKGGKGLGKGGAKRHRKV	6964	6480	4612
$H4_{1-21}$R3me^{1}	C-term	SGΞGKGGKGLGKGGAKRHRKV	5584	6008	5856
$H4_{1-21}$R3me^{2}a	C-term	SGΨGKGGKGLGKGGAKRHRKV	8584	4560	4272

$H4_{1-21}$R3me^{2}aK5ac	C-term	SGΨGΛGGKGLGKGGAKRHRKV	5960	5540	4480
$H4_{1-21}$S1pR3me^{2}aK5ac	C-term	ΣGΨGΛGGKGLGKGGAKRHRKV	5628	4332	4136
$H4_{1-21}$K5ac	C-term	SGRGΛGGKGLGKGGAKRHRKV	5568	5380	4544
$H4_{1-21}$K5acK8acK12ac	C-term	SGRGΛGGΛGLGΛGGAKRHRKV	3116	2616	2532
$H4_{1-21}$K5acK8ac	C-term	SGRGΛGGΛGLGKGGAKRHRKV	5360	4260	3796
$H4_{1-21}$K8ac	C-term	SGRGKGGΛGLGKGGAKRHRKV	5648	5424	4280
$H4_{1-21}$K8acK12ac	C-term	SGRGKGGΛGLGΛGGAKRHRKV	2760	4176	3620
$H4_{1-21}$K12me^{1}	C-term	SGRGKGGKGLGΦGGAKRHRKV	4348	6924	6048
$H4_{1-21}$K12me^{2}	C-term	SGRGKGGKGLGΠGGAKRHRKV	4928	4544	4120
$H4_{1-21}$K12me^{3}	C-term	SGRGKGGKGLGΘGGAKRHRKV	6188	6516	5368
$H4_{1-21}$K8acK12me^{1}	C-term	SGRGKGGΛGLGΦGGAKRHRKV	5776	4976	4608
$H4_{1-21}$K8acK12me^{3}	C-term	SGRGKGGΛGLGΘGGAKRHRKV	5856	4916	4660
$H4_{6-26}$K12me^{1}K16ac	C-term	Ac-GGKGLGΦGGAΛRHRKVLRDNI	1908	1776	1548
$H4_{6-26}$K12me^{3}K16ac	C-term	Ac-GGKGLGΘGGAΛRHRKVLRDNI	2176	2164	2052
$H4_{6-26}$K16ac	C-term	Ac-GGKGLGKGGAΛRHRKVLRDNI	2000	2076	1884
$H4_{11-31}$	C-term	Ac-GKGGAKRHRKVLRDNIQGITK	2016	1876	1812
$H4_{11-31}$K20ac	C-term	Ac-GKGGAKRHRΛVLRDNIQGITK	1416	1664	1632
$H4_{11-31}$K16acK20ac	C-term	Ac-GKGGAΛRHRΛVLRDNIQGITK	1484	1692	1480
$H4_{11-31}$K16acK20me^{1}	C-term	Ac-GKGGAΛRHRΦVLRDNIQGITK	1564	1668	1492
$H4_{11-31}$K16acK20me^{3}	C-term	Ac-GKGGAΛRHRΘVLRDNIQGITK	1444	1512	1296
$H4_{11-31}$K20me^{1}	C-term	Ac-GKGGAKRHRΦVLRDNIQGITK	1892	1860	1680
$H4_{11-31}$K20me^{2}	C-term	Ac-GKGGAKRHRΠVLRDNIQGITK	1676	1772	1716
$H4_{11-31}$K20me^{3}	C-term	Ac-GKGGAKRHRΘVLRDNIQGITK	2120	2016	1888
		no peptide	1316	1292	1232

Λ = acetyl-Lysine	Φ = monomethyl-Lys	Π = dimethyl-Lys	Θ = trimethyl-Lys
Σ = phospho-Ser	Ω = phospho-Thr	Ξ = monomethyl-Arg	Ψ = asym dimethyl-Arg
All the peptides have C-terminal amide groups (Ac-) unless specified			Spacer= aminohexanoic acid, Ahx

Table S5. RT-qPCR primer pairs used in this study. Related to Figs. 5 and 6

Target	Sequence
srw-85 F	GCGTGTCCCGAAATAAAGTC
srw-85 R	GATCTTCAAGTCTCGAATGCAG
C18D6.4 F	TACAGTGCTCATCAACTTGCC
C18D6.4 R	GCAATAAGAAGAGCATCTTCAAGG
pmp-3 F	GTTCCCGTGTTCATCACTCAT
pmp-3 R	ACACCGTCGAGAAGCTGTAGA
genomic *srw-85* F	GTGAGATGTGCCTGAGGAGT
genomic *srw-85* R	CCTACCGCTATCCATTCACG
genomic *C18D6.4* F	CGGGCTCTGGATGAGGTAAT
genomic *C18D6.4* R	TGCTATTGGCGGGAGGCTTA
hlh-1 F	CAAAGAACGTGTCCGAATCC
hlh-1 R	TGAGAGGAAGTCACATAATCGT
myo-3 F	AGACAGGTTGAGGAGGCTGA
myo-3 R	TCTGATAAGCGCACTGGATG
F21D9.4 F	CAGAGTATACTACAAAGGACTGGAG
F21D9.4 R	AGCCGATTGAGGTTGATGAC
C25F9.5 F	TTTCATCACACGAGATGAGATGG
C25F9.5 R	GTATACGTAGGTAGCAAGTCCTG
Y43F8A.5 F	TTAATGATCCTCAACATGCGCT
Y43F8A.5 R	GAGGTGCTATCCGTAAGTGTG
unc-98 F	TCCAGATACAACAATGGATGACGA
unc-98 R	TGAGCACTTGAACTTCCGACA
unc-45 F	GCTGATGAATTATACACTGAAGC
unc-45 R	GAGCCTCTTTTGCGTCTTGA
pal-1 F	GGAAGTAGCAGTAGTGATAGTGG
pal-1 F	GAATCCCTGAAACTGTTGATAATCC

Table S6. Depletion of nuclear envelope components to address CEC-4-mCherry perinuclear localization in worms. Referred in text section "*CEC-4 is intrinsically localized at the nuclear periphery*"

RNAi of NE related gene	CEC-4-mCh localization
anc-1	Perinuclear ring
baf-1	Perinuclear ring
emr-1	Perinuclear ring
lem-2	Perinuclear ring
lmn-1	Perinuclear ring
sun-1	Perinuclear ring
unc-83	Perinuclear ring
unc-84	Perinuclear ring
zyg-12	Perinuclear ring

Table S7. Yeast mutations in nuclear envelope components used to address CEC-4-mCherry perinuclear localization in yeast. Referred in text section "*CEC-4 is intrinsically localized at the nuclear periphery*"

Mutation Tested	CEC-4-mCh localization
mlp1 mlp2 esc1	Perinuclear ring
mlp1	Perinuclear ring
mlp2	Perinuclear ring
mlp1 mlp2	Perinuclear ring
mlp1 mlp2 siz2	Perinuclear ring
nup133	Perinuclear ring
mps3::mps3 delta75-150 tel1	Perinuclear ring
nup84	Perinuclear ring
nup120	Perinuclear ring
src1	Perinuclear ring

Supplemental References

Andrulis, E.D., Zappulla, D.C., Ansari, A., Perrod, S., Laiosa, C.V., Gartenberg, M.R., and Sternglanz, R. (2002). Esc1, a Nuclear Periphery Protein Required for Sir4-Based Plasmid Anchoring and Partitioning. Mol Cell Biol *22*, 8292-8301.

Berrow, N.S., Alderton, D., Sainsbury, S., Nettleship, J., Assenberg, R., Rahman, N., Stuart, D.I., and Owens, R.J. (2007). A versatile ligation-independent cloning method suitable for high-throughput expression screening applications. Nucleic acids research *35*, e45.

Bucci, M., and Wente, S.R. (1998). A novel fluorescence-based genetic strategy identifies mutants of Saccharomyces cerevisiae defective for nuclear pore complex assembly. Mol Biol Cell *9*, 2439-2461.

Ferreira, H.C., Luke, B., Schober, H., Kalck, V., Lingner, J., and Gasser, S.M. (2011). The PIAS homologue Siz2 regulates perinuclear telomere position and telomerase activity in budding yeast. Nat Cell Biol *13*, 867-874.

Frokjaer-Jensen, C., Wayne Davis, M., Hopkins, C.E., Newman, B.J., Thummel, J.M., Olesen, S.-P., Grunnet, M., and Jorgensen, E.M. (2008). Single-copy insertion of transgenes in *Caenorhabditis elegans*. Nat Genet *40*, 1375-1383.

Gaidatzis, D., Lerch, A., Hahne, F., and Stadler, M.B. (2015). QuasR: quantification and annotation of short reads in R. Bioinformatics *31*, 1130-1132.

Hediger, F., Dubrana, K., and Gasser, S.M. (2002). Myosin-like proteins 1 and 2 are not required for silencing or telomere anchoring, but act in the Tel1 pathway of telomere length control. J Struct Biol *140*, 79-91.

Hendriks, G.J., Gaidatzis, D., Aeschimann, F., and Grosshans, H. (2014). Extensive Oscillatory Gene Expression during C. elegans Larval Development. Molecular cell *53*, 380-392.

Ikegami, K., Egelhofer, T.A., Strome, S., and Lieb, J.D. (2010). Caenorhabditis elegans chromosome arms are anchored to the nuclear membrane via discontinuous association with LEM-2. Genome Biol *11*, R120.

Langmead, B., Trapnell, C., Pop, M., and Salzberg, S.L. (2009). Ultrafast and memory-efficient alignment of short DNA sequences to the human genome. Genome Biol *10*, R25.

Meister, P., Towbin, B.D., Pike, B.L., Ponti, A., and Gasser, S.M. (2010). The spatial dynamics of tissue-specific promoters during C. elegans development. Genes & Development *24*, 766-782.

Nagai, S., Dubrana, K., Tsai-Pflugfelder, M., Davidson, M.B., Roberts, T.M., Brown, G.W., Varela, E., Hediger, F., Gasser, S.M., and Krogan, N.J. (2008). Functional Targeting of DNA Damage to a Nuclear Pore-Associated SUMO-Dependent Ubiquitin Ligase. Science *322*, 597-602.

Rohner, S., Kalck, V., Wang, X., Ikegami, K., Lieb, J.D., Gasser, S.M., and Meister, P. (2013). Promoter- and RNA polymerase II-dependent hsp-16 gene association with nuclear pores in Caenorhabditis elegans. J Cell Biol *200*, 589-604.

Schindelin, J., Arganda-Carreras, I., Frise, E., Kaynig, V., Longair, M., Pietzsch, T., Preibisch, S., Rueden, C., Saalfeld, S., Schmid, B., *et al.* (2012). Fiji: an open-source platform for biological-image analysis. Nat Methods *9*, 676-682.

Schober, H., Ferreira, H., Kalck, V., Gehlen, L.R., and Gasser, S.M. (2009). Yeast telomerase and the SUN domain protein Mps3 anchor telomeres and repress subtelomeric recombination. Genes & development *23*, 928-938.

Sommer, C.S., C.; Köthe, U.; Hamprecht, F. A. (2011). ilastik: Interactive Learning and Segmentation Toolkit. Eighth IEEE International Symposium on Biomedical Imaging (ISBI) Proceedings, 230-233.
Stiernagle, T. (2006). Maintenance of C. elegans. WormBook, 1-11.

Taddei, A., Van Houwe, G., Nagai, S., Erb, I., van Nimwegen, E., and Gasser, S.M. (2009). The functional importance of telomere clustering: Global changes in gene expression result from SIR factor dispersion. Genome Research *19*, 611-625.

Thomas, B.J., and Rothstein, R. (1989). The genetic control of direct-repeat recombination in Saccharomyces: the effect of rad52 and rad1 on mitotic recombination at GAL10, a transcriptionally regulated gene. Genetics *123*, 725-738.

Timmons, L., Court, D.L., and Fire, A. (2001). Ingestion of bacterially expressed dsRNAs can produce specific and potent genetic interference in *Caenorhabditis elegans*. Gene *263*, 103-112.

Waterhouse, A.M., Procter, J.B., Martin, D.M., Clamp, M., and Barton, G.J. (2009). Jalview Version 2--a multiple sequence alignment editor and analysis workbench. Bioinformatics *25*, 1189-1191.

ABBREVIATIONS

3C	Chromosome Conformation Capture
3D	Three Dimensional
4C	Chromosome Conformation Capture on Chip
ac	Acetylation
BAF	Barrier-to-Autointegration Factor
Bio-ID	proximity-dependent Biotin IDentification
C. elegans	*Caenorhabditis elegans*
CDOM	Centromere-proximal DOMain
CEC-4	*Caenorhabditis elegans* Chromodomain protein 4
ChIP	Chromatin ImmunoPrecipitation
CREB	Cyclic AMP-responsive Element-Binding
CTCF	CCCTC-binding factor
DNA	Deoxyribonucleic acid
EM	Electron Microscopy
EMS	Ethyl MethaneSulfonate
Epha4	Eph receptor A4
ES	Embryonic Stem
EZH2	Enhancer of zeste 2 polycomb repressive complex 2 subunit
FISH	Fluorescence *in situ* hybridization
GFP	Green Fluorescent Protein
HDAC3	Histone Deacetylase 3
Hi-C	Genome-wide 3C
His	Histidine
HMTs	Histone MethylTransferases
HP1	Heterochromatin Protein 1
HPL-1/2	HP1 Like ½
HU	Hydroxyurea
H*x*K*x*	Histone *x* Lysine *x*
IF	ImmunoFluorescence
IgH	Immunoglobulin heavy chain complex
Ihh	Indian hedgehog
INM	Inner Nuclear Membrane
LAD	Lamina Associated Domain
LBR	Lamin B Receptor
LEM	LAP2, Emerin and MAN1 domain
Leu	Leucine
LINC	LInker of Nucleoskeleton and Cytoskeleton
LINE	Long Interspersed Nuclear Element
LMN-1	Lamin-1
LOCKs	Large Organized Chromatin K9-modifications
MBT	Malignant Brain Tumor
me (1,2,3)	Methylation (mono-, di-, tri-)
MNase	Micrococcal Nuclease
NE	Nuclear envelope
NET	Nuclear Envelope Transmembrane
OIS	Oncogene-Induced Scenescence

PARD3	Par-3 family cell polarity regulator
PARP1	Poly (ADP-ribose) polymerase 1
Pax3	Paired box 3
Pol	Polymerase
PPR14	PRoline-Rich protein 14
PRC2	Polycomb Repressive Complex 2
PRDM3/16	PR domain containing 3/16
PUS7	PseudoUridylate Synthase 7
rDNA	ribosomal DNA
RNA	Ribonucleic acid
RNAi	RNA interference
S. cerevisiae	*Saccharomyces cerevisiae*
S. pombe	*Schizosaccharomyces pombe*
SAHF	Senescence-Associated Heterochromatic Foci
SAMS	S-adenosylmethionine Synthetase
SetDB1	SET domain, bifurcated 1
SINE	Short Interspersed Nuclear Element
SIR	Silent Information Regulator
SPB	Spindle Pole Body
Suv39H1	Suppressor of variegation 3-9 homolog 1
TAD	Topological Associated Domain
TDOM	Telomere-proximal DOMain
TEX28	Testis EXpressed 28
TMCC1/2/3	TransMembrane and Coiled-Coil domain family 1/2/3
TRIP	Thousands of Reporters Integrated in Parallel
tRNA	transfer RNA
Trp	Tryptophan
vLADs	variable LADs
Wnt6	Wingless-type MMTV integration site family member 6
Y2H	Yeast two Hybrid
YY1	Ying-Yang-1

ACKNOWLEDGMENTS

I would like to thank Susan Gasser for her continuous support and encouragement throughout my PhD studies, without it, this doctoral thesis would not have been possible to be written.

Thanks as well to my committee members: Antoine Peters and Bas van Steensel, their insightful discussions during our meetings made the work of this thesis even better.

Special thanks to Benjamin Towbin for introducing me to the *C. elegans* world, providing me with all the necessary tools to start my project, inviting me to discuss every part of my work and teaching me how to be a scientist.

The Gasser lab members, past and present, were extremely important in my PhD achievements, without each of them the laboratory would not be the great working place it is. Thanks to all the colleagues for scientific discussions, technical help as well as proof-reading several reports and manuscripts, it has always been highly appreciated.

Big thanks to the amazing facilities at FMI and my collaborators from C-NIBR, without them my work would not have reached the level it has.

Thanks to all my friends at the FMI, their support made possible for me to continue working every day.

I am very thankful for the support of my family and friends. You are always here beside me, even though many of you are far away.

- A mis padres… gracias por el apoyo incondicional, estoy eternamente agradecida.

Muchas gracias to each of you!